LBL-1866 c.1

PHOTOCHEMICAL STUDIES OF ALKALI HALIDE VAPORS

Boyd Lorel Earl

(Ph. D. Thesis)

August 1973

Prepared for the U. S. Atomic Energy Commission
under Contract W-7405-ENG-48

For Reference

Not to be taken from this room

LAWRENCE BERKELEY LABORATORY
UNIVERSITY OF CALIFORNIA
BERKELEY

LBL-1866

DISCLAIMER

This document was prepared as an account of work sponsored by the United States Government. While this document is believed to contain correct information, neither the United States Government nor any agency thereof, nor the Regents of the University of California, nor any of their employees, makes any warranty, express or implied, or assumes any legal responsibility for the accuracy, completeness, or usefulness of any information, apparatus, product, or process disclosed, or represents that its use would not infringe privately owned rights. Reference herein to any specific commercial product, process, or service by its trade name, trademark, manufacturer, or otherwise, does not necessarily constitute or imply its endorsement, recommendation, or favoring by the United States Government or any agency thereof, or the Regents of the University of California. The views and opinions of authors expressed herein do not necessarily state or reflect those of the United States Government or any agency thereof or the Regents of the University of California.

0 0 0 0 3 9 0 , 2 4 2

PHOTOCHEMICAL STUDIES OF ALKALI HALIDE VAPORS

Contents

Abstract v

I. Introduction 1

References 6

II. Apparatus and General Experimental Conditions 8

A. Optics, Electronics and Vacuum Systems 8

1. Equipment 8

2. Signal Extraction and Signal-To-Noise Problems 17

B. The Hydrogen Arc 19

C. General Experimental Considerations 28

References 41

III. Potential Curves and Photodissociation 43

A. Introduction 43

B. Photodissociation Theory and Numerical Analysis 44

C. Potential Curves 50

D. Experiments and Results 51

1. Sodium Iodide 51

2. Sodium Bromide 60

3. Potassium Iodide 63

4. Lithium Iodide 71

5. Theoretical Intensity Distributions 72

E. Photodissociatively Produced Speed Distributions 72

1. Distribution Excluding the Effects of Molecular Rotation 75

2. Distribution including the Effects of Molecular Rotation 78

3. Full Experimental M* Speed Distributions 83

References 87

IV. Quenching Analysis and Theory 89

A. The Steady-State Treatment and Quenching and Mixing Rate Constants 89

1. General Formulation for Excited Doublets 90

2. Special Cases, Approximations, and Data Analysis . . . 93

B. Quenching Cross Sections 102

1. Initial Analysis: "Energy Independent" Cross Sections 102

2. Energy Dependence of Cross Sections 104

3. Decay of the Speed Distributions 115

4. Long-Range Forces 117

C. Theory of Quenching 124

References 133

V. Quenching of Excited Alkali Metals 136

A. Introduction 136

B. Experiments and Results 138

1. Quenching of First Resonance States 138

2. Quenching of $K^*(5p^2P)$ 155

3. Special Experimental Considerations 159

C. Discussion 181

1. Quenching Efficiencies 181

2. Comparison to Other Alkali Quenching Work 200

3. Comparison with Other Systems 204

D. Conclusion 210

References 212

Acknowledgements 216

0 0 0 0 3 9 0 7 2 4 3

PHOTOCHEMICAL STUDIES OF ALKALI HALIDE VAPORS

Boyd Lorel Earl

Inorganic Materials Research Division, Lawrence Berkeley Laboratory
and Department of Chemistry; University of California,
Berkeley, California 94720

ABSTRACT

An apparatus has been constructed for studying the photodissociation of alkali halides to produce excited alkali metal atoms. The key component is a low pressure H_2 arc continuum uv source. Radiation from this source, modulated by a chopping wheel and analyzed by a monochromator, enters a cell containing the alkali halide vapor. In the appropriate wavelength range, photodissociation occurs to produce the alkali atom in an excited ^2p state, the fluorescence from which is detected by a photomultiplier-lock-in amplifier combination.

Measurement of the relative intensity of this fluorescence as a function of uv wavelength for the pure vapor allows construction of an approximate potential curve for the dissociative molecular state. This has been done for the following photodissociation processes: $NaI \rightarrow Na^*(3p\,^2P)$, $NaBr \rightarrow Na^*(3p\,^2P)$, and $KI \rightarrow K^*(4p\,^2P)$. In addition, $KI \rightarrow K^*(5p\,^2P)$ and $LiI \rightarrow Li^*(2p\,^2P)$ were observed, but not fully characterized.

An analytic expression is derived for the distribution in speeds of atoms produced by dissociation at a single energy from a single vibrational level, taking into account effects of molecular translational and rotational energy. Combination of this result with the transition probability factors for the uv absorption process, which can be calculated if the upper potential curve is known, allows calculation of the experimental lab speed distributions of the excited atoms.

The measurement of the intensity of the atomic fluorescence as a function of the pressure of a foreign gas introduced into the cell allows extraction of a rate constant for collisional quenching of the fluorescence by the foreign gas. If this process is then studied at various uv wavelengths, information concerning the energy dependence of the quenching cross section can be obtained. For a system for which a repulsive potential curve has been found, the atomic speed distributions can be convoluted with the thermal speed distribution of the foreign gas, to provide the distributions in relative collision speeds. These distributions can then be used to deconvolute the energy dependence of the quenching cross section. Several gases were studied and analyzed by this technique with $Na^*(3p^2P)$ and $K^*(4p^2P)$.

In addition, a few quenching gases were studied without energy dependence with $Na^*(3p^2P)$ and $K^*(4p^2P)$, and several were studied with $K^*(5p^2P)$. An attempt is made to interpret the quenching efficiencies of all the gases studied in terms of molecular properties. The important properties seem to be electron affinity and the availability of a highly exoergic reaction path with the excited atom. With $Na^*(3p^2P)$ and $K^*(4p^2P)$, four classes of quenchers are proposed, ranging from very inefficient to "super-efficient". With $K^*(5p^2P)$, only noble gases were very inefficient, and all other gases were moderately efficient to efficient quenchers.

0 0 0 0 3 9 0 7 2 4 4

I. INTRODUCTION

Production of atoms in resonance states by photodissociation of diatomic molecules provides a method of investigating two sorts of phenomena. Following the discovery by Terenin,[1] in 1926, that photodissociation of sodium iodide produced the sodium D-lines fluorescence, this process was employed within a few years to study the quenching of atomic fluorescence by measurement of fluorescence intensity as a function of pressure of added foreign gas. Although many metal halides produce excited metal atoms upon exposure to appropriate radiation,[2] investigations through the years have concentrated primarily on sodium iodide[3-11] and thallium iodide,[8,9,12-15] with a small amount of work on sodium bromide[3,9] and potassium iodide.[16]

Following a period of considerable popularity in the thirties, this area of research become somewhat dormant during the forties and most of the fifties. In the last decade, however, molecular beam research has brought very powerful techniques to bear on the study of kinetics and dynamics of gas phase reactions, and the first subject of study by this method was alkali atoms.[17] The new insights gained into the kinetics of processes involving ground state atoms naturally led to a renewed interest in the kinetics of the excited species, and, at the same time, technological developments had been made which made better experiments possible. In particular, the use of continuous radiation sources[7,10] made possible better data analysis,[10] and the development of photon counting technology made direct lifetime measurements feasible.[9,11] On the theoretical side, improving computational methods

have begun to generate results on systems of experimental interest.[18,19] All these factors have led to a renaissance in the field.

Lijnse[20] has recently prepared a comprehensive review of the literature through about 1971 concerning experimental and theoretical work on quenching, excitation, and fine-structure mixing processes involving alkali atoms. This review includes not only photodissociation studies, but also the other two methods which have been applied in this area: the use of atomic vapors, in which excitation is produced by atomic resonance radiation, and fluorescence measurements proceed as in the photodissociation technique; and the use of flames, in which a salt vapor sprayed into a flame of known composition is irradiated with atomic resonance radiation, and the ratio of the absorbed to re-emitted radiation is used to extract information about quenching.

The photodissociation technique has some advantages over these other methods in studying quenching. Gases which react with the ground state atoms can be studied, which is not the case with the atomic vapor method, and molecules which would not survive in flames can be employed as quenchers. Also, by virtue of the very low concentrations of ground state atoms, no problems due to radiation imprisonment are encountered, and additionally, difficulties with collisional broadening of the absorption line are obviously avoided. Perhaps most significant, the photodissociation technique provides for the study of quenching as a function of collision energy over a considerable range, while the atomic vapor and flame techniques, restricted to thermal conditions, have much smaller energy ranges available. It is convenient in this regard that the atomic vapor

measurements, which are usually done at ~400°C, give results for collision energies somewhat lower than are accessible in photodissociation, and thus provide a useful check on the extrapolation of results to low energies.

The second kind of phenomenon which can be investigated by observing the fluorescence of the excited atom is the photodissociation itself as a function of the energy of the exciting radiation. This provides access to information concerning the potential curve for the dissociative molecular state (although, as the absorption process is continuous, the information is limited).[21] It was not until the advent of sufficiently powerful continuous radiation sources, however, that Hanson,[7] in 1955, was able, using a source similar to the one used in this study, to measure a curve of relative fluorescence intensity vs wavelength of exciting radiation (fluorescence efficiency curve) and to attempt to construct an upper repulsive potential curve, for sodium iodide. Recently, as detailed in Chapter III, more sophisticated computational techniques have been brought to bear on this problem, and the information which is obtained about the repulsive potential has been employed in calculating the experimental speed distributions of the excited atoms. These make possible the calculation of distributions in relative collision speed, which leads to full energy analysis of the results of quenching measurements.

There are two ways of studying quenching of excited atoms produced by photodissociation: the steady-state method and the direct lifetime measurement method. In the former, used in this study, the steady-state concentration of the excited species is monitored by measuring the

intensity of its fluorescence. The latter, in which the decay of the excited population is measured by photon counting following a short excitation pulse, is really the "right" way to do the experiments. Mainly this is because it avoids any possible errors due to influences which might cause the lifetime of the excited population in the absence of quenching gas to differ from the natural radiative lifetime, which has to be assumed in the steady-state method. The lifetime method also has the added convenience of not being susceptible to problems arising from absorption of the exciting or fluorescent radiation by the quenching gas or from reaction of this gas with the salt. However, it has one overriding disadvantage: it is extremely time-consuming. Typically, the collection of data on a single atom-gas system is a matter of several week's experiments. In the present study, the essential interest was in looking at a large number of quenching gases with different excited species, in order to try to discern general correlations between features of particular atom-gas systems and quenching behavior. This was only possible by using the steady-state method. Care in procedure and comparison with results of the lifetime method lend confidence to the results obtained here.

Presented here, then, are results on photodissociation of three alkali halides--NaI, NaBr and KI--to produce three excited atomic species--$Na^*(3p^2P)$, $K^*(4p^2P)$, and $K^*(5p^2P)$--and on quenching of these excited atoms by a variety of foreign gases, along with fragmentary results on the photodissociation of LiI to produce $Li^*(2p^2P)$. The primary hope for the results of the quenching experiments is that they will provide an enhanced understanding of the ways in which excited

alkali atoms might be expected to interact with various types of molecules. In particular, it is hoped that some insight can be provided into the behavior of second resonance states, a subject which has heretofore been investigated in only a single, not very extensive, flame study,[22] and into the similarities and contrasts which this behavior provides to that of the first resonance states.

REFERENCES

1. A. Terenin, Z. Physik. 37, 98 (1926).
2. G. G. Neuimin, Elementary Photoprocesses in Molecules, B. S. Neporent, ed. (Consultants Bureau, New York, 1968), p. 3.
3. J. G. Winans, Z. Physik. 60, 631 (1930).
4. A. Terenin and N. Prileshajewa, Z. Physik, Chem. (Leipzig) B13, 72 (1931).
5. B. Kiselbach, V. Kondratjew and A. Leipunsky, Physik. Z. Sowjetunion 2, 201 (1932).
6. V. Kondratjew and M. Siskin, Physik. Z. Sowjetunion 8, 644 (1935).
7. H. G. Hanson, J. Chem. Phys. 23, 1391 (1955).
8. D. J. Dowling, G. R. H. Jones and E. Warhurst, Trans. Far. Soc. 55, 537 (1959).
9. L. E. Brus, J. Chem. Phys. 52, 1716 (1970).
10. B. L. Earl, R. R. Herm, S-M. Lin and C. A. Mims, J. Chem. Phys. 56, 867 (1972).
11. J. R. Barker and R. E. Weston, Jr., Chem. Phys. Letters 19, 235 (1973).
12. N. Prileshajewa, Physik. Z. Sowjetunion 2, 351 (1932).
13. N. Prileshajewa, Physik. Z. Sowjetunion 2, 367 (1932).
14. N. Prileshajewa, Acta Physicochimica URSS 2, 647 (1935).
15. D. J. Dowling and E. Warhurst, Trans. Far. Soc. 55, 532 (1959).
16. J. Gatzke, Z. Physik. Chem. (Liepzig) 223, 321 (1963).
17. See for example, J. L. Kinsey, MTP International Review of Science, Phys. Chem. Series One, Chemical Kinetics, J. C. Polanyi (Butterworths, London, 1972), Vol. 9, Chap. 6.

0 0 0 0 5 9 0 , 2 4 7

18. E. E. Nikitin, Fast Reactions and Primary Processes in Chemical Kinetics, S. Claesson, ed. (Interscience, New York, 1967), p. 165.

19. E. Bauer, E. R. Fisher and F. R. Gilmore, J. Chem. Phys. 51, 4173 (1969).

20. P. L. Lijnse, Fysisch Laboratorium, Rijksuniversiteit Utrecht, The Netherlands, Report i 938, 1972.

21. Shen-Maw Lin, Molecular Beam Kinetics (Ph. D. Thesis), LBL-891, September 1972.

22. H. P. Hoomayers and P. L. Lijnse. J. Quant. Spectrosc. Radiat. Transfer 9, 995 (1969).

II. APPARATUS AND GENERAL EXPERIMENTAL CONDITIONS

A. Optics, Electronics and Vacuum Systems

1. Equipment

The apparatus employed in this study was fairly simple in concept, design, construction, and operation, with the exception of the hydrogen arc lamp, which will be discussed at some length later. A schematic of the apparatus, including a block diagram of the detection electronics, is shown in Fig. II-1. Early experiments, including most of the work on NaI, were done in the open air, so to speak, but subsequently the experiment was relocated so that the path of the ultraviolet (uv) radiation was entirely inside a metal vacuum chamber. Pumping this chamber to 1-10 mTorr with a mechanical pump trapped by liquid nitrogen to prevent back-diffusion of pump oil made available the upper wavelength ranges of the vacuum uv, and also improved the signal-to-noise ratio. This improvement was thought to be due to more efficient heating corresponding to lower temperatures of some of the heating wires (see part 2 of this section on signal-to-noise problems), and to better shielding of the photomultiplier from room light.

Following the path of the uv radiation from the hydrogen arc through the various components, then backtracking to the fluorescence radiation, provides a convenient way to describe the various parts of the experimental set-up and their relationships. The uv was focused by a 1 in., 5 cm focal length suprasil (synthetic fused quartz) lens into either a Heath Model EU-700 or a Jarrell-Ash 82-410 monochromator. The Heath instrument has a grating with 1180 lines/mm, blazed for 2500Å, in a Czerny-Turner mount, a focal length of 0.35 m, an aperture

0 0 0 0 5 9 0 7 2 4 8

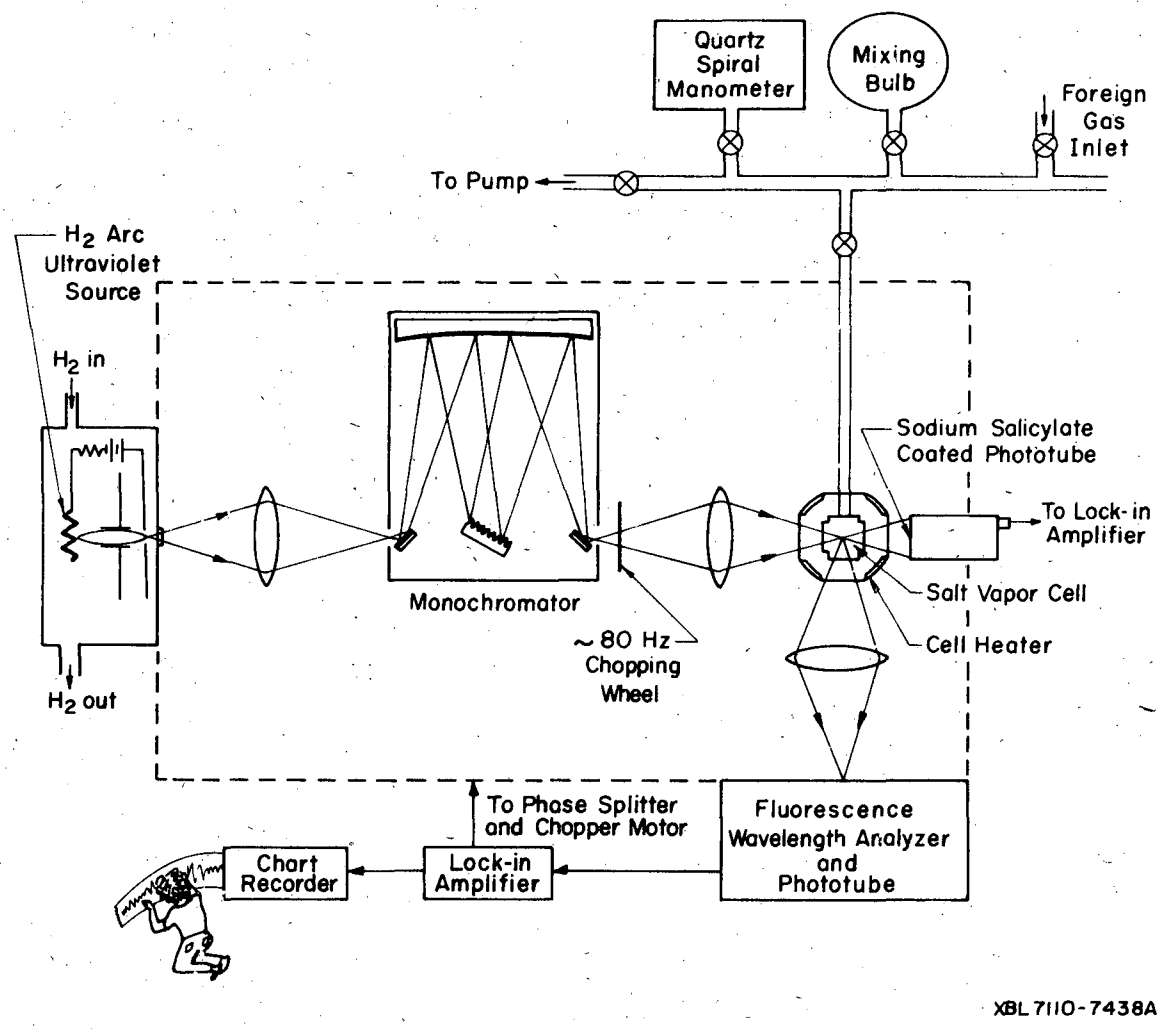

Fig. II-1. Schematic of the apparatus.

ratio of f/6.8 at 2000Å, and a reciprocal dispersion of ~24 Å/mm. It was employed in the experiments which did not use the vacuum chamber. The Jarrell-Ash monochromator has a grating with 1180 lines/mm, blazed for 1900Å, in an Ebert mount, a focal length of 0.25m, an aperture ratio of f/3.5, and a reciprocal dispersion of ~30 Å/mm. It was used inside the vacuum chamber with a simple rotary feed-through for the manual wavelength drive and a viewing window and a pair of mirrors to display the wavelength reading.

When the experiment was first put into the vacuum chamber, an assembly of two Jarrell-Ash 82-410 monochromators in tandem was introduced in an attempt to eliminate the small, but nevertheless bothersome, stray visible light passed by the Heath instrument. While this "white" stray light was effectively eliminated by the double monochromator assembly, two other difficulties arose. One of the monochromators proved to be ~4 times less efficient than the other in transmitting the uv around 2000Å, so, intensity considerations being paramount, it was removed. Furthermore, these monochromators exhibited multiple-path leakage[1] of visible light which allowed relatively very large amounts to pass at certain settings in the uv around 2000Å. This problem was overcome by placing a black paper mask ~1 in. wide vertically over the central portion of the concave mirror in the monochromator which was finally used. Quite probably this affected the efficiency of transmission at some wavelengths.* but it was necessary in order that the relative uv

---

*By comparing signal with and without this mask in its first configuration, it was estimated that it cut out about 30% at 1900Å, and did not affect transmission at 2500Å. In a later configuration (see Section B of this chapter) the effect of the mask was somewhat different.

intensity as a function of wavelength could be measured, which data were required for normalization of the fluorescence curves. Following this correction, there was, as with the Heath instrument, a small leakage of visible light, but in this case it was essentially independent of the monochromator setting, at least in the 1500-2750Å range, and could thus be properly accounted for in obtaining uv intensity measurements.

Following the monochromator, the radiation was chopped by a three-bladed wheel possessing C_3 symmetry, driven by a Globe model 53A112-2 ac hysteresis motor, which was in turn powered by a signal generated by a PAR model HR-8 lock-in amplifier operated in the internal reference mode. This signal passed through a phase splitter and was amplified by a Bogen CHB100 amplifier before reaching the motor.

A second suprasil lens, identical to the first, focused the chopped radiation into the cell containing the salt vapor. This fluorescence cell was constructed of quartz, with two suprasil windows in the uv path and two quartz windows in the perpendicular direction. The main body of the cell was a section of 30 mm tubing approximately 6 in. long, near the top of which the four 1 in. diameter, 1/16 in. thick windows were attached on short extensions so they protruded 1/4-1/2 in. from the body of the cell. The salt charge was placed in the lower end of this 30 mm section and a 10 mm finger extending down from it 3 or 4 in. At the upper end was attached a short section of ~3 mm i.d. capillary tubing to retard sublimation of the salt out of the main body of the cell. In early experiments, a magnet-controlled ground quartz rod was used to plug this 3 mm orifice except when a gas was introduced or the cell was to be pumped. This practice proved

troublesome for a couple of reasons--the subliming salt would occasionally seal the rod into the opening, and the rod, being thin, was very susceptible to breakage--and it was found to be unnecessary, as it was discovered that many hours of experiments could be run before sufficient salt sublimed to plug off the upper tube, and it was regarded as a good practice to change the salt charge regularly, anyway.

This upper tube, which led off from the short capillary section, provided connection with the glass vacuum system. This system was quite ordinary. The components which might merit mention in their applications in this study were a Granville-Phillips Co. Series 203 leak valve for the control of high-pressure gases from cylinders, a 5 ℓ mixing flask, the use of which will be discussed later, and a Texas Instruments Fused Quartz Precision Pressure Gage, model 141, supplied with a Bourdon Tube Capsule calibrated (and very nearly linear) from 0 to 1000 Torr. The resolution of this manometer was ~0.025 Torr. This vacuum system was pumped by a liquid-nitrogen-trapped mercury diffusion pump and a two-stage mechanical pump. The background pressure was in the range 10^{-5}-10^{-3} Torr, and the leak rate in the main manifold was found on two separate occasions to be ~1 mTorr/hr.

This aside, let us return to the experimentally interesting region. The fluorescence cell was heated by two Lindberg cylindrical ceramic heating units, 2 5/8 in. o.d., 1 3/4 in. i.d., one 8 in. long (type 1708-KSP) for the portion below the windows, and one 4 in. long (type 1704-KSP) for the portion above the windows. The windows separated these two heaters, and, although they did not extend beyond the outer surfaces, auxiliary heating was required to prevent condensation of salt vapor on them.

This was provided by Chromel A wire strung with ceramic beads and held in place either by being coiled around the window extensions, or later (and preferably) by a specially constructed stainless steel holder--a short section of pipe grooved for the beaded wire and drilled with holes for light passage. The entire heated assembly was insulated by two concentrically arranged metal cans for use in air, but only a small amount of aluminum or stainless steel foil was wrapped around the heating elements as heat shielding for operation in the vacuum chamber. In air, two chromel-alumel thermocouples were used to monitor the temperatures of the salt charge and the region immediately above the windows. In the vacuum chamber, three such thermocouples were used to monitor the temperatures of the salt charge, the window region and the region along the upper extension. The window temperature, which was taken to be the temperature at which the measurements were made, was usually maintained at 10-30°K above the salt temperature, which determined the vapor pressure. In the collection of the NaI fluorescence data, however, this differential was approximately 100°K, rendering knowledge of the true temperature in the fluorescence region somewhat uncertain. Salt temperatures were generally adjusted to provide 10-30 mTorr vapor pressure,[2] although values below this range could be used, especially with NaI. Data shown in Chapter III indicates a negligible variation in the NaI fluorescence efficiency curve over a salt temperature range of 535-605°C, which corresponds to a vapor pressure range of ~3-25 mTorr. Values above about ~30 mTorr could lead to problems, as will be discussed at various points in later chapters.

After exiting the cell the uv radiation passed through a suprasil window and struck a layer of sodium salicylate. This substance is a uv sensitizer whose fluoresence efficiency[3] has been shown to be flat over a wide range of uv wavelengths; a deterioration sometimes observed below 2000Å has been probably attributed to oil contamination in vacuum systems, and was not found when the sodium salicylate was kept scrupulously clean.[3] In these experiments, the sodium salicylate was not exposed to the vacuum, so presumably no oil contamination could occur. Furthermore, the flatness of the response is important here only in the measurement of uv intensity curves, for which purpose fresh coatings were applied. The fluorescent visible photons from this substance were detected by an RCA 1P21 photomultiplier, and their intensity taken as a direct measure of the uv intensity.

Meanwhile, back in the fluorescence cell, the excited metal atoms emitted fluorescent photons, the detection of which was the basis of this work. Various complicated arrangements of lenses and tubes were tried to optimize the collection of these sometimes elusive particles, but the final arrangement, which seemed to work best, was simply a 3/8 in. stainless steel tube, one end of which abutted against one of the quartz windows of the cell, and the other against either an interference filter (in air) or a pyrex window (in vacuum) immediately adjacent to an interference filter. Five interference filters were used at various times, depending on the species being detected. For the sodium D-lines fluorescence at 5890 and 5896Å, a single Baird Atomic type B-11 filter with peak transmission at 5892Å, of 42%, and a full width half maximum (FWHM) of 15Å served for simultaneous detection of both components.

This filter was found to have transmission of 39% at 5890Å and 32% at 5896Å. For the fluorescence of potassium at 7665Å ($4p^2P_{3/2}$), a filter of the same type with peak transmission of 53% at 7670Å and FWHM of 17Å was used and a similar filter with peak transmission of 50% at 6770Å and FWHM of 15Å was used in the brief LiI experiments. An Omega Optical filter with a 60% transmission peak at 7699Å and FWHM of 10Å was used to isolate the $K^*(4p^2P_{1/2})$ line at 7699Å. Finally a Corion Instrument Corporation filter with a 35% transmission peak at 4050Å and a FWHM of 60Å was employed for $K^*(5p^2P)$ lines at 4044 and 4047Å.

In connection with the use of the filters, a couple of questions arise. The first concerns the Doppler broadening of the atomic fluorescence lines. This was measured by Hanson,[4] and found to $\leqslant 0.15\ cm^{-1}$ for dissociation of NaI with wavelengths in the range 2144-2313Å. This broadening is clearly negligible in terms of the present measurements. The second question concerns the angular divergence of the fluorescent light which strikes the interference filter. The dimensions of the collimating tube are such as to allow a maximum angle of incidence of ~ 4° if the tube axis is precisely perpendicular to the filter surface. This corresponds to a maximum possible shift in the transmission peak of about minus 15Å for the $K^*(4p^2P)$ filters, and proportionally less for the others.[5] Even this maximum shift would not cause the 7699Å filter to transmit the 7665Å line, but these considerations do raise some questions, perhaps, concerning just what was seen with 5892Å filter. Early experiments using a lens placed in such a way as to theoretically

collimate the light incident on the filter, and experiments in which smaller (~1/8 in.) apertures were placed in the ends of the collimating tube showed the same behavior of the fluorescent signal as did the wide open tube experiments, which indicates that indeed, what was detected was what was expected.

It should be mentioned that attempts were made to detect the fluorescence signal through the Heath monochromator, which is the only excuse for the use of the term "wavelength analyzer" in Fig. II-1. This was done primarily with hope of being able to separate the sodium D-lines. However, it was not found to be feasible, due to the necessarily much smaller intensities, expecially at slit widths small enough to resolve the D-lines. It is believed that a noiseless photomultiplier would have rendered this experiment sucessful, but such an item, especially one with sensitivity at 5900Å, is far from reality. There are, of course, measures which can be taken to decrease photomultiplier noise, namely buying a new one and cooling it. However, at this point, the experimental road forked, and it was decided to take the path leading to KI and NaBr, for which the available instrumentation sufficed.

The radiation transmitted by whatever filter was being used fell upon an RCA 7265 photomultiplier, the output of which was the input signal to the PAR HR-8 lock-in amplifier. This lock-in was also used to make measurements of the uv, except in cases where simultaneous monitoring of the fluorescence and uv intensities was desired. In these cases, a second lock-in, a PAR JB-5, operated in the selective external reference mode on the reference output of the HR-8, was employed to measure the signal from the 1P21.

2. Signal Extraction and Signal-To-Noise Problems

The output signals from these lock-ins were fed to chart recorders, hence to a desk or table where a transparent straight edge and a pencil were used to draw the "best" straight lines through the recorder traces to obtain numbers proportional to the numbers of photons back at the signal source. With NaI, this "eyeball" averaging technique was generally quite easy, but with KI and NaBr, much less so.

The smaller signal-to-noise ratios in the latter cases derived from either or both of two causes. For example, in monitoring $K^*(4p^2P)$, the greatly increased black-body emission from the ovens, especially from the auxiliary window heaters, at 7665 or 7699Å, relative to 5890Å, increased the noise by orders of magnitude. With $K^*(5p^2P)$, on the other hand, smaller uv intensity at the operating wavelengths decreased the amount of signal. In the final case of NaBr, smaller uv intensity coupled with larger amounts of black-body radiation, which derived from the necessity of attaining higher temperatures in order to achieve the necessary salt pressure, combined to decrease the signal-to-noise ratio. In all three of these cases, the signal-to-noise ratios were approximately equal, and perhaps 50-100 times smaller than in the case of $Na^*(3p^2P)$ from NaI.

When the experiment was transferred to the vacuum chamber, one problem developed which caused considerable difficulty before it was finally discovered, somewhat by accident. This was the tendency of the two suprasil lenses to collect some sort of coating relatively opaque to the uv. This problem had not existed previously, and was discovered on observing that the uv intensity increased several-fold

when the second lens was removed from the path. The solution was simply to thoroughly clean these lenses before each experimental run.

It was then observed that, during the course of one run, there was a marked, even dramatic, deterioration in the signal which correlated with a loss of uv intensity greater than that due to the contamination of the lens surfaces. Again, this was a phenomenon not observed in the open-air configuration. According to Samson,[6] the transmission limit of synthetic fused quartz is ~1600Å at room temperature and exhibits a positive shift with increasing temperature of 1/4-1/3 Å/°K. So, on the suspicion that the cause of this deterioration was the intense heat of the ovens, especially as it affected the transmission characteristics of the nearer lens, a water-cooled copper shield was placed between the heated assembly and this lens. This did not prevent signal loss entirely, but it did control it sufficiently to allow experiments to proceed on the more difficult systems.

In general, it was found that the signal-to-noise ratio for a given system increased with temperature over a considerable range. However, there are several considerations which militate against higher temperatures. The higher the temperature, the greater the stresses on the entire heated assembly. Particularly notable in this regard was the tendency of the window heater wire to burn out. In the vacuum chamber experiments, higher temperature meant faster signal deterioration. This was definitely a noticeable effect with $K^*(4p^2P)$ from KI at 630°C (salt temperature) as compared to 580°C. With NaI and LiI, the tendency of the salt vapor to attack the quartz, rendering the windows ever less transparent was noted,

and this became more serious as the temperature was raised. In fact, this was the obstacle which was primarily responsible for the lack of success with LiI. A serious problem, from the point of view of interpreting the data, is the possibility that vapor pressures would be reached at which quenching of the atomic fluorescence by the parent salt molecules would become significant. This is discussed theoretically in Chapter IV and experimentally for the various systems in Chapter V.

B. The Hydrogen Arc

The single piece of equipment most crucial to this study, and at the same time most problematical, was the hydrogen arc lamp. This lamp was constructed early in the course of the work and was used to collect nearly all the data. It was modelled after the arc described in Finkelstein.[7] Samson[8] describes another similar lamp. The radiation from this source used in these experiments was part of the H_2 continuum, which results from the decay of a bound electronically excited state to a dissociative lower state.[7,9] Figure II-2 depicts the inner construction of the lamp together with the electronics required for dc operation.

In order to initiate operation of the lamp, the cathode is resistance heated, usually at 60-80 V, the arc power supply is turned up to about 260 V, and a tesla coil discharge is applied to the starting electrode, which is a ring of tantalum wire. At this stage the voltage divider chain determine the relative potentials on the various electrodes which help to guide the discharge. Further, a large molybdenum disc is screwed to the cathode end of the collimator to prevent the discharge from going around this piece. In operation, the cathode heater is off, the dc supply is at ~140-160 V, and the 4 ohm ballast is necessary to stabilize

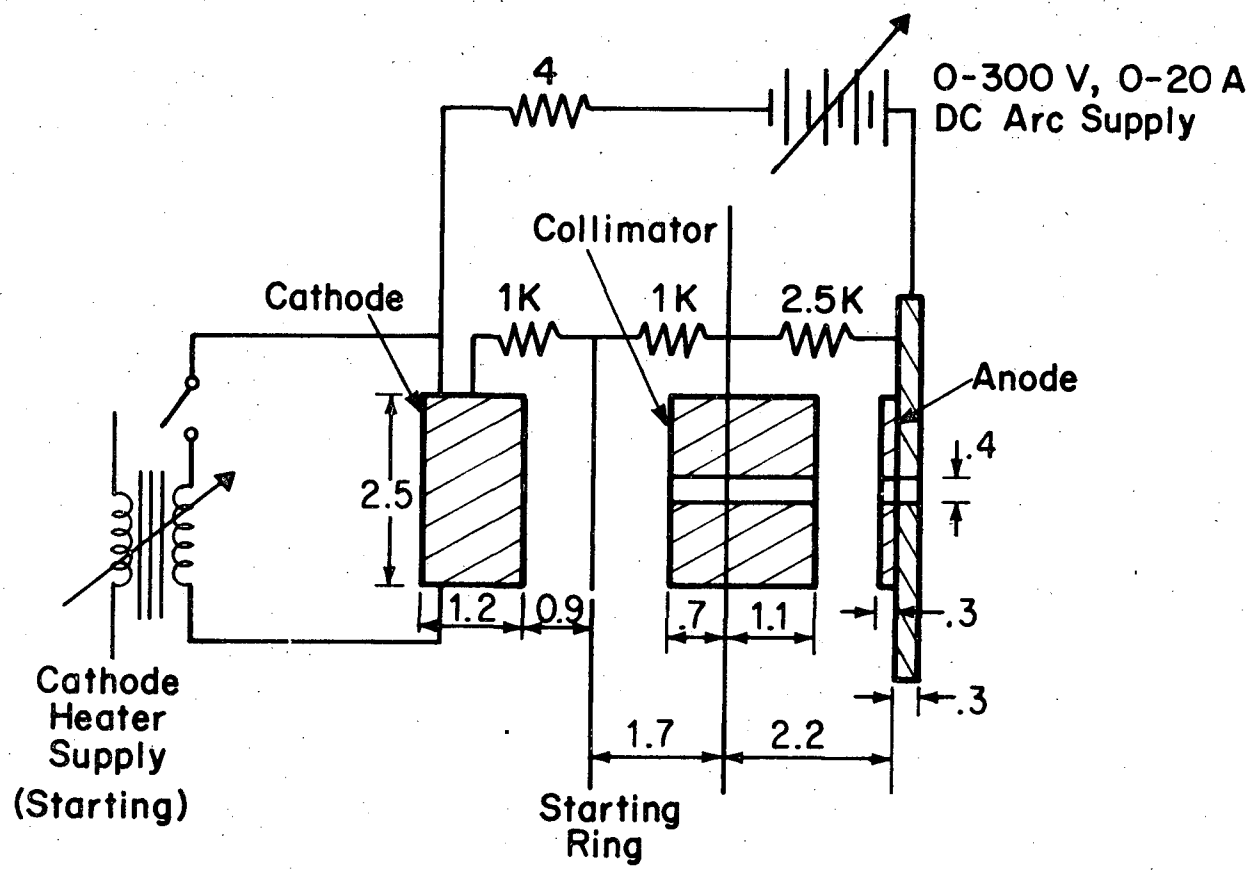

XBL 7012-7465

Fig. II-2. Schematic sectional view of the H_2 arc electrodes and associated electronics. Distances are in centimeters and resistances in ohms. The starting electrode is a ring of tantalum wire. The collimating electrode and anode are molybdenum.

the circuit, as the arc itself exhibits a characteristic "negative resistance".

The arc electrodes shown in Fig. II-2 are mounted inside a 5-1/8 in. i.d. brass cylinder, flanged on the cathode end for a large pyrex viewing window and on the anode end for a small 1/16 in. thick suprasil window and for attachment to either a support stand or the wall of the vacuum chamber. The cathode and starting ring are supported by 1/8 in. nickel rods which are held in metal-ceramic feed-throughs and which also provide electrical contact with the outside world. Likewise, the copper tubes which support the collimator and anode also supply cooling water and voltage to these pieces. The cooling water also circulates through a lengthy copper tube wound around the outside of the brass case.

The key to the operation of the arc is the cathode, which is formed of a piece of nickel screen (~50 mesh) ~1-1/2 in. wide and ~9 in. long, folded twice lengthwise around a narrow strip of tantalum sheet (~5 mil) for reinforcement, then folded several times crosswise, accordion-like. On this piece is deposited a solid solution of barium-strontium oxide. The procedure by which this is done needs to be followed quite carefully if proper operation is to ensue, as was emphasized by several unsuccessful attempts before the correct procedure was discovered in Ref. 10. First, an equimolar mixture of barium carbonate and strontium carbonate is triturated and mixed into a liquid consisting of 3 parts diethyl carbonate and 1 part diethyl oxalate and containing in solution ~0.15 g/ml nitrocellulose. It was found that 10 g of the carbonate mixture in 16 ml of the solution was sufficient to coat about 6 cathodes. This lacquer is painted onto the cathodes with a small brush or, just as

easily but more messily, with a finger. It is important to avoid deposition of large particles and to leave a uniform coating on the nickel screen. Following evaporation of most of the solvent, the cathode is put in place on the nickel rod supports inside the lamp, which is then pumped down through an auxiliary vacuum system using a small two-stage mechanical pump. The cathode is then "activated" by heating it gradually, over a period of about 1/2 hr, to ~1200°C, keeping it at this temperature for about 15 minutes, then cooling. This procedure converts the metal carbonate mixture to a solid solution of barium-strontium oxide, which has a low work function of 1.0 eV.[11] Initially, the temperature of the cathode during activation was monitored using an optical pyrometer, but later on an effective correlation with the pressure inside the lamp (due to the carbon dioxide being driven off) was developed which indicated when the temperature had reached approximately the desired maximum value.

After being properly activated, the cathode could usually be persuaded to produce an arc as described previously, with an H_2 pressure of about 3 Torr. This pressure was measured using a U-tube manometer containing Dow-Corning 704 oil (density 1.06 g/ml at room temperature). H_2 was flowed through the lamp constantly during operation and the pressure was controlled using a vernier needle valve. It was found to be advantageous to use pressures somewhat higher than 3 Torr for continuous operation, as greater intensities could be obtained with the same current through the arc. Figure II-3 shows the relationships of the several variables in lamp operation. The arc voltage was taken from the meter of the dc supply and corrected for the drop across the ballast resistance,

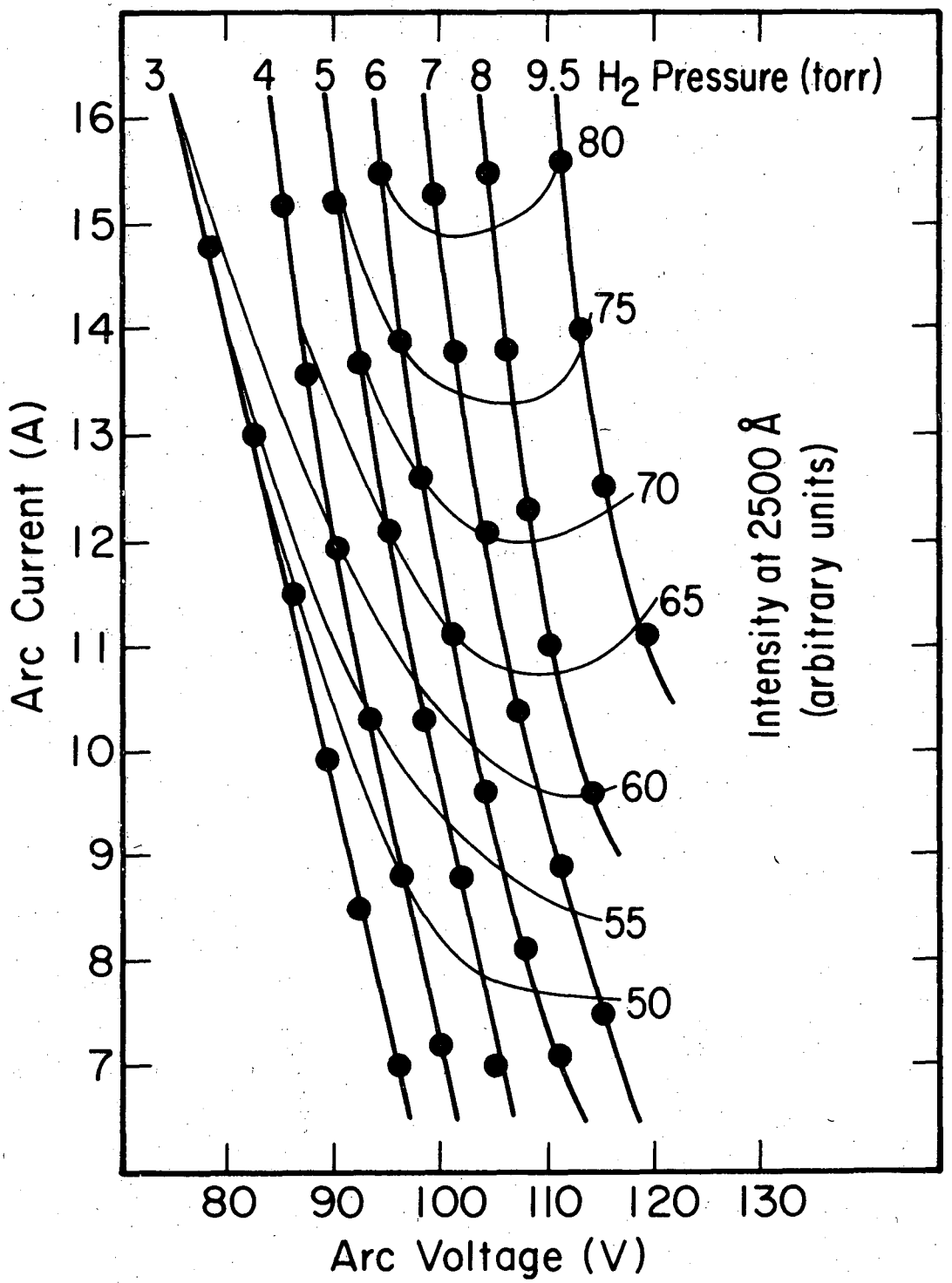

XBL 714-6643

Fig. II-3. Lamp performance curves. The data points and heavy curves show the current voltage characteristics for various H_2 pressures. The light curves show constant intensity contours measured at 2500Å.

and the current was measured using an ammeter across one of the 1 ohm resistors in the ballast series.

Construction of this lamp was undertaken because it was advertised as having a larger fraction of its output in the uv, and particularly as having more intensity in the region near the vacuum uv, compared to commercial xenon or xenon-mercury arcs, and because of Finkelstein's[7] claim that it was 50-100 times more intense than commercial H_2 arcs. No reason to contradict these claims was found. Figure II-4 shows a typical H_2 arc curve of intensity vs wavelength as measured through the Heath monochromator in air and similar curves for two 1 kW commercial arcs in the region 2000-2900Å. Data from the manufacturer[12] was used to plot the commercial arc curves. The comparison between the Xe-Hg arc and the H_2 arc was established, at least roughly, by comparing the fluorescence signal from NaI excited by the two different sources. This is why the ordinate is labelled "Usable Radiation Output". A comparison is somewhat difficult as the Xe-Hg arc emits into 4π steradians, while the H_2 arc has an aperture ratio of ~f/1. The fluorescence signal measurements indicated that the Xe-Hg arc output decreased more rapidly toward lower wavelengths than the curve in Fig. II-4 indicates.

The arc was also compared to an H_2 low-pressure glow discharge lamp, modelled after that of Hunter.[13] The glow discharge was roughly three times less intense overall, as might have been expected from its typical operating power of ~300 W, with relatively somewhat greater intensity below 2000Å. It was tried once in photodissociation of KI, and the signal was weaker than that produced with the arc, in the degree expected. In both these sources it was found, as has been reported[14]

0 0 0 0 3 9 0 7 2 3 6

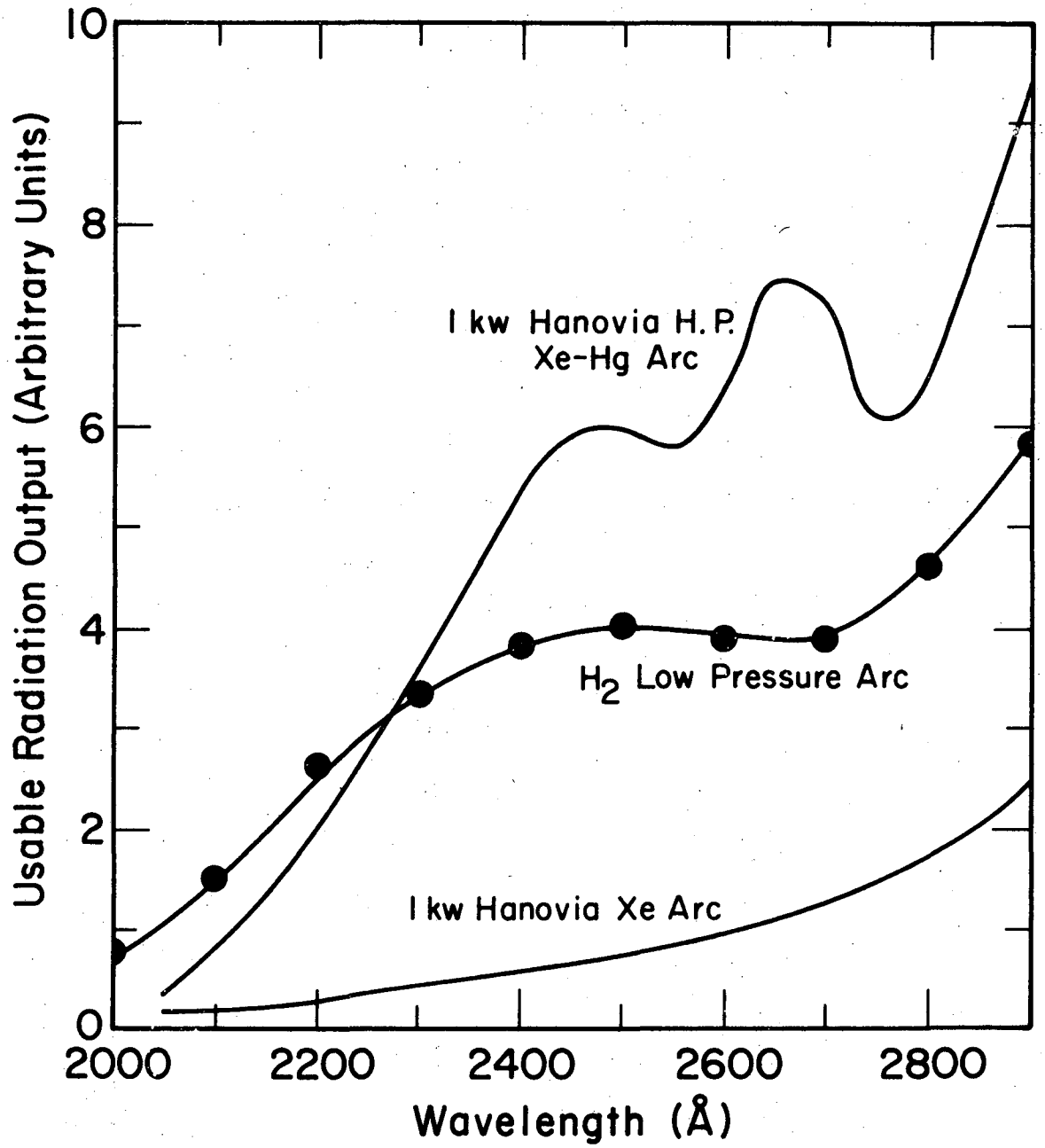

XBL 7012-7453

Fig. II-4. Comparison of intensities for H_2 arc and two commercial arcs. The relationship between the H_2 arc and the Xe-Hg arc was established roughly by comparison of fluorescence signal from photodissociation of NaI. The uv was collected by a 2 cm diameter lens, ~2 cm away from the source for the H_2 arc, and ~4 cm away from the source for the Xe-Hg arc. These arrangements seemed to maximize the fluorescence signal. The H_2 arc curve was measured through the Heath EU-700 monochromator with a bandpass of 48Å (FWHM).

for the glow discharge, that the use of D_2 as a discharge medium gave ~25% greater intensity in the region investigated (~2000-2500Å). D_2 was used experimentally in one case, the experiments on the quenching of $K^*(4p^2P)$ by I_2.

After the experiment was moved to the vacuum chamber and a new monochromator installed, new lamp curves were measured through the Jarrell-Ash monochromator in vacuum. Figure II-5 shows two of these curves, one taken just prior to measurement of the KI fluorescence efficiency curves, and the other just prior to measurement of the NaBr fluorescence efficiency curves. A relative maximum in the H_2 continuum below 2000Å is supposed to exist,[9] but it was observed only during the later measurements in vacuum. Probably this was due to the relocation of the paper mask, which had been removed during some of the intervening experiments. The presence or absence of the lower hump would not affect the results on KI, as the $K^*(4p^2P)$ fluorescence efficiency curves do not extend so low, and the $K^*(5p^2P)$ data was not energy analyzed. Fortunately, this peak in the vacuum uv was found prior to the NaBr experiments, in which the added intensity was certainly welcome. That this was indeed uv was proved by venting the vacuum chamber and watching it disappear.

In using the H_2 arc, it was found that the lifetime of the cathodes was limited mostly by the damage incurred during and immediately after starting. Usually the arc would jump about on the cathode for several seconds before it settled down to stable operation, and during this period bits and pieces of the cathode would go flying off. Examination of spent cathodes showed the central portion, i.e., that near the optical axis of the lamp, to be eaten away almost entirely. Death

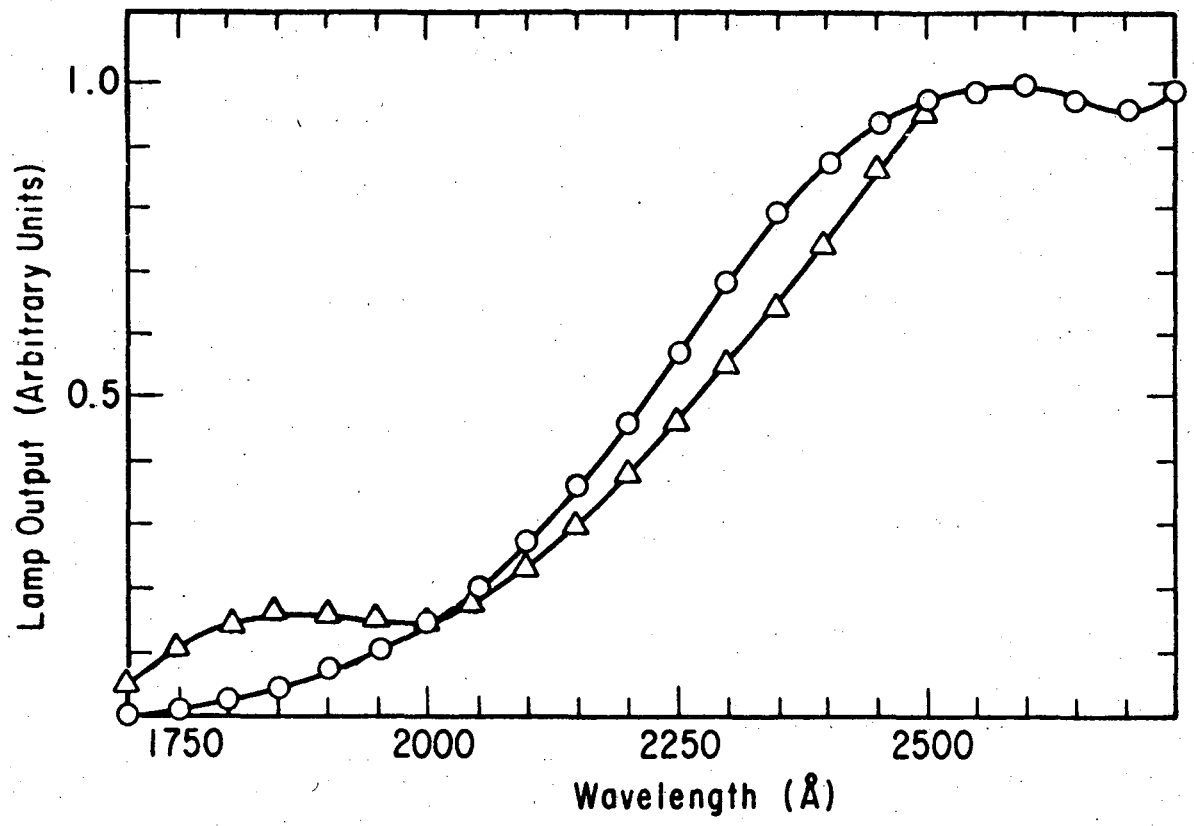

XBL 737-6563

Fig. II-5. Relative intensity vs nominal wavelength for the H_2 arc as measured through one Jarrell-Ash 82-410 monochromator with 60 Å (FWHM) bandpass for two configurations of the black paper mask which was used to eliminate multiple-path leakage. The circles represent the data points for the curve used to normalize the KI fluorescence, and the triangles represent the data points for the curve used to normalize the NaBr fluorescence.

0 0 0 0 6 9 4 7 2 3 7

usually resulted from burning out the remaining thin portion during an attempt at starting the lamp.

Once started, the arc would operate in quite stable fashion. Normal operation appeared to cause little cathode wear and there is no reason to believe that the lamp would not operate in the continuous mode for an essentially unlimited time. There would be occasional jumps in intensity of a few percent, presumably associated with a spontaneous self-reconfiguration of the discharge. There would also be rare negative spikes in the output. Observation of the lamp through the viewing window showed green flashes in the rear portion when these occurred, indicating a temporary arc to some portion of the copper--probably between the anode tubing and the lamp housing. These aberrations were nearly always self-correcting and were rare, but became more frequent when the lamp was operated at very high currents (~17A). Such currents were sometimes employed, although they tended to cause cathode wear as well as occasional instability problems, since signal intensity was extremely dear in some experiments.

C. General Experimental Considerations

In studying one of these alkali halide systems photodissociatively, the initial step was to load a charge of the salt into the fluorescence cell and degas it by heating it to 200-300°C for ~15 hrs under vacuum. This was particularly important with NaI, which exhibits a considerable affinity for atmospheric water. Following this initial degassing, the sample was heated to a temperature corresponding to a vapor pressure appropriate to the experiment. During this heating, the final traces of water would be driven off.

Upon exposure to uv radiation in the appropriate wavelength range, the fluorescence signal from the metal atom could be detected and studied as a function of wavelength for the pure salt or as a function of gas pressure and wavelength for some added foreign gas. Table I shows the general conditions under which these studies were conducted for the various systems.

In obtaining a fluorescence efficiency curve, the relative intensity of fluorescence was measured as a function of the nominal uv wavelength at several points across the range in which photodissociation to the desired product occurred. Then the value for each point was divided by the relative value of the uv intensity at that nominal wavelength to normalize the entire fluorescence efficiency curve to unit uv intensity. This yielded a curve which was still a function of the monochromator bandwidth, and subsequent calculations were done (see Chapter III) to relate this curve to the theoretical fluorescence curve for an infinitessimal uv bandwidth.

With NaI, fluorescence efficiency curves were measured under a wide variety of conditions. Except at the lowest temperatures and smallest bandwidths, it was possible to collect the data by setting the (Heath) monochromator at a slow automatic scan rate (1 or 1/2 Å/sec) and correlate the chart paper abscissa with wavelength by referencing the initial and final values. In collecting these data, no time-normalization problems were encountered. The other systems were studied under a single set of conditions, as data collection was much more difficult. In these cases, the (Jarrell-Ash) monochromator

Table I. Experimental conditions.

System	Subject	Temp. Range (°K)	Wavelength (Å)	Bandwidth (Å)
NaI→(Na*3p^{2}P)	Fluorescence Efficiency	870-1000	1900-2000	12-48
	Quenching	860-920 (870,960)*	2150-2400 (2125)*	48 (36,28)*
NaBr→Na*(3p^{2}P)	Fluorescence Efficiency	900	1700-2300	60
	Quenching	900	1875-2125	60
KI→K*(4p^{2}P)	Fluorescence Efficiency	870	2100-2800	60
	Quenching	870,890 (920)	2300-2525	60
KI→K*(5p^{2}P)	Fluorescence Efficiency (rough)	890	1750-2100	60
	Quenching	890	1925 Thermal (1925,1950, 1975 non-thermal)	60

*Values in parentheses refer to conditions which were used on single occasions, usually for a special purpose.

setting was varied manually and left at each value long enough to establish a level, usually three to five minutes. For the Na*($3p^2P$) from NaBr and K*($4p^2P$) from KI, there were real time-normalization problems deriving from the deterioration of the signal characteristic of the vacuum-chamber experiments. However, the slow, monotonic nature of this deterioration made it fairly straightforward to handle by using one monochromator setting as a reference and returning to it regularly, usually every third point. The fluorescence curve for K*($5p^2P$) from KI was examined only briefly as the presence of interfering processes (see Chapter V) rendered the results at lower wavelengths ambiguous.

In taking measurements on quenching by a foreign gas, a value of the unquenched fluorescence was obtained, then the gas was added at a known pressure and the value of the quenched fluorescence obtained, then the gas was pumped out at the unquenched level again established. If the foreign gas was added alone, its pressure was measured directly on the quartz spiral manometer. Since, even at the lowest pressures of quenching gases studied, the mean free path within the gas was much smaller than the i.d. of the tubing connecting the vacuum manifold to the fluorescence cell, the pressure measured in the manifold on the quartz spiral manometer could be equated to the pressure inside the cell (see Ref. 15 for a discussion of this problem). In a number of experiments, however, a known pressure of a foreign gas was premixed with several hundred Torr of argon and aliquots of this mixture were drawn off into the fluorescence cell, so that quenching occurred under thermal conditions. It was, of course, established that argon itself

did not produce measurable quenching at the pressures employed. The pressure of the foreign gas was then taken as its calculated partial pressure in the mixed sample.

The pre-mixing was done in a 5 ℓ flask equipped with a magnetically-driven stirring blade. It was necessary to check the thoroughness of the mixing procedure in order to be confident of the calculated gas pressures. This was done in two ways. First, visual checks were made using iodine and bromine vapors. These indicated that when argon was introduced into the flask over a low pressure (~1/2 - 10 Torr) of the vapor, the vapor was compressed toward the bottom of the flask, more noticeably for higher pressures, and that full mixing occurred quite readily when the gases were stirred. Second, absorption of the uv at 2100Å by SO_2 at calculated pressures in a mix was compared with absorption by pure SO_2 at directly measured pressures. The results of this check are shown in Table II. Since there are clearly departures from the Beer-Lambert law, it was important to compare points taken at nearly equal pressures. For such points, the ratio of the pressure of SO_2 to the quantity $[\ln(I/I_o)]$ should be the same. This requirement is well satisfied by the data of Table II.

When the foreign gas-argon mixture was added to the fluorescence cell at a few hundred Torr, the fluorescence signal would be depressed nearly to zero, and would then rise slowly and eventually establish a uniform level. This presumably was due to compression of the salt vapor into the lower portion of the cell by the initial high pressure wave, as it occurred almost immediately even though the gas mixture was added over a period of about 1-2 minutes, and then the subsequent

Table II. Mixing bulb check results.

Pure SO_2			3.5 Torr SO_2 in 650 Torr Argon		
P_{SO_2} (Torr)	$-\ln I/I_o$	$\lvert P/\ln I/I_o \rvert$	P_{SO_2} (Torr)	$-\ln I/I_o$	$\lvert P/\ln I/I_o \rvert$
3.45	0.82±0.03*	4.20±0.15	3.34	0.78±0.03	4.28±0.15
2.35	0.678±0.03	3.47±0.14	2.25	0.655±0.025	3.44±0.14
1.15	0.415±0.02	2.77±0.13	1.11	0.40±0.02	2.78±0.13

*Tolerances indicate the resolution of the measurement, which is ~1/2 division on 100 division/10 in. chart paper.

re-equilibration of the spatial distribution. Usually 3-5 minutes would pass before a measurement could begin. This phenomenon was also observed with comparable pressures of pure argon. As will be discussed in Chapter V, quenching experiments with CH_4, CD_4, C_2H_4, and CH_3OH, pure and in argon-gas mixtures, gave results which agreed within experimental error.

An additional complication arose when the foreign gas itself absorbed uv radiation at the wavelength being used. If this absorption was not too strong, and attempt was made to correct the data for it. To do this, the uv intensity was monitored continuously during and between quenching measurements. Values of $(I/I_o)_{uv}$ were obtained, and the I_o/I values for the fluorescence were divided by $(I/I_o)^x_{uv}$, where $x \approx 0.5$, corresponding to the fact that the zone from which fluorescence was detected was approximately halfway through the cell. This problem, of course, lessened the reliability of the results, and measurements were not attempted for cases in which the absorption of the uv accounted for about half or more of the observed drop in fluorescence intensity.

In the course of this work, many gases were tried as prospective quenchers, some of which proved unusable for various reasons, some of which quenched so little as to seem uninteresting, and some of which behaved in such a manner as to merit study. Three checks were employed on the behavior of gases in the fluorescence cell to try to ascertain that nothing untoward occurred, particularly for those gases which were studied at some length. The first was that the unquenched fluorescence level should return to its original value when the gas was pumped out of the cell. There were certain tolerances in this, of course, corresponding to normal fluctuations in the signal

level. Only one gas (CCl_4) failed this test, and it was reckoned that it reacted with the salt. The second check was that the pressure should remain constant while the gas was in the cell. This could be checked in one of two ways: the pressure could be monitored continuously, or the cell could be isolated, the manifold pumped out, and the pressure in the cell-manifold when the cell was opened could be compared to the value expected from the known volumes of the two parts. The third check was mass-spectrometric analysis. Spectra of gases which had been exposed in the cell were compared with those of gases directly from the reagent supply. Data from the spectra will be presented when the gases are considered in Chapter V.

Gases used were commercial reagent grade or better, where available, and were used directly from the cylinder. Liquid samples, likewise commercial reagent grade except for H_2O, which was obtained from the laboratory distilled water supply, were degassed by repeated freezing and thawing under vacuum before use. Deuterated compounds were 95% or better isotopic purity. In these experiments, where the quenching cross sections are large, small amounts of impurities would not be expected to introduce significant uncertainty into the results. Nevertheless, for most gases which were studied at some length, the mass spectra served to give a good indication as to the purity, both in the presence or absence of impurity peaks, and in comparison to standard spectra.

Table III presents a summary of the behavior and the kinds of results obtained for all the gases studied. Problems or special considerations for given gases will be discussed at the necessary length when the data are presented.

Table III. Summary of results.

System/Gas	Checks (i,p,m)*	Results**	Comments
$NaI \rightarrow Na^*(3p^2P)$			
I_2	i,~~m~~ (p res)	Qq vs g	
C_2H_4	i,p,m	Qq vs g	
CO_2	i,p,~~m~~	Qq vs g	
C_6H_6	i,m	Qq vs g	Absorbs uv/adsorbs slightly on glass-p inconclusive
SO_2	i,p,m	Qq vs g	Absorbs uv
CF_3Cl	i,p,m	Qq vs g	Signal drops slowly at higher pressures--NaCl?
CH_3CN	i,p,m	Qq vs g	Isomerization?
CH_3OH	i,m	Qq vs g and kq thermal	Adsorbs on glass, p inconclusive
H_2	i,p,~~m~~	kq thermal	Enhancement observed
D_2	i,p,~~m~~	kq thermal	Enhancement observed
H_2O	i,~~m~~ (p res)	kq thermal--very small enhancement T-dependent?	Adsorbs on glass
D_2O	,~~m~~ (p res)	kq unobservable irregular enhancement	Adsorbs on glass

Table III. Continued.

System/Gas	Checks	Results	Comments
NaI→Na*($3p^2P$)			
CH_4		kq very small	
C_2H_6		kq very small	
CF_3H	i,p,No m	Enhances to 50 Torr	
CS_2			Absorbs too much uv
SF_6	Fails m	Apparent kq very large	
Propene	Fails p		Decomposes?
2-butene	Fails p		Decomposes?
NO_2		Signal drops-rises slowly	Decomposes?
BF_3		Signal drops-rises slowly	Decomposes?
CCl_4	Fails i		Reacts with salt?
NaBr→Na*($3p^2P$)			
Br_2	i,~~m~~	Qq vs g	Pressure drops slowly, p inconclusive-reacts with stopcock grease?

0 0 0 0 5 9 0 1 2 6 2

Table III. Continued.

System/Gas	Checks	Results	Comments
$KI \rightarrow K^*(4p^2P)$			
C_2H_4	i,p,~~n~~	Qq vs g and kq thermal	
CF_3Cl	i,p,~~n~~	Qq vs g	Signal drops slowly at higher pressures, cannot be thermal
SO_2	i,p,~~n~~	Qq vs g and kq thermal	
CH_3OH	i,~~n~~, ~~p~~	kq thermal	
H_2	i,p,~~n~~	kq thermal	
D_2	i,p,~~n~~	kq thermal	
H_2O	i,~~n~~ (p res)	kq thermal--very small	Adsorbs on glass
CF_4	i,p,~~n~~	kq very small	
CH_4	i,p,~~n~~	kq very small	
CF_3H		windows become coated	HF? KF?
I_2	i,~~n~~, (p res)	kq non-thermal	

Table III. Continued.

System/Gas	Checks	Results	Comments
$KI \rightarrow K^*(5p^2P)$			
CF_3Cl	i,~~m~~,~~p~~	kq thermal	No signal drop
CF_4	i,~~m~~,~~p~~	kq thermal	
CH_3OH	i,m,~~p~~	kq thermal	
N_2	i,~~m~~,~~p~~	kq thermal	
H_2O	i,~~m~~,(p res)	kq approx thermal	Adsorbs on glass, cannot do thermal
D_2O	i,m,(p res)	kq approx thermal	Adsorbs on glass, cannot do thermal
HCl	i,~~m~~	kq non-thermal	Pressure drops slowly, p inconclusive reacts with metal tubing?
DCl	i,~~m~~	kq non-thermal	Pressure drops slowly, p inconclusive reacts with metal tubing?
C_2H_4	i,p,~~m~~	kq thermal and non-thermal	
C_2D_4	i,~~p~~,~~m~~	kq thermal	
H_2	i,p,~~m~~	kq thermal	

Table III. Continued.

System/Gas	Checks	Results	Comments
$KI \rightarrow K^*(5p^2P)$			
D_2	i,p,~~m~~	kq thermal	
CH_4	i,p,m	kq thermal and non-thermal	
CD_4	i,p,m	kq thermal and non-thermal	
C_2H_6	i,m,~~p~~	kq thermal	
C_2D_6	i,~~m~~,~~p~~	kq thermal	
I_2	i,~~m~~ (p res)	kq non-thermal	

*i,p and m refer to the checks on the behavior of gases in the fluorescence cell: i the unquenched fluorescence intensity check, p the pressure check, and m the mass spectral check. Entry of one of these symbols indicates that the check was passed.
(p res) indicates the pressure was maintained in equilibrium with a reservoir, so no check was possible.
~~p~~ denotes a case in which no pressure check was made because all measurements were done with argon mixtures.
~~m~~ denotes a case in which the mass spectral check was considered unnecessary, because of the gas itself or because a check had been made for the gas and with another system.
**Qq denotes the quenching cross section, g the relative velocity. If "Qq vs g" is entered, this indicates full energy analysis of the data as described in Chapter IV; kq denotes the quenching rate constant, and its entry indicates that it was measured but full energy analysis was not done.

REFERENCES

1. Joshua J. Mitteldorf and Donald O. Landon, Appl. Opt. 7, 1431 (1968) and references therein.
2. John L. Margrave, ed., The Characterization of High Temperature Vapors (John Wiley and Sons, New York, 1967), p. 503.
3. J. A. R. Samson, Techniques of Vacuum Ultraviolet Spectroscopy (John Wiley and Sons, New York, 1966), p. 212.
4. Howard G. Hanson, J. Chem. Phys. 47, 4773 (1967).
5. Oriel Optics Corp., Stamford, Connecticut, Catalog (1970), p. C6.
6. J. A. R. Samson, Techniques of Vacuum Ultraviolet Spectroscopy (John Wiley and Sons, New York, 1966), p. 181, discusses the effect of temperature on transmission.
7. N. A. Finkelstein, Rev. Sci. Instr. 21, 509 (1950).
8. J. A. R. Samson, Techniques of Vacuum Ultraviolet Spectroscopy (John Wiley and Sons, New York, 1966), p. 145.
9. J. A. R. Samson, op. cit., p. 95 for a discussion of the H_2 continuum.
10. G. Herrmann and S. Wagner, The Oxide Coated Cathode (Chapman and Hall, London, 1951), pp. 20, 38, 58.
11. J. Hasted, Physics of Atomic Collisions (Butterworths, London, 1964), p. 75.
12. Hanovia Lamp Division, Newark, N. J., Data File: Hanovia Compact Arc Lamps.
13. W. R. Hunter, Proceedings of the Xth Colloquium Spectroscopicum Internationale, Ellis R. Lippincott and Marvin Margoshes, eds. (Spartan Books, Washington, D. C., 1962), p. 247.

14. A. S. Coolidge, Phys. Rev. 65, 236 (1944).

15. J. A. Bellisio and P. Davidovits, J. Chem. Phys. 53, 3474 (1970).

III. POTENTIAL CURVES AND PHOTODISSOCIATION

A. Introduction

In these experiments, photodissociation of an alkali halide molecule, MX, occurs when a molecular transition from the ground electronic state to an excited repulsive electronic state is induced by the absorption of a uv photon. The atoms, one or both of which may be excited, then separate as the system "rolls down" the potential curve of the upper state. There is experimental evidence which indicates that the photodissociation of NaI to produce Na*($3p^2P$) and ground state I proceeds by a direct transition to the repulsive state involved in the dissociation. By photon counting, the natural radiative lifetime of the Na*($3p^2P$) atoms has been observed following short uv pulses.[1,2] Reference 1 also reports no indications of delay in the fluorescence of Na*($3p^2P$) from NaBr, again leading to the probable conclusion that the mechanism of photodissociation is a direct one. This is assumed to be the case for the other systems studied as well. It is further assumed that the upper potential is purely repulsive, although a small well[3,4] of ~0.2 eV has been considered in the upper curves of several alkali halides, and is not ruled out by the results of this work. This well, however, is less probable for iodides than for other halides.[3]

Since the metal atom produced by photodissociation in these experiments is in an excited state, whose steady-state population can be monitored by observing the emission from it, the intensity of this emission can be taken as a measure of the relative efficiency of the photodissociation process. That is, the fluorescence efficiency curve

provides a measure of the relative absorption probability vs energy for the molecular electronic transition. This in turn provides a handle on the upper potential curve, if an acceptable representation of the ground state potential curve is available. The numerical analysis of this problem and the calculations for NaI are primarily due to Shen-Maw Lin, and are detailed in his thesis,[5] as well as being described in Ref. 6. They are presented here for the sake of completeness, along with the results on NaBr and KI.

Knowledge of the upper potential makes possible the calculation of the speed distribution of the photodissociatively produced atoms. The latter part of this chapter develops the analytic expression for this distribution for the case of a single vibrational level at a single frequency neglecting and including the contribution of the molecular rotational energy, and describes the additional numerical steps involved in obtaining the full experimental speed distributions.

B. Photodissociation Theory and Numerical Analysis

Consider the hypothetical situation of a sample of MX molecules, all in vibrational state v, of thickness Δx, and number density N_v. If uv radiation at frequency ν_o, of intensity I_o (energy/cm^2 sec), falls on this sample, the intensity absorbed, I_a, is given by[7]

$$I_a = I_o N_v \Delta x h \nu_o B_{\varepsilon,v} \quad , \tag{1}$$

where h is Planck's constant and $B_{\varepsilon,v}$ is the Einstein absorption coefficient for the transition connecting the eigenstate v of the ground electronic state with the eigenstate ε of the repulsive electronic state, having energy ε above the dissociation limit. In

terms of ω_e, the vibrational frequency of MX, D_e, the well-depth of the ground electronic potential, and E*, the excitation energy of the excited M* atom

$$\varepsilon = h\nu_o + \hbar\omega_e(v + 1/2) - D_e - E^* \quad . \tag{2}$$

The relationship of the various energy quantities is indicated in Fig. III-1 for a hypothetical case. $B_{\varepsilon,v}$ is given in the Franck-Condon approximation[7,8] by

$$B_{\varepsilon,v} = (8\pi^3/3\hbar c)\ \bar{\mu}_e^2(r)\ |\langle\varepsilon|v\rangle|^2 \quad , \tag{3}$$

where $\bar{\mu}_e^2(r)$ is the average value of the electronic transition moment and $\langle\varepsilon|v\rangle$ represents the overlap integral between the wave functions of the states v and ε.[†]

Combination of Eqs. (1) and (3) gives an expression in terms of molecular parameters for I_a in units of energy/cm^2 sec, while the number of excited metal atoms produced, which is what is detected in these experiments, is proportional to I_a', in units of photons/cm^2 sec. I_a' is just $I_a/h\nu_o$, which eliminates the factor of ν_o, which appears on the right side of Eq. (1), from the expression for the experimental fluorescence intensity. However, the reduced fluorescence efficiency, that is, the fluorescence efficiency normalized to unit incident uv intensity (in units of photons/cm^2 sec), is proportional to I_a'/I_o', where I_o' is just $I_o/h\nu_o$, which reintroduces the factor of ν_o. Recognizing this, and collecting constant terms, the reduced metal atom fluorescence intensity for a given vibrational level,

---

[†] In calculating transition probabilities for these molecules, the effect of rotation was ignored by setting J=0 for both the upper and lower states.[5]

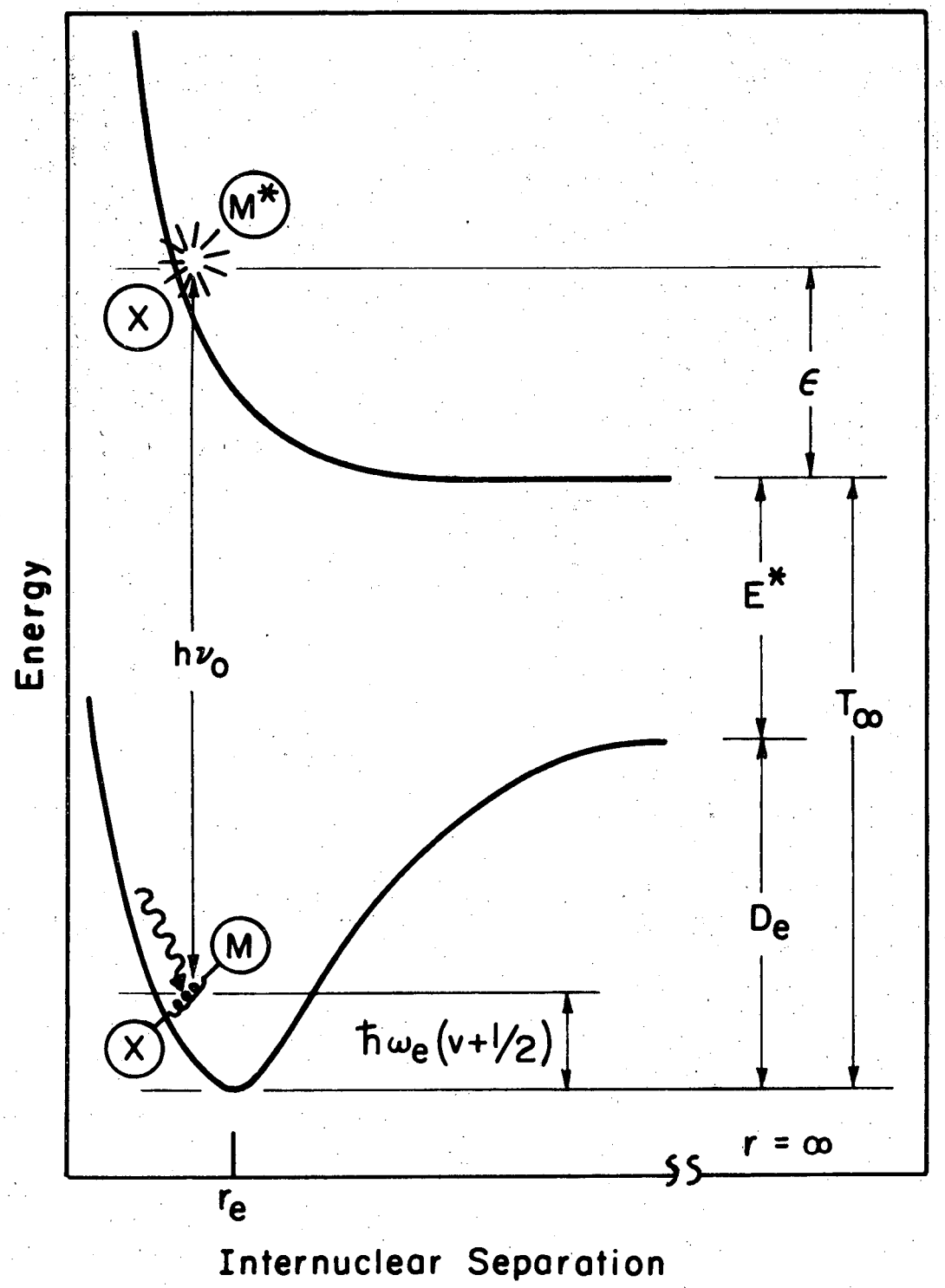

Fig. III-1. Schematic of the photodissociation process, showing the various energy quantities involved.

$I_v(\nu_o)$, can be expressed as a function of frequency as

$$I_v(\nu_o) = CN_v\nu_o|\langle\varepsilon|v\rangle|^2 \quad , \tag{4}$$

where it should be noted that ε is also a function of ν_o.

This equation relates the fluorescence efficiency curve for a given vibrational level to the two potential curves for a particular transition. Given computer time, any of the three can be calculated from the other two, although there seems to be no rigorous proof that the relationship is unique. In the real case, in which more than one vibrational level is populated, Eq. (4) is easily generalized to

$$I(\nu_o) = \sum_{v=0}^{\infty} I_v(\nu_o) \quad , \tag{4a}$$

where now ε also depends on v, as per Eq. (2).

A computer program[5] was written which, given the two potential curves, found the wave functions, did the integrals, and carried out the summation indicated in Eq. (4a). The solution of the Schroedinger equation for the ground state was done by the method of Zare and Cashion,[9] as applied in the program of Zare[9b] for intensity calculations for two bound states. This latter program was modified for the present calculation. The continuum wave functions were obtained from a one-dimensional, box (energy) normalized solution to the radial Schroedinger equation for a given trail potential.[5] In this method, the wave functions were restricted to a maximum internuclear separation of $12a_o$, and the continuous infinity of solutions was replaced by a discrete infinity. Tests were made to insure that the maximum separation was sufficient so that changing it did not affect the results. After

calculating the theoretical fluorescence efficiency curve of Eq. (4a), the program then convoluted it with the bandpass function of the monochromator, $M(\lambda,\lambda_o)$ to obtain the total intensity, I_T, for comparison with experimental data. Converting to the wavelength (λ) domain,[6]

$$I_T(\lambda) = \int_\lambda I(c/\lambda_o)\, M(\lambda,\lambda_o)(c/\lambda_o^2)d\lambda \qquad (5)$$

As discussed in Ref. 5, previous attempts to extract repulsive potential curves from molecular absorption spectra[3,10,11] or atomic fluorescence data[4] have used the so called delta-function approximation, in which the overlap integral is replaced by the value of the bound state wave function at the internuclear separation corresponding to the frequency being considered. This approximation, as previously used, gave considerably different results for the repulsive curve than are given by the full Franck-Condon factor calculation as employed here. However, recent studies by other workers[12,13] have indicated that at least a part of the problem with previous delta-function approximation calculations was improper energy normalization for the upper state.

It is conceivable that the atomic fluorescence produced in these photodissociation experiments is polarized to some degree. This could give rise to problems in interpreting the data, as the polarization would be accompanied by spatial anisotropy[14] which could then vary as a function of uv wavelength, and which would be expected to vary as a foreign gas was added, possibly giving rise to spurious differences in the detected intensity.

On the atomic level, polarization means a non-statistical population of m_J levels, which can occur for J = 3/2, but not for J = 1/2. There is apparently no experimental evidence of this in photodissociation of alkali halides, and, if it did occur, the cross-sections for its collisional destruction by the parent salt vapor molecules would probably be very large indeed, as the cross section for depolarization of the J = 3/2 level of $Na^*(3p^2P)$ by helium, with which the interaction should be very weak, has been found to be 95 Å.[2,15] However, the possibility that it might be produced will be considered a bit further.

Defining the atomic coordinate system in terms of the instantaneous M-X axis at the time of transition to the upper state seems reasonable, for at least a short time after dissociation. Then, if the m_J levels are not statistically populated, the atomic fluorescence would be polarized and anisotropic with respect to this axis. This could lead to anisotropy in the angular distribution of photons in the lab if the axes of dissociated molecules are not isotropically distributed, which condition would produce a spatial anistropy of photodissociation products. This problem, as discussed by Zare and Herschbach,[16] involves the question of whether the molecular transition is $\parallel(\Sigma\rightarrow\Sigma)$ or $\perp(\Sigma\rightarrow\Pi)$. In these experiments one might reasonably expect some admixture of both types of transitions, which would produce an only slightly anistropic product distribution for completely polarized uv. The uv through the monochromator would be expected to be only slightly polarized, as all experiments were done near the blaze settings.[17] For the Jarrell-Ash monochromator, the ratio of the two polarized components ($\parallel$ and $\perp$ to the grating grooves) was found to ~1/2 at 4860Å, and so would be expected to

be quite near 1 at settings within 800Å of the 1900Å blaze setting.

All these considerations lead to the expectation that polarization effects would not be important in these or similar experiments. In fact, experimental attempts[18] to observe anisotropy in the angular distribution of NaI photodissociation products using polarized uv have led to the conclusion that no such anisotropy existed.

To be convinced of the lack of importance of polarization effects in the present case, one need only consider that addition of high pressures of argon, which should depolarize quite efficiently, produced no permanent change in the intensity of fluorescence from either $Na^*(3p\,^2P)$ or $K^*(5p\,^2P)$. In these cases, as J = 1/2 and J = 3/2 were observed simultaneously, as opposed to the $K^*(4p\,^2P)$ case, any overall intensity change would have been readily detectable.

C. Potential Curves

The lower state potential curves for the systems studied here were based on the Rittner polarizable ion model,[19] which has been shown[20] to account well for the dipole moments and dipole derivatives of several alkali halides. This model was modified slightly by the inclusion of a scaling factor, β, to fit the potential minimum to the known dissociation energies to ions.[21] The expression for the interatomic potential near the minimum is then

$$V(r) = \beta[Ae^{-r/\rho} - e^2/r - e^2(\alpha_+ + \alpha_-)/2r^4 - C_6/r^6 - 2e^2\alpha_+\alpha_-/r^7] \quad (6)$$

where α_+ and α_- are the polarizabilities of the alkali and halide ions (values from Ref. 22). C_6, the dispersion constant, was calculated from the Slater-Kirkwood approximation.[23] The constants A and ρ were evaluated by demanding $(dV/dr)_{r=r_e} = 0$ and by fitting $(d^2V/dr^2)_{r=r_e}$

to the experimental (harmonic) force constant. Values of ω_e and r_e were taken from Ref. 24, and values of D_o for the process $MX \rightarrow M^+ + X^-$ were taken from Ref. 21 and corrected by $\omega_e/2$ to get D_e for evaluation of β. Table I lists the values of the input and output parameters of this model for the molecules under consideration, along with values of $\omega_e x_e$[24] and $\omega_e y_e$[25] which were used in calculating trial energy levels for the computer program. Although the Rittner potential gives the dissociation energy to ions, it is valid in the region near the minimum for a system which is considered to dissociate to neutrals. Its applicability is indicated by the fact that the vibrational levels found by solving the Schroedinger equation for this potential agreed to within 1% with the spectroscopic data.

The upper state potential curves were found by trial and error, being adjusted in a given case until the program results, corresponding to Eq. (5), fit the experimental fluorescence efficiency curve satisfactorily. It should be kept in mind, in considering these curves, that there may be several molecular states which can dissociate to the particular atomic states in question, and that the curves which are found would then be regarded as "average" curves for all such states.

D. Experiments and Results

1. Sodium Iodide

As mentioned in Chapter II, fluorescence efficiency curves for NaI were measured under a wide variety of conditions. Experimental points for three sets of conditions are shown in Fig. III-2, along with the "best-fit" calculated curve for one set, corresponding to Eq. (5), and including two distinct processes, as discussed below. It should be

Table I. Parameters for alkali halides.

Parameter/Salt	NaI	NaBr	KI
Input			
D_e(eV)	005.095	005.3955	004.5211
ω_e(cm^{-1})	258.0	298.5	186.5
r_e(Å)	002.7115	002.5020	003.0478
α_+($Å^3$)	000.15	000.15	001.20(0.9)*
α_-($Å^3$)	007.0	004.5	007.0
C_6($eVÅ^6$)	015.41	011.98	099.96(78.03)
Output			
A(eV)	1629.7	1672.63	2753.4(2728.8)
ρ(Å)	0000.3813	0000.3511	0000.3896(0.3876)
β	0001.022	0001.012	0001.008(1.011)
Extra			
$\omega_e x_e$(cm^{-1})	0000.96	1.16	0.57
$\omega_e y_e$(cm^{-1})	0000.001	0.001	0.001

Reference 22 gives various values for the polarizabilities of Na and K*. Those chosen seem to be the most popular. The differences in the potential curves calculated for KI using values of 1.20 and 0.90 (values in parentheses) were negligible for the purposes of this study (<25 cm^{-1} over the important range of r). The value of 1.20 gave a slightly better fit to D_e. α_+ for Na*, being an order of magnitude smaller, would affect the potential curves even less.

0 0 0 0 3 9 0 7 2 7 0

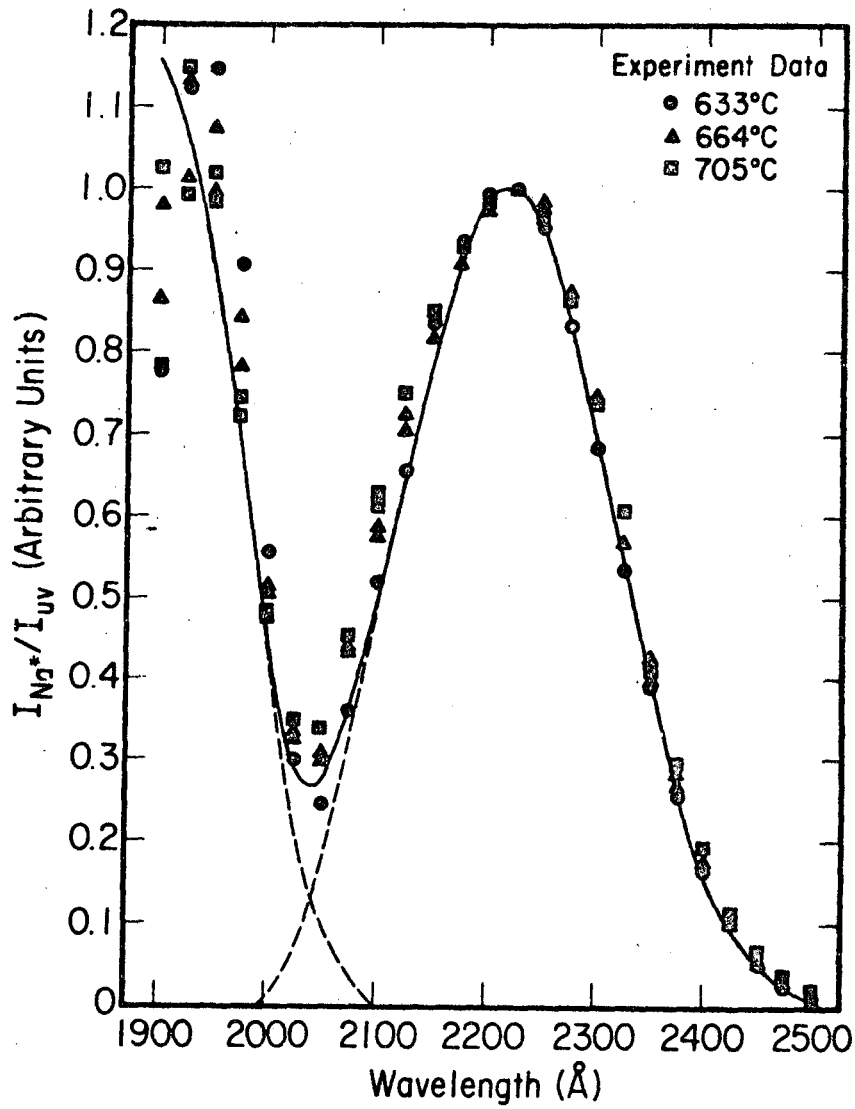

XBL 713-6601

Fig. III-2. Fluorescence efficiency curves for Na*($3p^2P$) from NaI. The data points, normalized to unit uv intensity, are given as solid symbols. The temperatures listed are those of the window region of the cell for each case. The salt temperatures were 100°C lower. The uv bandwidths were 24Å (FWHM) for the 633°C data, and 36Å (FWHM) for the 664 and 705°C data. The solid line shows the best fit calculated for the 633°C data for both fluorescence processes, Eqs. (7) and (8). The lines show the separate contributions in the region of overlap. All three sets of data were normalized to the same height at the long wavelength relative maximum.

noted that, as the data points indicate, the uncertainty in the data increases toward lower wavelengths, expecially below 2000Å. However, even considering this, it seems likely that the lower wavelength peak would be more intense than the upper.

The process of primary interest here in the photodissociation of NaI can be represented as

$$\mathrm{NaI} \xrightarrow{\sim 2000\text{-}2500\text{Å}} \mathrm{Na}^*(3p\,^2P) + \mathrm{I}(^2P_{3/2}) \quad . \tag{7}$$

A portion of the adjacent lower-wavelength peak in the fluorescence efficiency curve was observed, and may be due to either or both of two processes

$$\mathrm{NaI} \xrightarrow{?\text{-}\ \sim 2100\text{Å}} \mathrm{Na}^*(3p\,^2P) + \mathrm{I}^*(^2P_{1/2}) \tag{8a}$$

or

$$\mathrm{NaI} \xrightarrow{?\text{-}\sim 2100\text{Å}} \mathrm{Na}^*(4s\,^2S) + \mathrm{I}(^2P_{3/2}) \tag{8b}$$

The additional energy required for the process of Eq. (8a)[26c] 7600 cm^{-1}, and for process (8b) [26a] is 8800 cm^{-1}. If the potential curves for these processes are similar in shape to that for process (7), these energy increments would correspond to wavelength shifts of ~320Å and ~360Å, respectively, placing the fluorescence efficiency peak at or below 1900Å. The domain of the study of these two (or three) processes was 1900-2600Å. This work was done in air, and, after transferring to the vacuum chamber, further investigation of the lower peak was not thought worthwhile for several reasons, among which were: the ambiguity as to which process was going on; the

much-decreased intensity at lower wavelengths; the lack, even in vacuum, of sufficiently low wavelengths to permit investigation over the full energy range; and the fact that interfering processes could be expected to lead to further ambiguity at lower wavelengths.

Figure III-3 shows the potential curves used for NaI to calculate the best-fit curve, along with several examples of ground- and excited-state wavefunctions. The parameters of the ground-state curve are given in Table I. The calculated fluorescence efficiency curve of Fig. III-2 was calculated from these potential curves using 10 vibrational levels of the ground state. The main interest was in fitting the longer wavelength peak, but it was decided to include calculations of the contribution of the shorter wavelength process peak through the experimental region, based on certain assumptions: (1) the lower peak is due to process (8a); (2) $\mu_e(r)$ is the same for transitions of processes (7) and (8a); and (3) the upper potential curve for process (8a) can be obtained by simply displacing the curve for process (7) upward by 7600 cm^{-1}. The fluorescence curve calculated on the basis of these assumptions certainly provides an adequate fit to the lower wavelength data, but these data are hardly good enough to provide a definitive test. The total fluorescence curve provides an excellent fit to the data throughout the full wavelength range of process (7). In the region in which the two processes overlap, the separate contributions are indicated by dashed lines.

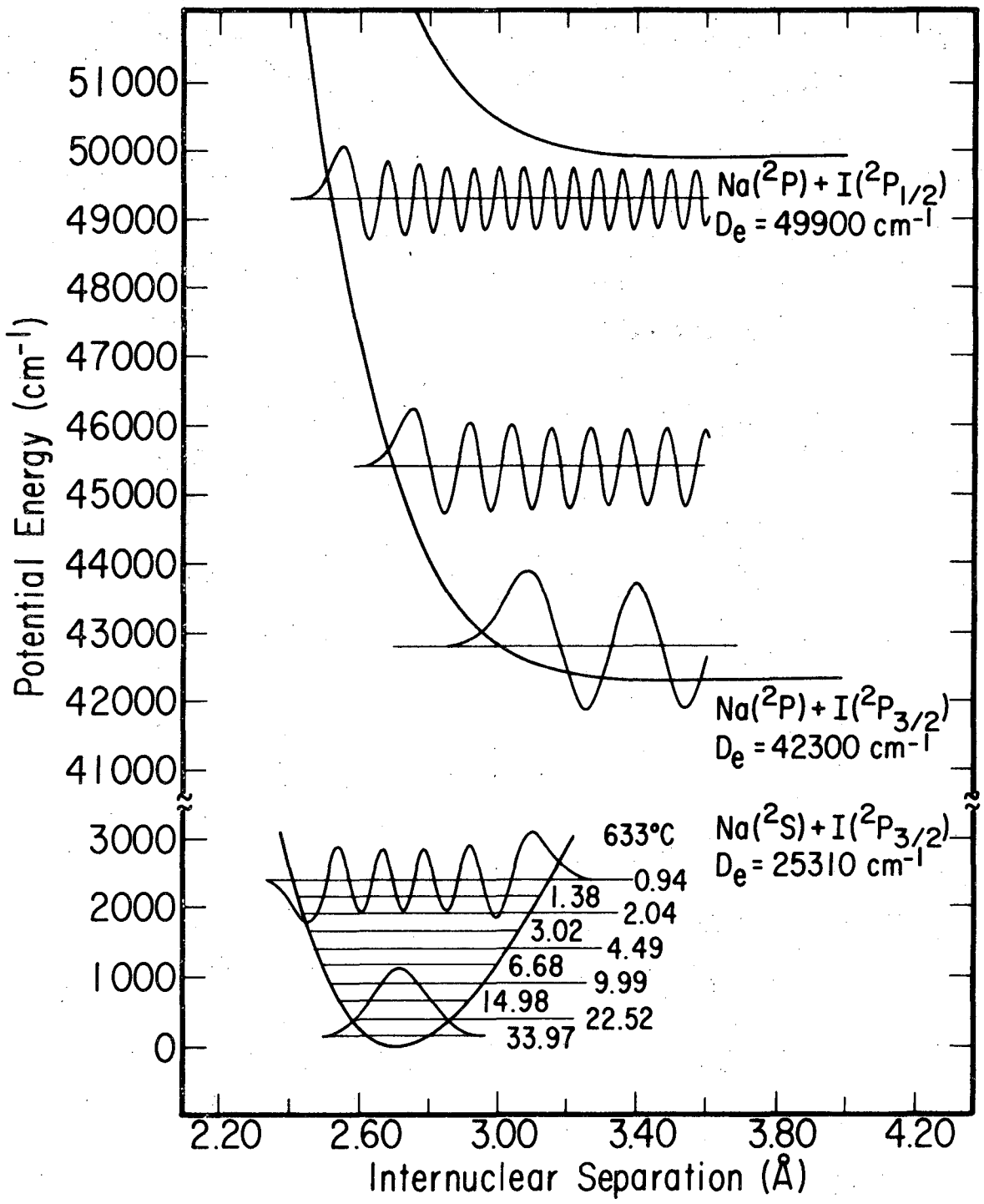

XBL713-6600

Fig. III-3. Potential curves for NaI used to construct the fit shown in Fig. III-2. Also shown are: the first ten vibrational levels of the ground state and their relative thermal populations at 633°C; unnormalized wavefunctions for v = 0 and v = 9 of the ground state; and three examples of continuum wavefunctions for the lower of the two repulsive states.

One of the conditions which must be met in order for the fluorescence efficiency data to be valid is that the uv must be absorbed negligibly upon traversing the cell. If this is not true, the uv normalization is invalid. A significant loss of uv before the uv beam reaches the zone from which fluorescence is detected would depress the peak fluorescence efficiency relative to values away from the peak. Ultraviolet absorption cross-sections from Ref. 3, combined with vapor-pressure data from Ref. 2, Chapter II, indicate that the peak absorption through a 5 cm cell would vary from ~1% to ~7% over the temperature range included in the data of Fig. III-2. The value of 7%, which would correspond to ~3-4% absorption at the detection zone, is perhaps pushing the limit of acceptability.

Another condition necessary to the validity of the data is that the fraction of molecules dissociated is negligible. To see the necessity of this, consider Eq. (4). N_v is just the number density of molecules in vibrational level v, which is given in terms of N, the total number density, and Q_v, the vibrational partition function, by

$$N_v = N \exp[-\hbar\omega_e(v + 1/2)/kT]/Q_v \tag{9}$$

The analysis of the data using Eq. (4) and those derived from it assumes that N and hence all the N_v's are independent of frequency. If a significant fraction of molecules is dissociated, this is not true; the "reservoir" is depleted and again, this would lead to a flattening of the fluorescence efficiency curve, although in a slightly different

way from the previous problem, as the effect would be greatest for the largest number of uv photons absorbed, as opposed to the largest fraction of the uv absorbed, and thus would be shifted slightly to longer wavelengths (to the experimental peak).

In the vapor pressure region in which the fraction of the uv absorbed is small, this fraction will increase approximately linearly with pressure, so the fraction of molecules dissociated will be approximately independent of pressure. The problem, then, is to be sure that the uv intensity is not so great that too much dissociation occurs. Perhaps the best way to do this would be to combine uv absorption cross-sections with absolute intensity data for the uv source, although the difficulty in estimating the geometry of the fluorescence zone makes this non-trivial. Lacking the uv intensity data, the problem was attacked experimentally by comparing fluorescence efficiency curves taken at the same temperature but with monochromator bandwidths of 12Å and 48Å. Since the uv intensity is proportional to the square of the bandwidth, the curves represent a factor of 16 in the intensity, and the agreement between them, shown in Fig. III-4, indicates little, if any, problem with excessive dissociation at 603°C. The larger values for the 48Å curve at the long wavelength tail and through the minimum around 2000Å would be expected from the added bandwidth. A similar comparison between two such curves taken at 635°C showed a slight but probably real difference between the two, which was probably due to excessive uv absorption. Note that these temperatures are salt temperatures, while the temperatures shown in Fig. III-2 are window temperatures.

0 0 0 0 3 9 0 7 2 7 3

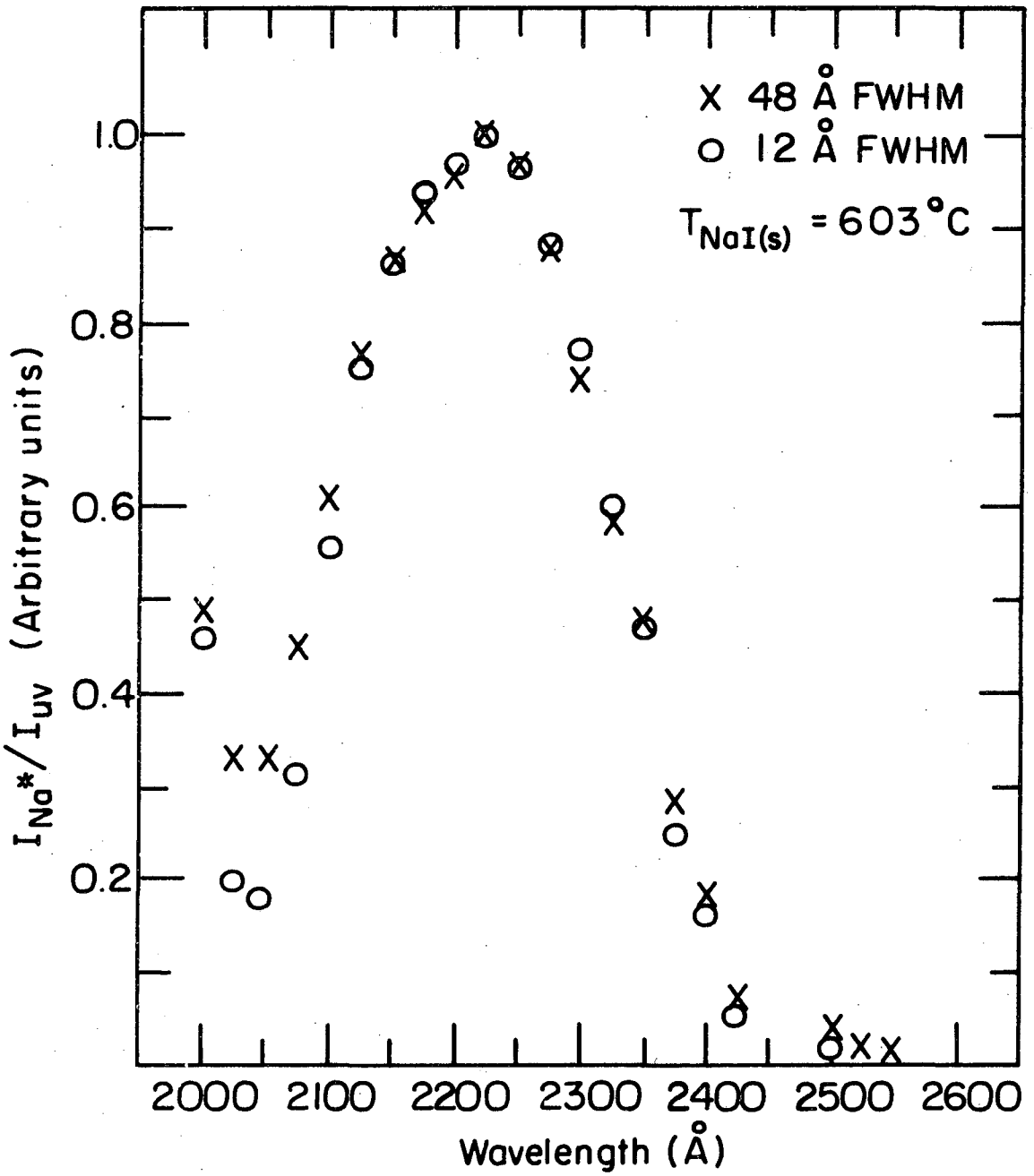

XBL 737-6557

Fig. III-4. Comparison of fluorescence efficiency data for NaI at bandwidths representing a factor of 16 in uv intensity. As discussed in the text, the agreement indicates little or no difficulty with excessive uv absorption or excessive dissociation at 603°C, salt temperature.

Fluorescence efficiency curves for NaI have been reported in at least one previous study.[4] The two curves shown there, covering the range 2100-2500Å, for temperatures of 581°C and 668°C, peak at ~2250 Å and 2300Å, respectively, whereas the results of the present work show a peak at ~2220Å, with no apparent temperature dependence. The present results coincide closely with the reported absorption spectrum for this process,[3] which shows a peak at ~2200Å.

2. Sodium Bromide

The sodium D-lines fluorescence from photodissociation of NaBr has been observed, but apparently not previously studied as a function of wavelength. Brus[1] reported that photodissociation over the full wavelength range by an H_2 spark lamp was necessary to produce sufficient signal to allow data collection. Winans,[27] in 1930, studied the quenching of the D-lines radiation by Br_2 at three wavelengths using atomic line sources. Assignment of this fluorescence to the process

$$NaBr \xrightarrow{\sim 1750\text{-}2300\text{Å}} Na^*(3p\,^2P) + Br(^2P_{3/2}) \qquad (10)$$

seems obvious for several reasons. This is the region where the process would be expected to occur energetically; this is the longest wavelength absorption[3] which produces sodium fluorescence; and this is the third absorption peak,[3] as is the NaI peak for process (7). Furthermore, Ref. 1, as previously mentioned, states that there is no indication of delay in the D-lines fluorescence observed in this region. The absorption spectra of Ref. 3 were quite helpful in providing

corroboration of assignments for the fluorescence spectra of NaBr and KI. For these salts, as well as for NaI, the fluorescence data agreed well with the absorption spectra in the regions where the measurements overlapped.

The experimental points for the fluorescence efficiency curve of NaBr are shown in Fig. III-5, along with the best calculated fit. As shown, no fluorescence could be measured at a monochromator setting of 1700Å, although the uv intensity there had been measurable, albeit small, in the measurements done just prior to the collection of the fluorescence data. Processes analagous to those of Eq. (8) for NaI might be expected to come into the picture at lower wavelengths, but in this case the production of the excited halogen atom, $Br(^2P_{1/2})$ would involve only 3700 cm^{-1} additional energy,[26b] which would place the peak for such a process at ~1840Å. The data seem to indicate quite definitely that this is not occurring with a significant probability. The process analagous to (8b) would be expected to peak at ~1680Å, and a contribution from it is not ruled out entirely, although comparison to the lower peaks in the NaI and KI cases indicates that it would be very weak. Further clouding this low wavelength picture is the fact that the uv intensity data used to normalize the fluorescence efficiency were taken at room temperature, and at the temperature used in collecting the fluorescence data, there might well have been some relative changes in the uv intensity around the lower wavelength limit (cf. Chapter II, Section A-2). All these considerations render the interpretation of the NaBr fluorescence below, say, 1850Å, somewhat problematical.

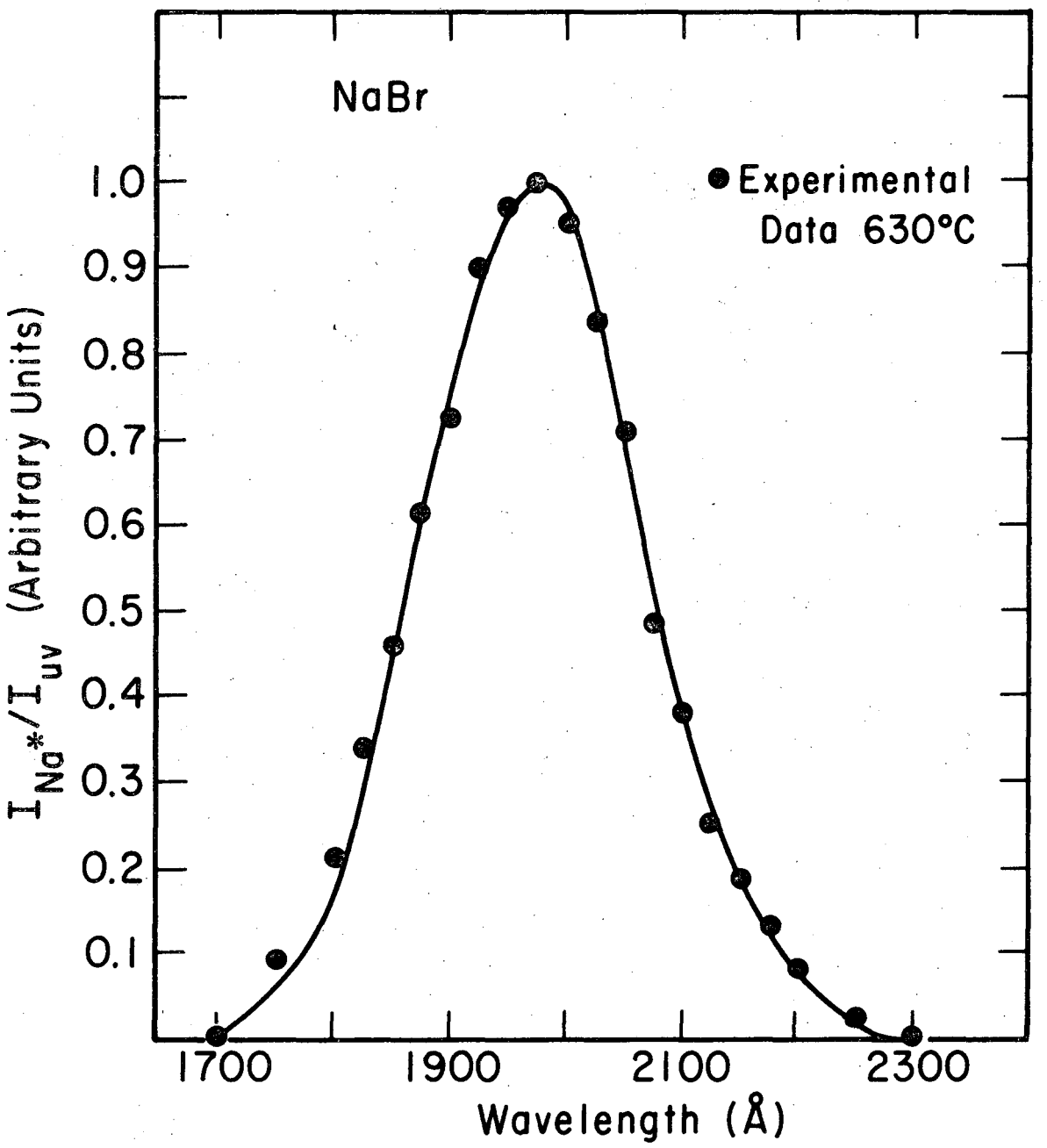

XBL 737-6562

Fig. III-5. Fluorescence efficiency curve for Na*($3p^2P$) from NaBr. The data points were taken at 630°C, window temperature, 610°C, salt temperature. The uv bandwidth was 60Å (FWHM). The solid curve is the fit calculated from the potential curves of Fig. III-6.

It was decided, primarily on the basis of the zero value at 1700Å, to try to fit all the data to process (10), without stressing exact coincidence below 1850Å.

The potential curves used to calculate the solid curve of Fig. III-5 are shown in Fig. III-6. The parameters of the ground state curve are given in Table I. Ten vibrational levels of the ground state were used in the calculation. The upper curve for NaBr is somewhat steeper and covers a somewhat greater energy range than those for NaI and KI. There have apparently been no previous calculations of an NaBr repulsive potential curve, though Ref. 3 presents results of such calculations for a few alkali halides.

3. Potassium Iodide

As in the case of NaBr, fluorescence from the first resonance state of the metal atom has been observed in photodissociation experiments, but not studied as a function of wavelength,[28] although quenching experiments were carried out at three wavelengths using atomic resonance lamps (Hg at 2537Å and Cd at 2288Å) and an H_2 arc similar to the one described in Chapter II at 2400Å. The same considerations discussed for NaBr lead to the assignment of the first fluorescence peak of KI to the process

$$KI \xrightarrow{\sim 2150\text{-}2750\text{Å}} K^*(4p\,^2P_{1/2,3/2}) + I(^2P_{3/2}) \qquad (11)$$

In this case, there is apparently no experimental data on the fluorescence lifetime of the $K^*(4p\,^2P)$ atom from this process.

A rise in the fluorescence efficiency below ~2200Å was observed,

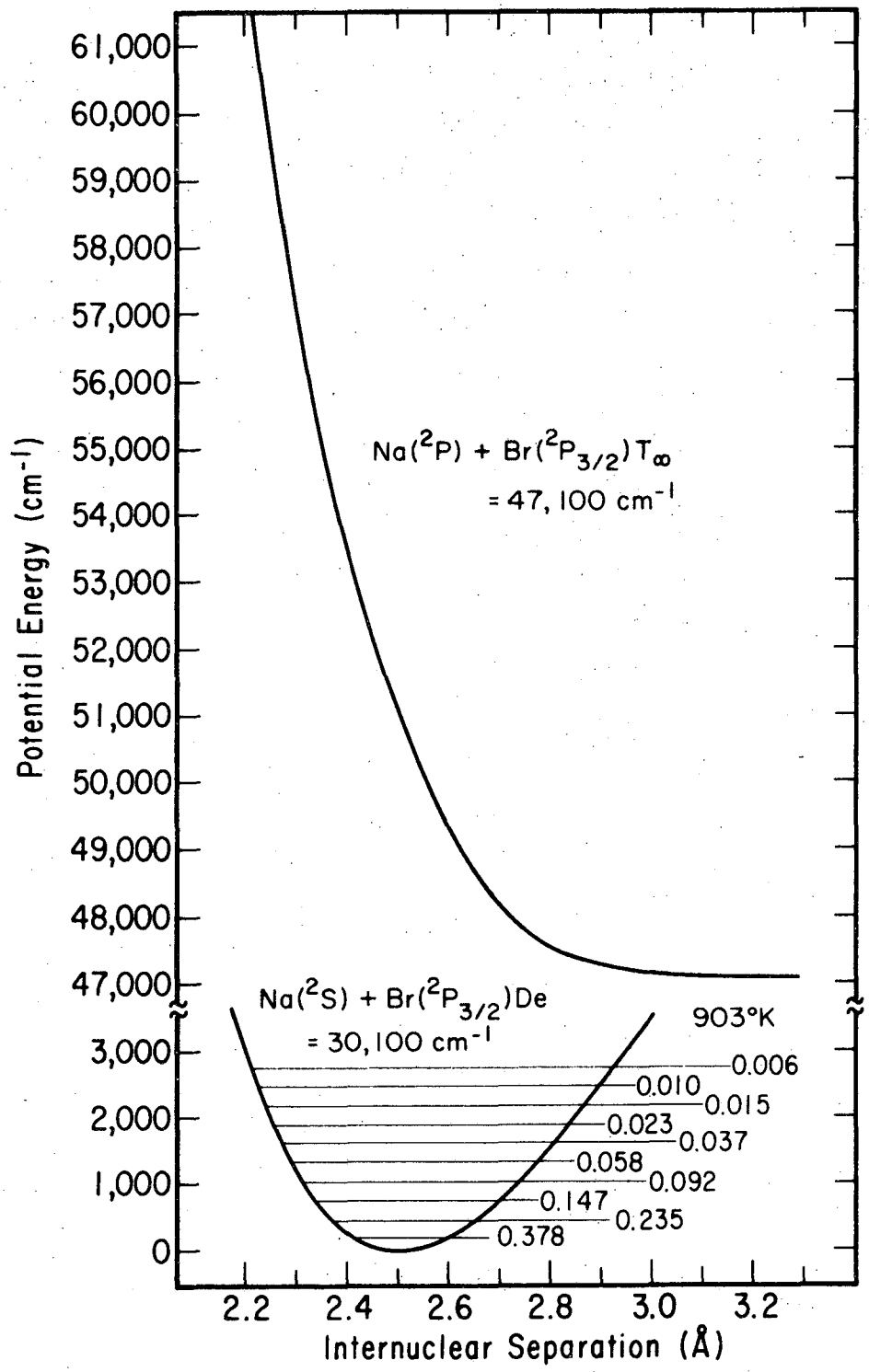

XBL 737-6564

Fig. III-6. Potential curves for NaBr, used to calculate the fit shown in Fig. III-5. Also shown are the first 10 vibrational levels of the ground state, and their relative thermal populations at 903°K.

but no attempt was made to characterize it. For purposes of analysis, it was assumed to be due to a process analagous to Eq. (8a) for NaI. For KI, the energy difference between the two processes[26] corresponding to Eq. (8) would be ~500 cm^{-1}, so any possible distinction between the two would be less clear than in the case of NaI.

The inclusion of the subscripts in the term symbol of K* in Eq. (11) is meant to indicate a complication in this case which did not occur with any other fluorescence studied. The K*($4p^2P$) lines lie at 7665Å ($4p^2P_{3/2}$) and 7699Å ($4p^2P_{1/2}$), and the separation rendered their simultaneous detection impractical. If much better signal to noise had been available, this would have provided more experimental possibilities, but, as it turned out, it was no more than an added difficulty. As discussed in Chapter II, the two lines were detected separately. The resulting experimental points are shown in Fig. III-7, along with the calculated fits, as discussed a bit later. For the purposes of comparing the two fluorescence efficiency curves, both were normalized to the same height. There is a displacement of the 7699Å curve by about 15Å to longer wavelengths along the right side of the spectra. In order to indicate this more clearly, the fit to the 7699Å data is shown as a dashed line on the 7665Å panel. This displacement, though small compared to the bandpass of the monochromator (FWHM = 60Å), is much larger than any difference to be expected solely on the basis of the doublet splitting, as 60 cm^{-1} corresponds in this region to ~3Å . The fluorescence efficiency curves come together at ~2300Å, and coincide to within experimental error at lower wavelengths.

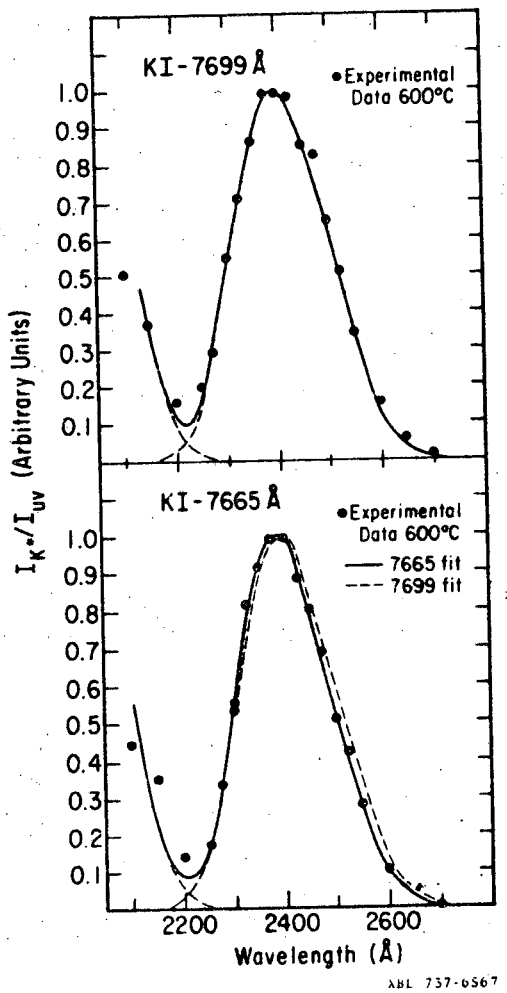

Fig. III-7. Fluorescence efficiency curves for $K^*(4p\,^2P_{1/2,3/2})$ from KI. The data points were taken at 600°C, window temperature, 580°C, salt temperature, with a uv bandwidth of 60Å (FWHM). The solid curves represent the fits calculated from the potential curves of Fig. III-8. The dashed curves in the region of the relative minima represent the calculated contributions of the two distinct fluorescence processes in the region where they overlap. In the lower panel, the dashed curve above 2300Å is the 7699Å fit, given for purposes of comparison. The 7665 and 7699Å curves were normalized to the same peak height for this figure.

For the purpose of generating the transition probability factors to be used in construction of the K* speed distributions, as discussed in Section C of this chapter, it was decided to fit a potential curve to the total fluorescence efficiency, which would clearly be just a weighted average of the curves of Fig. III-7. This potential would be adequate for the purpose mentioned, as the asymptotic energy difference[26b] of 58 cm^{-1} is much smaller than any recoil energies of interest in the quenching experiments.

In order to construct a total fluorescence efficiency curve, and in order to combine the quenching data for the two components, as discussed in Chapter IV, it was necessary to establish the relative intensities of the two independent of apparatus parameters. This was accomplished by finding the true ratio of the intensities at one wavelength, 2400Å. The relative detection efficiency for the two components was established by measuring their intensities with 600 Torr argon in the cell, under which condition the true ratio of the J = 3/2 to J = 1/2 intensities should be just 2 $\exp(-58\ cm^{-1}/kT)$. Then, with no argon present, combination of the relative detection efficiency with the experimental intensity ratio yielded a value for the true ratio of J = 3/2 to J = 1/2, in the argon-free KI vapor, of 2.4, with an estimated uncertanity of ~0.1. This ratio, combined with the full fluorescence efficiency curves, suffices to calculate the true ratio at any wavelength. As the high pressure of argon employed did cause some excitation transfer between the doublet levels, the apparent total intensity increased, as the detection efficiency was greater for the

7699Å component. However, using the newly derived value for the true ratio to properly weigh the contributions, the total intensity was found to be independent of the argon, within experimental uncertainty. This is not at all unexpected, as the same result was observed in the cases of $Na^*(3p^2P)$ and $K^*(5p^2P)$.

The potential curves for KI, used to obtain the fits shown in Fig. III-7, are given in Fig. III-8. The parameters for the ground state curve are in Table I. It was necessary to use a dissociation energy for KI 100 cm^{-1} below the "best" value of Table I to obtain the fits at long wavelengths. As this corresponds to only ~1/4 kcal/mole, which is within the uncertainty in the experimental dissociation energy, it was not regarded as significant. Fifteen vibrational levels of the lower state were used for the calculations.

As in the NaI case, contribution of the lower wavelength process was included in the calculated fluorescence curves, based on the same assumptions as in that case. This contribution was calculated for the 7665Å component and was just shifted by the appropriate amount for the 7699Å component, as the long wavelength tail indicated that the two should be related to each other by such a shift, according to the assumptions employed. The potential curves for the lower wavelength process would be obtained by displacing the upper curves in Fig. III-8 to higher energies by 7600 cm^{-1}.

The fluorescence efficiency of KI to give $K^*(5p^2P)$ was investigated briefly and the results are shown in the upper panel of Fig. III-9. The 4d and 6s levels of potassium lie only 2690 cm^{-1} and 2740 cm^{-1}, respectively, above the 5p level,[26b] and since both may decay to the 5p

0 0 0 0 3 9 0 7 2 7 6

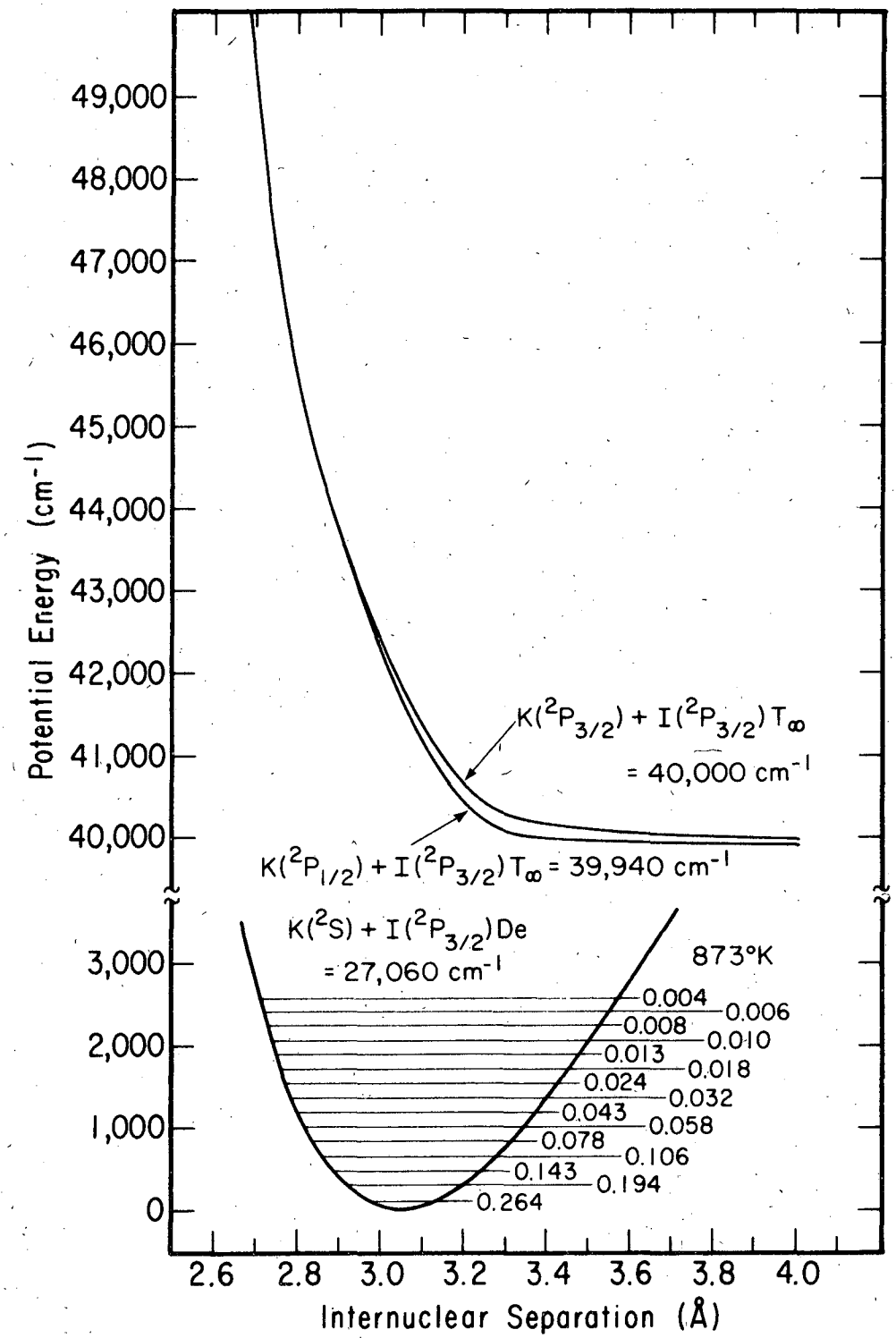

XBL 737-6566

Fig. III-8. Potential curves for KI. The repulsive curves used to calculate the low wavelength contributions to the fluorescence efficiency curve are obtained by displacing those shown by 7600 cm^{-1} to higher energies. Also shown are the first fifteen vibrational levels of the ground state, and their relative thermal populations at 873°K.

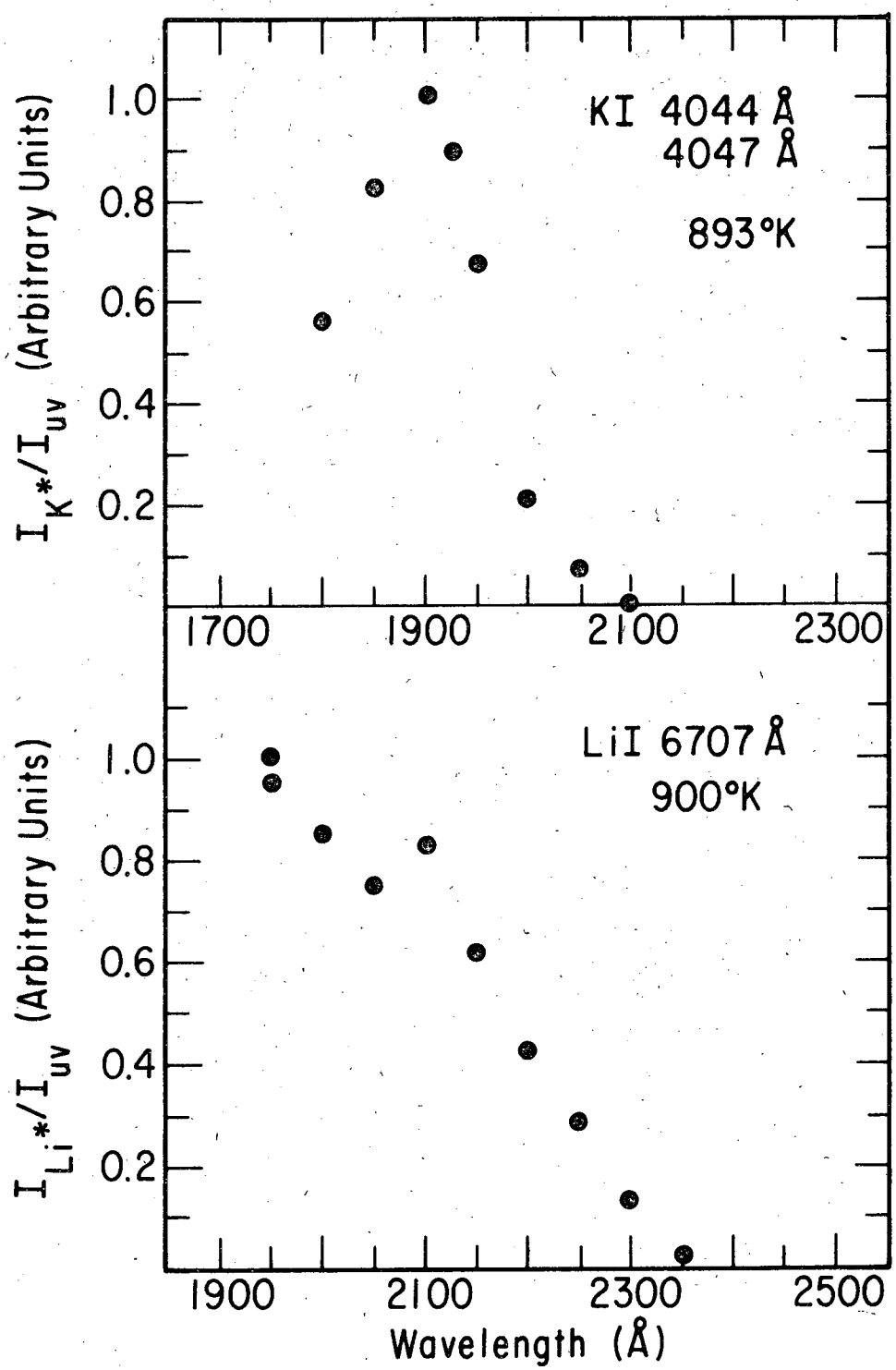

XBL 737-6565

Fig. III-9. Fluorescence efficiency data for $K^*(5p^2P)$ from KI (upper panel) and $LI(2p^2)$ from LiI (lower panel). The temperatures given are window temperatures. The salt temperature was 873°K for KI, and 865°K for LiI. The uv bandwidths were 60Å (FWHM) for the KI data and 48Å (FWHM) for the LiI data.

level, the data may be regarded as ambiguous below ~1925Å. At any rate, it was not possible to investigate this fluorescence to its lower wavelength limit with the available uv. Even if the uv had extended to sufficiently low wavelengths, however, the ambiguity in interpreting the data would have precluded the construction of any upper potential curve, and of excited atom speed distributions. For this reason, the speed distributions were thermalized, where possible, for quenching experiments, so that their exact character was known.

4. Lithium Iodide

As indicated earlier, fragmentary results were obtained on the fluorescence of $Li^*(2p^2P)$ produced from LiI. This salt is ideal kinematically for quenching studies, as the mass ratio would cause nearly all the excess energy to go into the Li*, making available a very wide range of collision energies. However, the strong tendency of the LiI vapor to attack quartz rendered the cell windows opaque to the uv quite quickly at the pressures required to produce sufficient fluorescence signal. The fluorescence efficiency data which was obtained is shown in the lower panel of Fig. III-9. As these data were taken in air, the lower wavelength limit was 1900Å.

5. Theoretical Intensity Distributions

The calculated fits to the experimental data shown in Figs. III-2, III-5 and III-7 are averaged over the appropriate monochromator bandwidths, and thus do not represent the "true" theoretical intensity distributions which are calculated for zero bandwidth, Eqs. (4) and (4a). The four experimental fits are shown again in Fig. III-10, accompanied in each case by the theoretical intensity distribution. The former are shown as solid lines and the latter as dashed lines in the regions in which they are distinguishable. As would be expected, the role of the monochromator bandwidth is simply to broaden the distributions at the marginal wavelengths. The relatively small effect in the NaI case is due to the fact that the bandwidth was 24Å(FWHM) as compared to 60Å for the other cases.

E. Photodissociatively Produced Speed Distributions

For the purpose of analyzing the quenching data, as discussed in Chapters IV and V, it is necessary to know the experimental distributions in speeds of the excited M* atoms. Although, as discussed in Chapter I, photodissociation quenching studies have been going on for about 40 years, there has been no previous attempt to properly account for these distributions in discussing the energy dependence of the quenching cross sections. The full experimental distribution involves the monochromator bandwidth, the uv intensity distribution, and the transition probability distributions for each vibrational level of the molecule, aside from purely kinematic factors. In the latter category, one must consider the thermal distributions in molecular translational, vibrational, and rotational energy as well as the

0 0 0 0 3 9 0 7 2 7 8

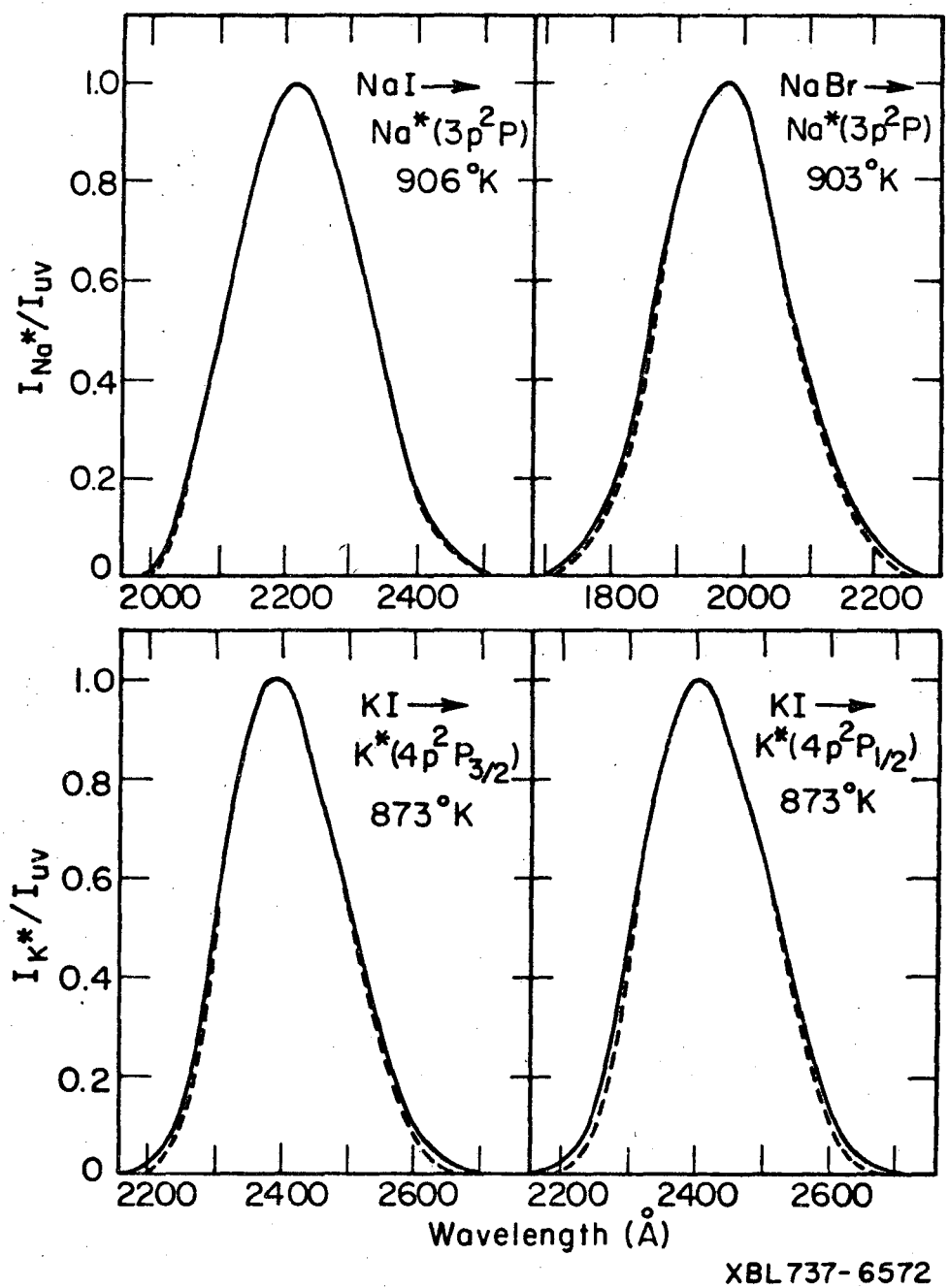

Fig. III-10. Theoretical intensity distributions for the fluorescence processes indicated. The theoretical distributions are calculated for infinitessimal uv bandwidth, and are shown as dashed curves where they are distinguishable from the solid curves, calculated for the experimental bandwidths, and reproduced from Figs. III-2, III-5, and III-7. The bandwidths (FWHM) were: for NaI, 24 Å, and for everything else, 60 Å.

distribution in the orientation of the M* recoil velocity with respect to the molecular velocity. Initially, all of this was put into a computer program and done numerically, but this process proved prohibitively expensive. Given an analytic solution for the problem of a single dissociating frequency and a collection of molecules in single vibrational level, the remainder of the averaging could be done within reasonable cost, but a search of the literature provided no such analytic solution. There were partial solutions which had been derived for the speed distribution of particles in dissociative electron attachment in a high recoil energy approximation,[29] and for the kinetic energy distributions of fragment ions in a mass spectrometer.[30] These results, however, neglected the effect of the rotational energy of the molecule which, it turns out, is quite significant in these photodissociation experiments. A result equivalent to that of Ref. 30 was obtained independently before it was realized that molecular rotation should, in fact, be included in the calculation. This derivation is presented here first, as it provides a convenient prelude to the more difficult problem, and is followed by the derivation, which was finally accomplished, of the analytic result including the effect of molecular rotation. The last section then briefly describes the numerical averaging required to obtain the full experimental distributions.

1. Distribution Excluding the Effects of Molecular Rotation

If a molecule, MX, in vibrational level v, is dissociated by radiation of frequency ν_o, the center of mass (c.m.) recoil speed, u, of the M* atom has a unique value, u_v, related to the excess energy of dissociation ε, through conservation of energy and linear momentum, by

$$m_M u_v^2/2 = E_v = (m_X/m_{MX})\ \varepsilon \quad , \tag{12}$$

ε having been defined in Eq. (2). The quantities m_M, m_X and m_{MX}, are just the masses of the respective particles, and E_v then represents that portion of the excess energy which goes into kinetic energy of the metal atom.

The laboratory (lab) velocity of M*, $\vec{V}$, is just $\vec{V} = \vec{u} + \vec{v}_{MX}$, where $\vec{u}$ is the CM recoil velocity of M* and $\vec{v}_{MX}$ is the lab velocity of the MX molecule. The distribution in $\vec{V}$ can be expressed formally in terms of the distributions in $\vec{u}$ and $\vec{v}_{MX}$, as

$$P_{v,\nu_o,T}(\vec{V}) = \int_{\vec{u}} P_{v,\nu_o}(\vec{u})\ P_T(\vec{v}_{MX}) \left|\partial\vec{v}_{MX}/\partial\vec{V}\right| d\vec{u} \tag{13}$$

where the subscripts index the variables on which the various distributions depend. Since the Jacobian factor for the two Cartesian coordinate systems is unity, the solution for $P_{v,\nu_o,T}(\vec{V})$ can be obtained by putting in the expressions for the other two distributions, substituting for $\vec{v}_{MX}$ in terms of $\vec{u}$ and $\vec{V}$, and carrying out the integration. Using the result of Eq. (12)

$$P_{v,\nu_o}(\vec{u})\ d\vec{u} = (4\pi)^{-1}\ \delta(u - u_v)\ \sin\theta d\theta d\phi du \tag{14}$$

since the distribution in values of the vector $\vec{u}$ is just the distribution in values of the scalar u divided by $4\pi u^2$. This equation indicates an isotropic distribution in recoil velocities with respect to some coordinate system, but, as will be discussed shortly, the final speed distribution is independent of initial assumptions concerning the spatial character of the $\vec{u}$ distribution.

The distribution in MX velocities is just the Boltzmann distribution

$$P_T(\vec{v}_{MX})\ d\vec{v}_{MX} = (\pi^{3/2}\bar{v}_{MX}^3)^{-1}\ \exp(-v_{MX}^2/\bar{v}_{MX}^2)\ d\vec{v}_{MX} \tag{15}$$

where $\bar{v}_{MX} = (2kT/m_{MX})^{1/2}$ is the most probable molecular speed, so Eq. (13) becomes

$$P_{v,\nu_o,T}(\vec{V}) = (4\pi)^{-1}\ (\pi^{3/2}\bar{v}_{MX}^3)^{-1} \times \int_{\vec{u}} \exp(-V^2/\bar{v}_{MX}^2)\ \exp(-u^2/\bar{v}_{MX}^2)\ \exp(2\vec{V}\cdot\vec{u}/\bar{v}_{MX}^2)\ \sin\theta_u d\theta_u d\phi_u du \tag{13a}$$

where $\vec{v}_{MX}$ has been substituted for in terms of $\vec{V}$ and $\vec{u}$. Invoking the delta function and integrating over u yields

$$P_{v,\nu_o,T}(\vec{V}) = (4\pi)^{-1}\ (\pi^{3/2}\bar{v}_{MX}^3)^{-1}\ \exp(-V^2/\bar{v}_{MX}^2)\ \exp(-u_v^2/\bar{v}_{MX}^2) \times \int_0^{2\pi}\int_0^{\pi} \exp(2\vec{V}\cdot\vec{u}_v/\bar{v}_{MX}^2)\ \sin\theta_u d\theta_u d\phi_u \tag{16}$$

The trick now is to let $\vec{V}$, which is a constant vector in the integration, define the polar axis. Then $\theta_u = \theta, \phi_u = \theta$, $\vec{V}\cdot\vec{u}_v$ becomes $Vu_v\cos\theta$, and the integration over angles can be done easily[31] to give

$$P_{v,\nu_o,T}(\vec{V}) = (2Vu_v\pi^{3/2}\bar{v}_{MX})^{-1}\ \exp(-V^2/\bar{v}_{MX}^2)\ \exp(-u_v^2/\bar{v}_{MX}^2) \times \sinh(2Vu_v/\bar{v}_{MX}^2) \tag{17}$$

To get the distribution in M* speeds, is it only necessary to integrate $P(\vec{V})\, d\vec{V}$ over angles, which yields a result which is conveniently expressed in terms of the reduced variables $A_v = u_v/\bar{v}_{MX}$ (the reduced c.m. recoil speed), and $A = V/\bar{v}_{MX}$ (the reduced M* lab speed):

$$P_{v,\nu_o,T}(A) = \pi^{-1/2}(A/A_v)\{\exp[-(A - A_v)^2] - \exp[-(A + A_v)^2]\} \quad (18)$$

As mentioned, this problem has been solved previously. Chantry and Schulz[29] have given the high recoil energy limit, which discards the second exponential if $A_v \gtrsim 3$. Stanton and Monahan[30] have derived an expression exactly equivalent to Eq. (18) in terms of the kinetic energy of ions in mass spectrometer studies. Furthermore, Ref. 31 derives the same expression for the distribution in relative speeds between a monoenergetic beam and a thermal gas in a scattering cell.

In this last regard, it is clear that both results obtain from convolution of a delta function distribution with a full Boltzmann distribution. Note, however, that in the case of the monoenergetic beam, the distribution in beam velocities is <u>vector</u> delta function; i.e., if the beam direction defines the polar axis, and v_o is the beam speed

$$P(\vec{v})\, d\vec{v} = \delta(v_x)\, \delta(v_y)\, \delta(v_z - v_o)\, d\vec{v} \quad . \qquad (19)$$

This is just the opposite extreme from the isotropic expression of Eq. (14), yet the final distribution in terms of speeds is identical. To understand this, consider riding on one of the particles in the monoenergetic beam. The distribution in <u>velocities</u> which you see clearly depends on the orientation of the particle's velocity relative to the chosen coordinate axes. However, the distribution in <u>speeds</u> of the

thermally distributed particles which you see, will be independent of the direction in which you are traveling, as long as the distribution of the thermal particles is completely isotropic. So, since a monoenergetic particle sees the same distribution in speeds of other particles relative to itself regardless of its direction, any assumption about the directional character of the monoenergetic distribution will not affect the final relative speed distribution.

The same idea applies to the dissociation problem. One can formulate this problem by letting u_v define the polar axis,[6] in which case $P(\vec{u})\, d\vec{u}$ is analagous to Eq. (19). The distribution in lab speeds derived will then apply to any direction of u_v as long as the parent molecule speed distribution is fully isotropic. This approach shows the interesting result that the distribution in lab velocities of M* is just the thermal distribution in molecular velocities with its origin centered about u_v.

2. Distribution Including the Effects of Molecular Rotation

If the MX molecule which is dissociated has rotational energy, E_r, this energy must appear at "large" M-X separations as translational energy, so E_r will supplement ε, and the c.m. recoil speed for this case, U, will be related to the recoil speed for the no-rotation case, by

$$U^2 = u^2 + 2Er/\kappa \tag{20}$$

with $\kappa = m_M m_{MX}/m_X$, so

$$P_{v,\nu_o,T}(U) = \int P_{v,\nu_o}(u)\, P_T(E_r)\, |\partial E_r/\partial U|\, du \tag{21}$$

with the Jacobian $|\partial E_r/\partial U| = \kappa U$. For these alkali halides at

temperatures around 900°K, the average value of J, the rotational quantum number, is very large, so the rotation may be treated classically, and the relative contributions of different rotational states to the intensity of the transition are just proportional to their populations, so the distribution function in rotational energy as it contributes to the recoil energy is simply a Boltzmann factor

$$P_T(E_r) = (kT)^{-1}\, e^{-E_r/kT} \tag{22}$$

and

$$\begin{aligned} P_{v,\nu_o,T}(U) &= (\kappa U/kT) \int_u \delta(u - u_v)\, \exp[-\kappa(U^2 - u^2)/2kT]\, du \\ P_{v,\nu_o,T}(U) &= (\kappa U/kT)\, \exp(\kappa u_v^2/2kT)\, \exp(-\kappa U^2/2kT);\ U \geqslant u_v \end{aligned} \tag{23}$$

Note that U must be greater than u_v, as the contribution of the rotational energy will always be to increase U. As before $P_{v,\nu_o,T}(\vec{U})$ can be obtained from Eq. (22) by dividing by $4\pi U^2$, and $P_{v,\nu_o,T}(\vec{U})\, d\vec{U}$ can then be inserted into Eq. (13) in place of $P_{v,\nu_o}(\vec{u})\, d\vec{u}$, with integration to be performed over $\vec{U}$. (Although different symbols have been used to denote the c.m. recoil velocities in the two cases as it was necessary to express a functional relation between them, V will be used for the M* velocity in both cases.)

The working expression for the distribution in M* velocities is now

$$\begin{aligned} P_{v,\nu_o,T}(\vec{V}) = {} & (\kappa/4\pi kT)(\pi^{3/2}\bar{v}_{MX}^{3})^{-1}\, \exp(\kappa u_v^2/2kT)\, \exp(-V^2/\bar{v}_{MX}^2) \times \\ & \int_{\vec{U}} \exp(-U^2/\bar{v}_{MX}^2)\, \exp(2U\cdot V/\bar{v}_{MX}^2)\, U \sin\theta_u d\theta_u d\phi_u du \end{aligned} \tag{24}$$

The same technique as before is used to allow integration over the angles to give the following expression for the integral of Eq. (23).

$$(\pi\bar{v}_{MX}^{2}/V)\int_{u_v}^{\infty} \exp[-(m_{MX} + \kappa)\ V^2/2kT][\exp(2VU/\bar{v}_{MX}^{2}) - \exp(-2VU/\bar{v}_{MX}^{2})]\ dU$$

The evaluation of this integral was accomplished "with a little help from my friends,"[31] by changing variables to $x = U - u_v$, so the limits went from zero to infinity, converting to scalar V and integrating over angles, then breaking the integrand apart, doing all the integrals separately, and reassembling the results into an expression which falls into two parts, depending on the relative magnitudes of V and u_v. Using the mass ratio $\eta = m_M/m_X$, the reduced M* lab speed, B, and the reduced CM recoil speed, B_v, are defined as

$$\begin{aligned} B &= (1 + \eta)^{-1/2}\ (V/\bar{v}_{MX}) \\ B_v &= (1 + \eta)^{1/2}\ (u_v/\bar{v}_{MX}) \end{aligned} \tag{25}$$

which allows expression of the final distribution in reduced M* lab speeds as

$$P_{v,\nu_o,T}(B) = \eta(1 + \eta)^{1/2}\ B\ \exp[\eta B_v^2/(1 + \eta)]\ \exp(-\eta B^2)\ G(B,B_v)$$

where

$$G(B,B_v) = \begin{cases} \mathrm{erf}(B + B_v) + \mathrm{erf}(B - B_v), & B > B_v \\ \mathrm{erf}(B + B_v) - \mathrm{erf}(B_v - B), & B < B_v \end{cases} \tag{26}$$

and erf(x) is just the error function.[31]

Figure III-11 shows probability curves calculated from Eqs. (18) and (26) for various values of $E_0 = m_M u_v^2/2$, the c.m. recoil energy of M*. Values of E_0 between ~kT/2 and ~10 kT were actually used in the

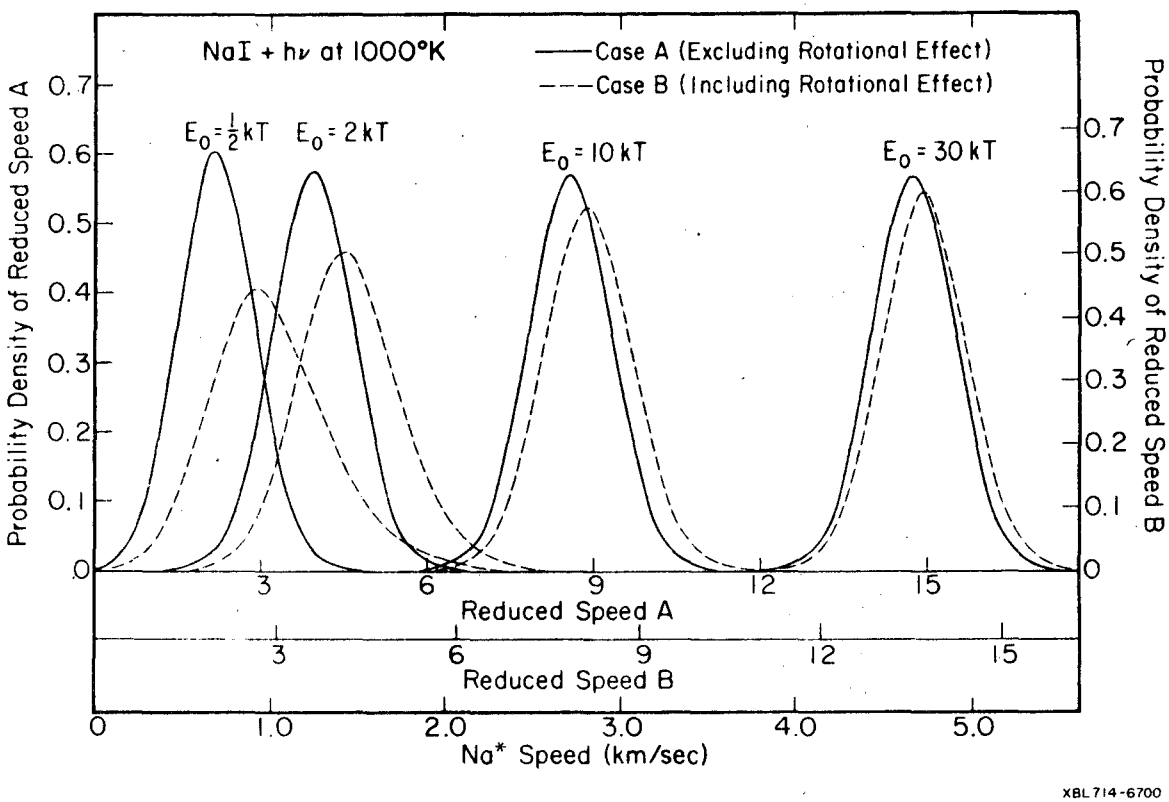

Fig. III-11. Normalized probability density distributions for the lab speed of an atom ejected from a diatomic molecule with c.m. recoil energy E_0, corresponding to E_v of Eq. (12). The solid curves, calculated from Eq. (18), account for the thermal translational distribution of the parent molecule, but neglect its rotational energy. The dashed curves, calculated from Eq. (26), account for thermal distributions in translational and rotational energies of the parent molecule. The ordinate scale for the lab speed, V, is not given. The relationship between this speed and the reduced speeds is appropriate to NaI at 1000°K.

experiments. The particular relationship between the two reduced speed axes in the Figure III-11 is valid for a value of η appropriate to the case of NaI. The other axis is just the Na* lab speed produced by photodissociation of NaI at 1000°K. The curves are normalized to unit area, as were all probability distributions for speeds in this work, thus the difference in ordinate scales (the ordinate scale for the M* speed is not shown).

As would be expected the rotational contribution broadens the distributions and shifts them to higher speeds. At high recoil energies, however, the effect of the rotational contribution becomes very small in both respects. To understand this, consider Eq. (23) for $P_{v,\upsilon_0,T}(U)$. This function is zero for $U < u_v$, then rises abruptly to a value proportional to u_v at $U = u_v$, then falls off exponentially as $\exp[-(U^2 - u_v^2)]$. Two things are noteworthy about this behavior. The peak height, which occurs at $U = u_v$, increases for greater u_v, and the fall-off is steeper for greater u_v. That is, as the CM recoil energy increases, this distribution becomes higher and narrower, tending to concentrate the probability at u_v, which makes it similar in effect to the delta function distribution of the no-rotation case, so at high recoil energies the M* lab speed distributions become similar to those of the other case as well.

That the broadening of the M* distribution due to the thermal translational energy distributions of the MX molecules is not very different over the range of E_0 values displayed in Fig. III-11, can be understood by examining Eq. (18). Except for very small values of E_0, the second exponential will be negligible. For example, if

$E_0 = 2kT$, then for the mass values of NaI, $A_v = 3.6$, which is well above the "high energy limit" of Chantry and Schulz. In this case, the maximum value of the second exponential, which occurs at $A = 0$, is 2.3×10^{-6}. For $E_0 = kT/2$, $A_v = 1.8$, which gives a maximum for this term of 0.04. Clearly, for small enough E_0, the second exponential would come into play, and would broaden the distribution. However, for all the solid curves of Fig. III-11, the first exponential dominates, giving a fall-off from the peak as $\exp[-(A_v-A)^2]$, which is independent of the value of A_v, being the square of the difference. In the case of the rotational contribution discussed in the previous paragraph, the exponent which controlled the fall-off was a difference of squares, hence gave steeper fall-off for larger u_v.

The physical interpretation of this difference seems to be that the change produced in u_v by a given increment of <u>energy</u> (E_r) will decrease with increasing u_v, whereas the change produced in u_v by a given increment of velocity (v_{MX}) will be independent of the value of u_v.

3. <u>Full Experimental M* Speed Distributions</u>

The M* speed distribution including all vibrational levels at a given frequency, ν_o, and a given temperature, T, is obtained by summing the weighted contributions over levels:

$$P_{\nu_o,T}(V) = \left[\sum_{v=0}^{\infty} I_M(\nu_o,v)\ P_{v,\nu_o,T}(V)\right]\Big/F_o$$
$$F_o = \int_0^{\infty} P_{\nu_o,T}(V)\ dV \qquad (27)$$

Where the transition probability factor is defined in Eq. (4). This summation was actually carried out over 10 levels for NaI and NaBr and over 15 levels for KI.

In practice, because of the logistics of the calculations, Eq. (27) was not employed directly. Instead, the probability factors for each vibrational level, N_v and $f_v(\nu_o) = \nu_o |\langle \varepsilon | v \rangle|^2$ were normalized at each wavelength such that

$$\sum_{v=0}^{\infty} N_v f_v(\lambda_o) = 1 \tag{28}$$

Then the speed distribution, indexed now by wavelength, $P_{v,\lambda_o,T}(V)$, was combined with Eq. (28) to give

$$P_{\lambda_o,T}(V) = \sum_v P_{v,\lambda_o,T}(V)\ N_v f_v(\lambda_o) \tag{29}$$

Equation (29) gives the speed distribution at a given wavelength, without consideration for the factors which weight various wavelengths. In the experimental distributions, these factors are three: The monochromator bandpass, $M(\lambda,\lambda_o)$, the relative uv intensity, $I_{uv}(\lambda_o)$, and the relative total fluorescence intensity, $I(\lambda_o)$, which is related to $I(\nu_o)$ of Eq. (4a) by $I(\lambda_o)\ d\lambda_o = I(\nu_o)\ d\nu_o$. The full experimental speed distributions are given by

$$P_{\lambda,T}(V) = \left[\int_{\lambda_o} P_{\lambda_o,T}(V)\ M(\lambda,\lambda_o)\ I_{uv}(\lambda_o)\ I(\lambda_o)\ d\lambda_o \right] \Big/ F$$
$$F = \int_0^{\infty} P_{\lambda,T}(V)\ dV \tag{30}$$

Figure III-12 shows plots of this function, obtained by doing the summation and integration of Eqs. (29) and (30) by computer, for various values of uv wavelength for NaI. The effect of different temperatures and bandwidths is also indicated for each wavelength. Comparison of the curves in Fig. III-12 with each other and with the curves of

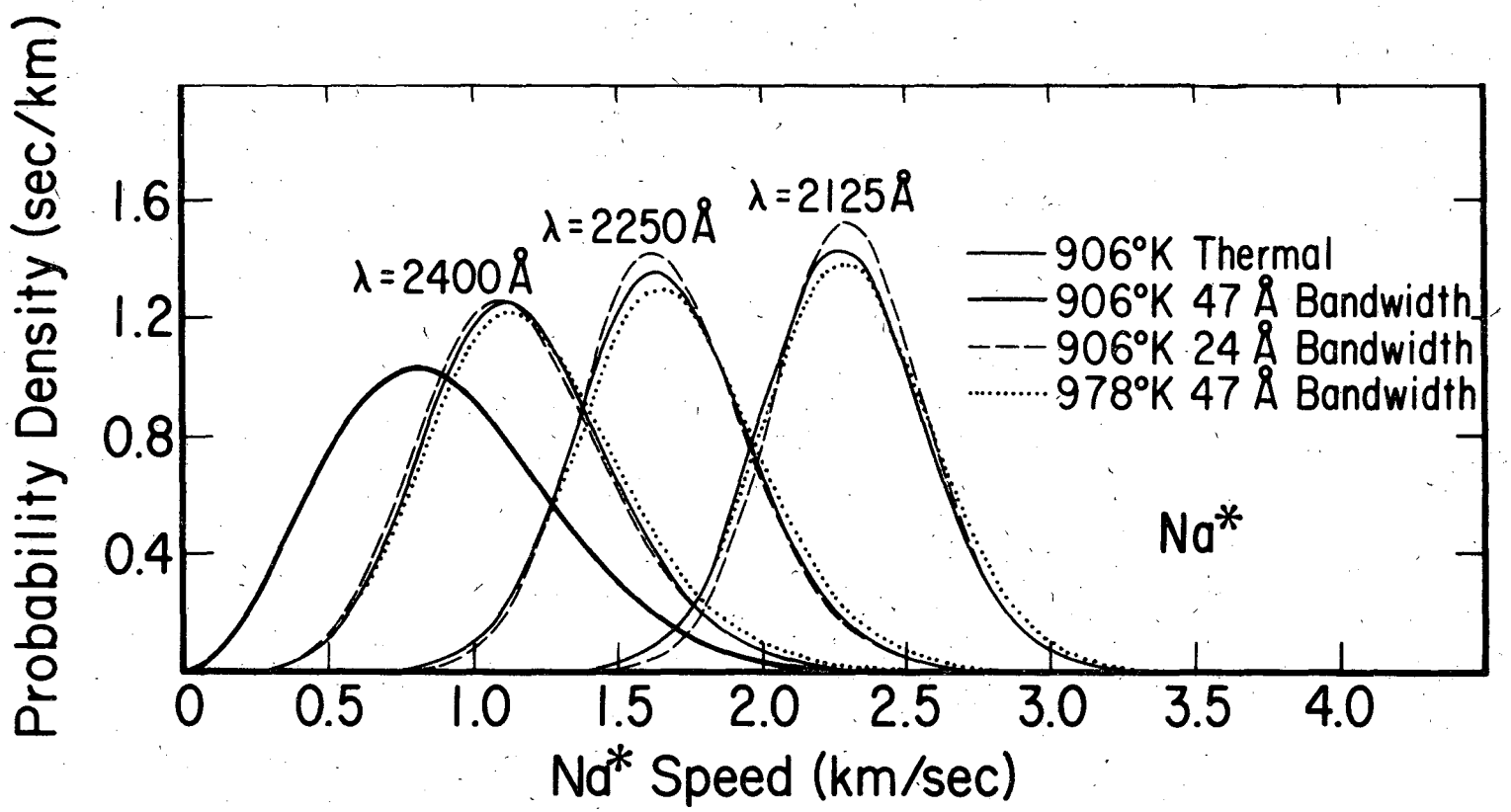

XBL 714-6673A

Fig. III-12. Full experimental speed distributions calculated for Na*($3p^2P$) from NaI for the indicated temperatures, monochromator settings, and bandwidths (FWHM). The thermal distribution at 906°K is also given.

Fig. III-11, indicates that the three weighting functions have relatively little effect on the distributions. In particular, the experimental monochromator banwidth, which controls the contributions of the two intensity distributions, introduced very little additional broadening into the speed distributions.

REFERENCES

1. L. E. Brus, J. Chem. Phys. 52, 1716 (1970).
2. J. R. Barker and R. E. Weston, Jr., Chem. Phys. Letters 19, 235 (1973).
3. P. Davidovits and D. C. Brodhead, J. Chem. Phys. 46, 2968 (1967).
4. H. G. Hanson, J. Chem. Phys. 23, 1391 (1955).
5. Shen-Maw Lin, Molecular Beam Kinetics (Ph. D. Thesis), LBL-891, Sept. 1972.
6. B. L. Earl, R. R. Herm, S-M. Lin and C. A. Mims, J. Chem. Phys. 56, 867 (1972).
7. G. Herzberg, Spectra of Diatomic Molecules (D. Van Nostrand Company, Inc., Princeton, New Jersey, 1967), p. 20.
8. G. Herzberg, op. cit., pp. 20, 199.
9. (a) R. N. Zare and J. K. Cashion, The IBM SHARE Program D2 NU SCHR 1072 for Solution of the Schrodinger Radial Equation, UCRL-10881, 1963.

   (b) R. N. Zare, Programs for Calculating Relative Intensities of Vibrational Bands in Electronic Transitions, UCRL-10925, 1963.
10. C. F. Goodeve and A. W. C. Taylor, Proc. Roy, Soc. (London) A154, 181 (1936).
11. J. F. Ogilvie, Trans. Far. Soc. 67, 2205 (1971).
12. G. H. Dunn, Phys. Rev. 172, 1 (1968).
13. E. A. Gislason, University of Illinois-Chicago Circle (private communication).
14. E. U. Condon and G. H. Shortley, The Theory of Atomic Spectra (University Press, Cambridge, 1967), p. 90.

15. F. Masnou-Seeuws and E. Roueff, Chem. Phys. Letters 16, 593 (1972).

16. R. N. Zare and D. R. Herschback, Proc. IEEE 51, 173 (1963).

17. Diffraction Grating Handbook (Bausch and Lomb, Inc., Rochester, N. Y., 1972).

18. (a) A. C. G. Mitchell, Z. Physik. 49, 228 (1928).
(b) H. G. Hanson, J. Chem. Phys. 41, 4773 (1967).

19. E. S. Rittner, J. Chem. Phys. 19, 1030 (1951).

20. C. Maltz, Chem. Phys. Letters 3, 707 (1969).

21. L. Brewer and E. Brackett, Chem. Rev. 61, 425 (1961).

22. A. Dalgarno, Advan. Phys. 11, 281 (1962).

23. (a) J. C. Slater and J. G. Kirkwood, Phys. Rev. 37, 682 (1931).
(b) J. G. Kirkwood, Physik. Zeits. 33, 57 (1932).

24. J. R. Rusk and W. Gordy, Phys. Rev. 127, 817 (1962).

25. G. Herzberg, Spectra of Diatomic Molecules (D. Van Nostrand Company, Inc., Princeton, New Jersey, 1967), Table 39.

26. Charlotte E. Moore, Atomic Energy Levels, Circular of the National Bureau of Standards 467, United States Department of Commerce, National Bureau of Standards, (a) Vol. I, 1949, (b) Vol. II, 1952, (c) Vol. III, 1958.

27. J. G. Winans, Z. Physik 60, 631 (1930).

28. J. Gatzke, Z. Physik, Chem. (Leipzig) 223, 321 (1963).

29. P. J. Chantry and G. J. Schulz, Phys. Rev. Letters 12, 449 (1964).

30. H. E. Stanton and J. E. Monahan, J. Chem. Phys. 41, 3694 (1964).

31. I. S. Gradshteyn and I. M. Ryzhik, Table of Integrals, Series, and Products (Academic Press, N. Y., 1965).

32. Fr. von Busch, H. J. Strunck and Ch. Schlier, Z. Physik 199, 518 (1967).

IV. QUENCHING ANALYSIS AND THEORY

A. The Steady-State Treatment and Quenching and Mixing Rate Constants

The interpretation of quenching data collected by the steady-state method has been historically by the Stern-Vollmer method,[1] according to which the ratio of unquenched to quenched fluorescence intensity should vary linearly with quenching gas pressure, the slope of the line being given by the ratio of the quenching rate constant to the natural radiative decay rate of the excited species. The derivation of this simple relationship assumes a single excited state, which is not the case for the ^2P states of alkali metals. Thus, interpretation of alkali quenching data by this relationship provides an "average" or "overall" rate constant for the quenching of the excited state. McGillis and Krause[2] have presented the full picture, according to the steady-state approximation, for the case in which only one of the doublet components is excited by radiation, which is feasible in atomic vapor studies, and Hoomayers and Lijnse[3] have developed the analysis of the general situation in flame experiments in which both doublet components are measured together. This section presents the full analysis of the experimental situation encountered in photodissociation, where an arbitrary mixture of the two components is initially excited, in terms of the steady state approximation. Subsequently, various special cases and approximations are discussed.

1. General Formulation for Excited Doublets

The processes occurring in the fluorescence cell, during photodissociation of MX molecules, including deactivation by foreign gas molecules, A, but ignoring effects such as collisions with the cell wall, can be represented by

$$MX \xrightarrow[h\nu]{s_1} M_1 + X \tag{1}$$

$$MX \xrightarrow[h\nu]{s_2} M_2 + X \tag{2}$$

$$M_1 \xrightarrow{\tau_1^{-1}} M_0 + h\nu_1 \tag{3}$$

$$M_2 \xrightarrow{\tau_2^{-1}} M_0 + h\nu_2 \tag{4}$$

$$M_1 + A \xrightarrow{Z_{12}} M_2 + A \tag{5}$$

$$M_2 + A \xrightarrow{Z_{21}} M_1 + A \tag{6}$$

$$M_1 + A \xrightarrow{Z_{20}} M_0 + A \tag{7}$$

$$M_2 + A \xrightarrow{Z_{20}} M_0 + A \tag{8}$$

In these equations, $M_0 = M(^2S)$, $M_1 = M^*(^2P_{1/2})$, $M_2 = M^*(^2P_{3/2})$, s_a represents the rate of creation of M_a, τ_a is the natural radiative lifetime of the M_a population, $h\nu_a$ represents the fluorescence of M_a, and Z_{ab} represents the rate of collisions of M_a with A which produce M_b. In terms of the quenching rate constants, k_{10} and k_{20}, and the mixing rate constants, k_{12} and k_{21}, $Z_{ab} = k_{ab}N_A$ where N_A is the number density of A. Thus, Eqs. (1) and (2) represent photodissociation to the excited states, Eqs. (3) and (4) represent fluorescence, Eqs. (5)

and (6) represent mixing, and Eqs. (7) and (8) represent quenching. Equations (1) through (8) and subsequent developments assume that the concentrations of M_0 and MX are small enough that the rates of collisions of M_1 or M_2 with these species and absorption of fluorescence by M_0 can be neglected. It has been indicated previously that extremely small concentrations of ground state atoms are produced in the experiments and the assumption with respect to MX concentrations can be fulfilled experimentally, as well, simply by maintaining sufficiently low vapor pressures.

The time-honored technique of analyzing such a system of equations in order to discern the dependence of measurable quantities on rate constants is to introduce the steady-state approximation, which says that the concentrations of excited species are constant under a given set of conditions. That is, if N_a represents the number density of M_a,

$$dN_a/dt = 0, \; a = 1,2 \quad . \tag{9}$$

This leads to the following two equations

$$\begin{aligned} S_1 + Z_{21}N_2 - N_1(Z_{12}+Z_{10}+\tau_1^{-1}) &= 0 \\ S_2 + Z_{12}N_1 - N_2(Z_{12}+Z_{20}+\tau_2^{-1}) &= 0 \end{aligned} \tag{10}$$

The solutions for N_1 and N_2, whose relative magnitudes under different conditions can be measured by monitoring the fluorescence, is a reasonably unpleasant algebraic exercise, yielding, for N_1,

$$\begin{aligned} N_1 &= [S_1\tau_1(1 + \tau_2Z_{20} + \tau_2Z_{21}) + S_2Z_{21}\tau_1\tau_2]/D \\ D &= (1 + \tau_2Z_{21} + \tau_2Z_{20})(1 + \tau_1Z_{12} + \tau_1Z_{10}) - \tau_1\tau_2Z_{12}Z_{21} \end{aligned} \tag{11}$$

and the expression for N_2 is clearly obtainable by permutation of the subscripts 1 and 2, which, incidentally, affects only the numerator. The rate of fluorescence of M_a is simply N_a/τ_a, so if I_{a0} represents the fluorescence intensity from M_a with no A present, and I_a the fluorescence intensity with A present, the following expression obtains for I_{10}/I_1 as a function of N_A

$$I_{10}/I_1 = D/(1 + \tau_2 Z_{20} + \tau_2 Z_{21} + f_2^o Z_{21}\tau_2) \qquad (12)$$

where $f_2^o = I_{20}/I_{10} = s_2/s_1$. The analagous expression for I_{20}/I_2 is again obtained by interchanging 1 and 2. This gives two equations involving experimentally measurable quantities on the one hand, and the Z_{ab} (or k_{ab}) on the other. A third independent equation is obtained for f_1, the ratio I_1/I_2

$$f_1 = [SZ_{21}\tau_2 + s_1(1 + \tau_2 Z_{20})]/[SZ_{12}\tau_1 + s_2(1 + \tau_1 Z_{10})] \qquad (13)$$

where $S = s_1 + s_2$ is the total excitation rate. Thus, the steady-state analysis yields three equations for the four unknowns, k_{ab}. (Of course, four quantities are measured, I_{10}, I_{20}, I_1 and I_2, but one of the relations among them is just the initially excited ratio, which is of no use in elucidating the rate constants.) The problem, if one wishes to extract information about all the k_{ab}'s, is to find an additional constraint, either experimental or theoretical.

2. Special Cases, Approximations, and Data Analysis

Krause[2] and his co-workers, doing atomic vapor experiments, are able to achieve an experimental constraint by creating a situation containing more information initially. Namely, only one of the two components is excited, by resonance radiation. If, for instance, M_2 is produced initially, then extrapolation of a plot of f_1 to very low pressures will yield a value for k_{21}, since N_1 is negligible in comparison to N_2. In practice, experiments were done with each component initially excited, and the rate constants were found by fitting the four plots (of I_{10}/I_1, I_{20}/I_2, f_1 and f_2 vs foreign gas pressure) to the forms required by the steady-state equations by an iterative method on a computer.

In photodissociation experiments, one cannot obtain two independent measurements for f_1 and f_2, as the initial ratio is experimentally constant at a given uv wavelength. The principle of detailed balancing[4] provides, in theory, the additional constraint which is required. This principle states that cross sections for collisional transitions between two states of a system, x and y, which have equal total energy, must be related in a particular way:

$$p_x^2 Q_{xy} = p_y^2 Q_{yx}$$
$$E_x(\text{int}) + p_x^2/2\mu_x = E_y(\text{int}) + p_y^2/2\mu_y \qquad (14)$$

where p_a represents the relative linear momentum of collision of the system with internal energy $E_a(\text{int})$ and μ_a is the reduced mass of the collision partners. In a case where $\mu_x = \mu_y$ Eq. (14) can be expressed

in terms of collision energy E_a. Rearranging and making the energy dependence of the cross sections explicit:

$$Q_{xy}(E_x) = Q_{yx}(E_y)\ E_y/E_x \tag{14a}$$

Since Eq. (14a) relates cross sections at <u>different</u> energies, it is not exactly clear how one would apply it to data analysis in a general case. Presumably, measurements at several energies would allow extraction of the desired information from Eq. (14a) along with Eqs. (12) and (13), but the process would probably be complicated

In the one experimental case in which this arose here, however, a simplifying approximation can be made. For $K^*(4_p\,^2P_{1/2,3/2})$, the doublet splitting is 58 cm^{-1} (the collision energies actually differ, on the average, by ~45 cm^{-1}, due to the mass factor M_I/M_{KI} which appears in the photodissociation energy partitioning). These energies are small enough, compared to collision energies in the experiments, ~500-~5000 cm^{-1}, that one might simply neglect the energy difference between the states. Then, since for a given energy distribution, k_{ab} is directly proportional to Q_{ab}, Eq. (14a) can be written approximately as

$$k_{xy} = k_{yx} \tag{14b}$$

This result would apply, in this experimental case, to transfer between each pair of m_J levels. To illustrate the problem of using it, it is instructive to consider a simplified model system consisting of an upper level, u, with two sublevels denoted by 1 and 2, and a lower level, ℓ, with one sublevel denoted by 3. Then, for the rate constants for transitions among the sublevels, one can write, from Eq. (14b)

$$k^o_{31} = k^o_{13}$$
$$k^o_{32} = k^o_{23} \tag{15}$$

Now, the total transfer rate from u to ℓ and vice versa can be written, with the concentration of the foreign gas implicit, as

$$R_{u\ell} = n_1 k^o_{13} + n_2 k^o_{23}$$
$$R_{\ell u} = n_3 (k^o_{31} + k^o_{32}) \tag{16}$$

where the n_a are the number densities in each sublevel. Since the overall rate constant is just the overall rate divided by the total population, $k_{u\ell}$ and $k_{\ell u}$ can be written, using Eq. (15), as

$$k_{u\ell} = (n_1 k^o_{13} + n_2 k^o_{23})/(n_1 + n_2)$$
$$k_{\ell u} = (k^o_{13} + k^o_{23}) \tag{17}$$

Now, $k_{u\ell}$ and $k_{\ell u}$ correspond to experimentally observable quantities. The difficulty in obtaining a usable relation between them lies in the fact that populations of the sublevels appear in Eq. (17), and these are not known. It is necessary to make some assumption about them, in order to proceed, and the only useful assumption to make is that they have statistical values within each J level. This requires, that, if photodissociation does not produce a statistical distribution of sublevel, i.e., m_J populations, these populations relax much faster than the J populations. This means that the depolarization cross sections, for m_J transitions within one J state, should be much bigger than the inelastic cross sections, for transitions from one J state to the other. Theoretical and experimental results[5] for collisions with noble gases

indicate that this requirement is not at all satisfied in the case of $Na^*(3p^2P)$, where the doublet splitting is only 17 cm^{-1}. However, separate detection of the two components is very difficult in this case anyway, as discussed in Chapter II. There is evidence in the case of $Rb^*(5p^2P)$, with a doublet splitting of 238 cm^{-1}, that the depolarization cross sections are about two orders of magnitude larger than the inelastic cross sections.[6] Presumably, the case of $K^*(4p^2P)$, with a doublet splitting of 58 cm^{-1}, would be reasonably good for the assumption in question.

If one then takes $n_1 = n_2$ in Eq. (17), one can obtain a ratio of mixing rate constants

$$k_{u\ell}/k_{\ell u} = 1/2 \tag{18}$$

Returning to the experimental case of J = 3/2, 1/2, four and two sublevels, respectively, one would obtain precisely the same equation. That is, in terms of the previous subscripts, u goes to 2, ℓ goes to 1, and

$$k_{12} = 2k_{21} \tag{18a}$$

which is just what one would expect statistically, since the energy difference was neglected. Hence, Eq. (13) for the ratio of the two components becomes

$$f_1 = [SZ_{21}\tau_2 + s_1(1 + \tau_2 Z_{20})]/[2SZ_{21}\tau_2 + s_2(1 + \tau_1 Z_{10})] \tag{19}$$

It might be noted that this development does not apply when gas pressures become high, as the M* speed distribution will be relaxed, so the energy relationship on which the detailed balancing argument rests will not

be satisfied. At high enough gas pressures, in fact, the ratio f_1 will simply be the Boltzmann factor weighted by the degeneracy

$$f_1(\text{thermal}) = (1/2)\exp[-(h\nu_1 - h\nu_2)/kT] \tag{20}$$

This condition, in combination with Eq. (13), says that at high pressures, i.e., thermal conditions, if quenching is negligible, the measured ratio of the mixing rate constants, k_{12}/k_{21}, must go to the statistical value, since τ_1 is very nearly equal to τ_2. This is what must obtain as it is the consequence of detailed balancing under equilibrium conditions, whether quenching is occurring or not. In this regard, it was noted that the ratios of cross sections reported in Ref. 2, which correspond to k_{12}/k_{21} for $Cs^*(6p^2P)$, are approximately half again as large as the statistical value. However, more recent results by the same workers give ratios which agree, within experimental error, with that prescribed by detailed balancing.[2b]

If it is assumed that Eq. (19) is accepted, at least tentatively, the four rate constants in the steady state analysis have been reduced to three, and the three measurable intensity ratios, plotted against N_A, should allow extraction of the constants, although the process might be somewhat complicated. In practice, it would have been very nice if mixing effects had appeared at pressures low enough that quenching could have been neglected, in which case Eqs. (18) and (19) would have allowed calculation of k_{12} and k_{21}. Attempts were made to observe such effects with $K^*(4p^2P)$, but no changes in the intensities of the components were observable at very low pressures. Still, it would have been possible to get information about mixing if the I_0/I vs pressure plots for the two components had had significantly different

slopes, corresponding to f_1 changing with pressure. Even this was not observed with the gases studied as quenchers, so the attempt to extract quantitative information concerning the mixing rate constants was abandoned.

As has been indicated, some doublet mixing effects were observed with argon, and the same is true of CH_4 and CF_4, two gases which quench $K^*(4p^2P)$ very weakly, if at all. No attempt was made to extract quantitative information about these processes, as they were not regarded as highly interesting per se, and also because doublet mixing large enough to allow extraction of such information could only be observed very near threshhold, as reference to the fluorescence efficiency curves will show, since the doublet ratio did not vary greatly from the statistical value elsewhere.

Returning to the quenching data, it was decided to fit the I_0/I plots for the individual components to the simple Stern-Vollmer equation. As has been indicated, this equation is obtained by steady-state analysis of a system involving only a single excited state. One case in which it falls out of the more complicated development is if there is no doublet mixing. Then Eq. (12) becomes, for each component

$$I_{a0}/I_a = 1 + Z_{a0}\tau_a \tag{21}$$

In the case of doublet mixing which is strong compared to quenching one would observe, on combination of both components, the same pressure dependence, but the overall quenching rate constant, k_q, would be an "average" of the quenching rate constants for the individual components:

$$k_q = (k_{10}N_1 + k_{20}N_2)/(N_1 + N_2) \tag{22}$$

This equation does not provide a direct basis for data analysis in general, as the observed attenuations of the individual components correspond not to k_{10} and k_{20}, but to complicated combinations of all four of the k_{ab}'s, and N_1 and N_2 are themselves functions of pressure.

The Stern-Vollmer equation expressed in terms of k_q, is given, on converting from number density of A to pressure in Torr, by

$$I_0/I = 1 + k_q\tau(9.65\times10^{18}/T)\ P_A \tag{21a}$$

where T is the experimental temperature in degrees Kelvin. What was done, in effect, was to combine the data for both components, taking into account the appropriate weighting factor corresponding to the real difference in unquenched intensities. That is, Eq. (21a) was used with $I_0 = I_{01} + I_{02}$ and $I = I_1 + I_2$. This gives a rate constant for the overall quenching of the excited state, which is just what was obtained directly in the cases of $Na^*(3p^2P)$ and $K^*(5p^2P)$ by simultaneous measurement of the two components.

In the latter cases, the raw quenching data was fit to Eq. (21a) by the least squares method, the slope then being equal to $9.65\times10^{18}k_q\tau/T$. In the case of $K^*(4p^2P)$, linear least-squares fits were done for each component, and the data were then combined to yield the overall result. Since

$$I/I_0 = I_1/I_0 + I_2/I_0 \tag{23}$$

combination must proceed by inverting the Stern-Vollmer plots, at least formally. In the general case, it would be necessary to construct the overall I_0/I vs P curve by using the ratio f_1^o. Since $I_{10} + I_{20} = I_0$ and $f_1^o = I_{10}/I_{20}$, I_0 can be expressed as $I_{10}(f_1^o + 1/f_1^o)$ or $I_{20}(1 + f_1^o)$. Then Eq. (22) becomes

$$I/I_0 = (I_1/I_{10})\ f_1^o/(1 + f_1^o) + (I_2/I_{20})\ 1/(1 + f_1^o) \qquad (23a)$$

which gives the prescription for constructing the overall plot. However, under certain conditions, it is possible to obtain an expression for the slope, m, for the overall plot, which is all that is needed, in terms of the slopes, m_1 and m_2, of the plots for the individual components. Given

$$\begin{aligned} I_{10}/I_1 &= 1 + m_1P \\ I_{20}/I_2 &= 1 + m_2P \end{aligned} \qquad (24)$$

then, using Eq. (23a)

$$I/I_0 = [(1 + m_2P)\ f_1^o + 1 + m_1P]/[(1 + m_1P)(1 + m_2P)(1 + f_1^o)] \qquad (25)$$

Hence,

$$I_0/I = (1 + f_1^o)[1 + (m_1 + m_2)\ P + m_1m_2P^2]/[1 + f_1^o + (m_2f_1^o + m_1)\ P] \qquad (26)$$

Clearly, if $m_1 = m_2 = m$, this reduces to the simple Stern-Vollmer plot of slope m. However, even if $m_1 \neq m_2$, the right side of this expression can be divided out to yield

$$I_0/I = 1 + P\ (m_1f_1^o + m_2)/(1 + f_1^o) + P^2f_1^o(m_2 - m_1)^2/(1 + f_1^o)^2 + \ldots \qquad (27)$$

The coefficient of the linear P term is just the appropriately weighted average of m_1 and m_2, and if $m_2 - m_1 << m_1$, this coefficient can simply be used as the desired slope of the overall plot. In all the measurements on $K^*(4p^2P)$, m_1 and m_2 agreed within experimental error, so this method was used to find m. It should be noted that this is purely an algebraic artifice, devoid of physical significance.

So far, the data have been treated to yield rate constants for the quenching of the excited species under investigation. The next step

0 0 0 0 3 9 0 7 2 8 4

is to convert these rate constants into cross sections, and to see what can be learned from the energy dependence and magnitudes of these cross sections.

B. Quenching Cross Sections

1. Initial Analysis: "Energy Independent" Cross Sections

The rate constants are, of course, a perfectly good expression of the primary results if the conditions under which they are obtained (e.g., "thermal, 900°K" or "photodissociation, 2300Å") are given. Traditionally, however, data in this field have been converted to cross sections or, in some cases, squares of collision diameters, vs relative collision speeds (or energies). The justification for this, beyond the facts that it provides a convenient pictorial representation and that cross sections seem perhaps more "physical" than rate constants, lies in the fact that this form of the information is more directly related to the parameters of the long-range attractive forces between the excited atom and the quenching gas molecule.

The usual analysis,[7,8] which is followed here as an initial step, and which does not account for the distributions in collision energies, extracts a value of a "phenomenological cross section," $\langle Q_q \rangle$, which is assumed to be independent of relative collision speed over the available range, at a "characteristic collision speed," $\langle g \rangle$. The c.m. recoil speed, u_v, of the metal atom, may be modified to account approximately for the thermal distributions in MX rotational and vibrational energies at temperature T simply by adding an increment of 2kT to the c.m. recoil energy for the zeroth vibrational state, $E_{v=0}$ as defined in Eq. (12) of Chapter III. Let u_T denote this "thermal average" c.m. recoil speed. Then

$$m_M u_T^2 = E_{v=0} + (m_X/m_{MX})\ 2kT \tag{28}$$

The most probable lab speed of the excited atom is obtained, according to this analysis, by assigning to MX its most probable speed and averaging over orientations of u_T with respect to $\bar{v}_{MX}$, to give

$$V_T = u_T + \bar{v}_{MX}^2/3u_T, \quad u_T > \bar{v}_{MX}$$
$$V_T = \bar{v}_{MX} + u_T^2/3\bar{v}_{MX}, \quad u_T < \bar{v}_{MX} \tag{29}$$

From kinetic theory comes the relation, for the frequency of collisions of an M* atom with A molecules under these conditions, which yields the phenomenological cross section:[7]

$$k_q = \pi^{-1/2} \langle Q_q \rangle \bar{v}_A \psi(x)/x$$
$$\psi(x) = x \exp(-x^2) + (2x^2 + 1)(\pi^{1/2}/2) \operatorname{erf}(x) \tag{30}$$

where $x = V_T/\bar{v}_A$, $\bar{v}_A$ being the most probable thermal speed of A, $(2kT/m_A)^{1/2}$, and k_q is the rate constant from Eq. (21a). The characteristic relative collision speed is given by

$$\langle g \rangle = V_T + \bar{v}_A^2/3V_T \ , \ V_T > \bar{v}_A$$
$$\langle g \rangle = \bar{v}_A + V_T^2/3\bar{v}_A \ , \ V_T < \bar{v}_A \tag{31}$$

In the case of thermal measurement, the approximation corresponding to Eqs. (30) and (31) is embodied in the simple expression

$$k_q(\text{thermal}) = \langle g \rangle \langle Q_q \rangle \tag{32}$$

where $\langle g \rangle = (8kT/\pi\mu)^{1/2}$, is just the thermally most probable collision speed, μ being the reduced mass of the collision pair.

Examination of the non-thermal data, or comparison of thermal results at widely different temperatures from different studies provides a clear indication that the quenching cross sections increase with

decreasing collision energy. This indicates the desirability of investigating the energy dependence of the cross sections more accurately. One of the goals in this study was to provide and utilize a method for "deconvoluting" the measured rate constants at different energies to obtain the true cross section as a function of energy. This method and its application here will now be discussed.

2. Energy Dependence of Cross Sections

The "right" expression for the rate constant in terms of the true cross section, Q_q, and relative speed, g, is simple in appearance:

$$k_q = \int_0^\infty g P_{T,\lambda}(g)\ Q_q(g)\ dg \tag{33}$$

where $P_{T,\lambda}(g)$ is the experimental distribution in relative speeds at temperature T and monochromator setting λ. The difficulty with evaluating the integral is that it requires knowledge of the dependence of Q on g and of the probability distribution of the relative speed. It is this latter requirement which has, in the past, provided the big obstacle to evaluating Eq. (33) for non-thermal conditions. However, the construction of the distribution in M* speeds, V, in Chapter III, permits the evaluation of $P_{T,\lambda}(g)$ by numerical convolution of $P_{T,\lambda}(V)$ with the thermal distribution in v_A, the speed of the A molecules. This was carried out using a simple "bin-counting" program which was checked on thermal cases to ensure that it worked properly. Some of the results of these calculations are shown in Fig. IV-1, for Na* from NaI with two gases which represent extremes in mass among those for which energy dependence of quenching was studied. The corresponding distributions

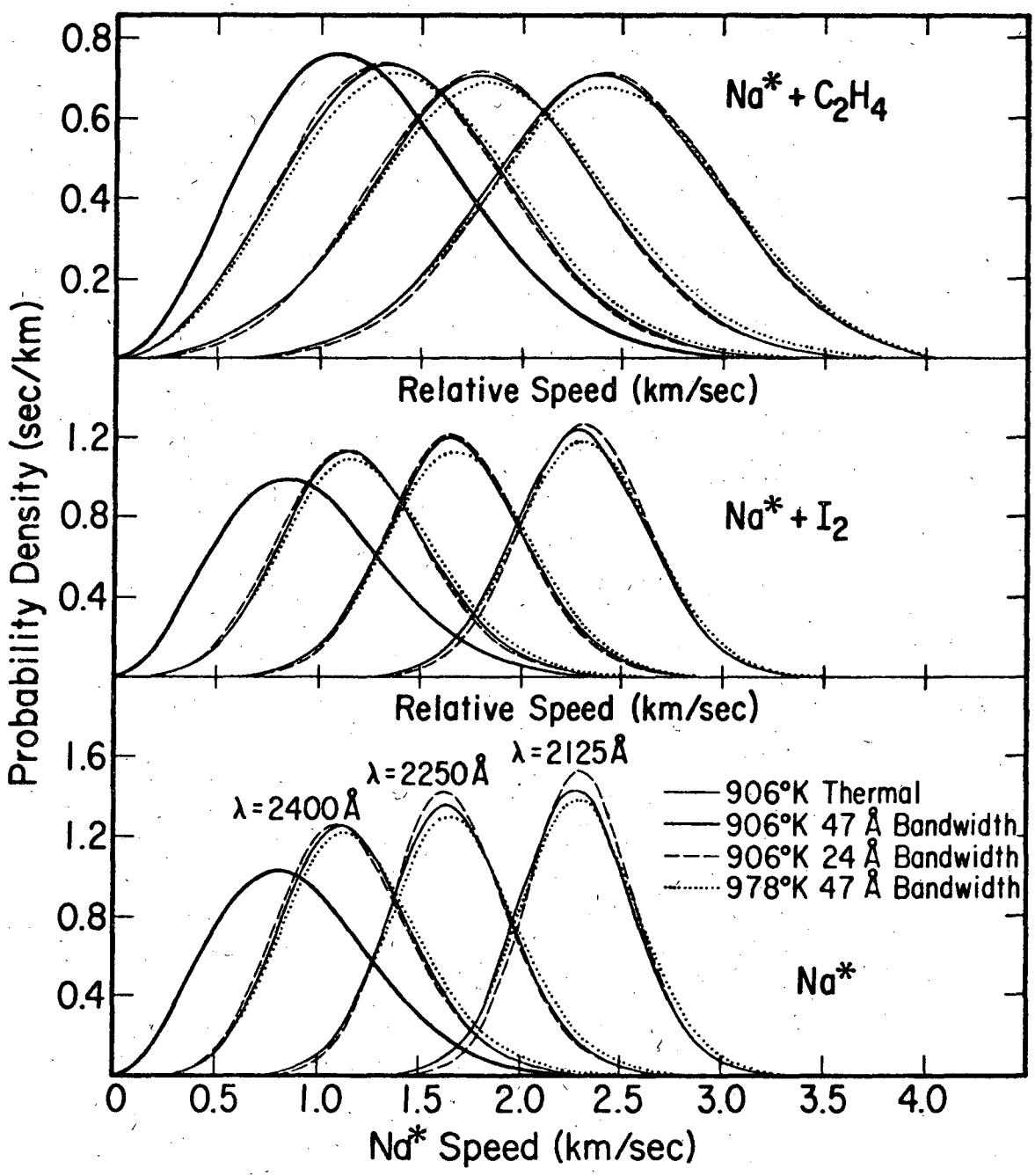

XBL 714-6673

Fig. IV-1. The lower panel shows calculated speed distributions for $Na^*(3p^2P)$ from NaI for various combinations of temperature, monochromator setting, and bandwidth (FWHM). Also shown is the thermal distribution at 906°K. The upper two panels show the corresponding distributions in relative speeds calculated for $Na^*(3p^2P)$ with I_2 and C_2H_4.

in Na* speeds, and a thermal distribution for each case, are also shown for comparison.

Once $P_{T,\lambda}(g)$ has been calculated, various forms of $Q_q(g)$ can be inserted into Eq. (31) to try to obtain the best fit to the experimental k_q's. In the cases where several quenching experiments were done with a single gas at different energies, this should provide a reasonably good test of the dependence of Q_q on g, as the various $P_{T,\lambda}(g)$ curves will sample different portions of the $Q_q(g)$ curve, although, as Fig. IV-1 indicates, the energy resolution is not especially good, particularly for the lighter gases. This would prevent observation of any "fine structure" in the $Q_q(g)$ curve. However, the energy resolution which is attained is sufficient to allow discernment of smooth variation of Q_q with g, which is what one is inclined to expect. In cases where only a thermal rate constant was measured, it was not possible to determine anything about the dependence of Q_q on g.

The dependence of a cross section for some inelastic (or reactive) process on collision energy is, in general, determined by the potential curves for the initial and final states and by what occurs in getting the system from the first of these to the second. In a full analysis of the problem, one would have to consider the perturbations on these potential curves due to interactions with each other or with some other curve which provides coupling between them, as well as the fact that the probabilities of making transitions between curves are themselves, in general, dependent on energy.

In the case in which the coupling between the initial and final states is strong, however, it might be expected that the predominant influence on the energy dependence would be the long-range forces, i.e.,

the unperturbed potential curve, in the incoming channel, as the strong coupling would provide a high probability of exiting in the inelastic (or reactive) channel once some critical region of interaction, as yet undefined, is reached.

There are reasons to believe that this strong coupling situation applies at least to the more efficient quenchers studied here. In the first place, the very fact that the cross sections are large indicates strong coupling of the excited and quenched states. Secondly, molecular beam scattering data[9] on ground state alkali metals indicates such strong coupling in some reactive processes. Namely, the absence of wide-angle elastic scattering indicates that close approach leads to reaction with a high probability. Since the reactive processes involved are generally pictured in terms of the same electron transfer model which is considered to apply to quenching of the excited states, (see Section C of this chapter) one is led to expect similar strong coupling, particularly in view of the much lower ionization potentials of the excited atoms. Finally, calculations which will be discussed in some detail in Section C lend support to the notion of strong coupling. Furthermore, these same calculations, neglecting long-range attractive forces, yielded no significant energy dependence for the calculated cross sections, contrary to experimental observations.

For these reasons, the energy dependence of the cross sections in this study will be considered in terms of the long-range attractive forces between M* and A. One useful way to investigate this relationship is through the classical orbiting model,[10] which has been applied quite extensively in the study of ion-molecule reactions.[11] In this model,

the effective potential, U, is obtained by adding the angular energy of the colliding pair, $L^2/2\mu r^2$, to the true potential energy, which is assumed to be dominated by a single term of the form $V(r) = -C_s/r^s$, $s > 2$. The angular momentum of the colliding pair, L, is given by μgb, where g is the "asymptotic" relative speed, that is the relative speed at distances large enough that V(r) is not appreciable, and b is the impact parameter for the collision, which is the distance of closest approach in the absence of any interaction.

The angular energy provides a "centrifugal barrier" in U, and conservation of energy provides a path to calculating which incoming trajectories get inside this barrier. The situation is depicted in Fig. IV-2, where U is shown for a given value of collision energy $E = \mu g^2/2$, and three different impact parameters. The turning points of the corresponding three trajectories are indicated by the arrow heads. What happens is that at a given energy, since the angular energy term grows as b^2, an impact parameter is reached beyond which the centrifugal barrier prevents close approach. The critical orbiting trajectory for a given energy, defined by E and $b_o(E)$, is the one which "orbits", i.e., has its turning point precisely at the top of the barrier in the effective potential (point B in Fig. IV-2). The orbiting distance, $r_o(E)$ is given by

$$r_o(E) = [(s - 2)\ C_s/2E]^{1/s} \tag{34}$$

and the height of the barrier, $U[r_o(E)]$, by

$$U_o = (Eb^2/2)^{s/(s-2)}\ (1/sC_s)^{2/(s-2)}\ (1/2 - 1/s) \tag{35}$$

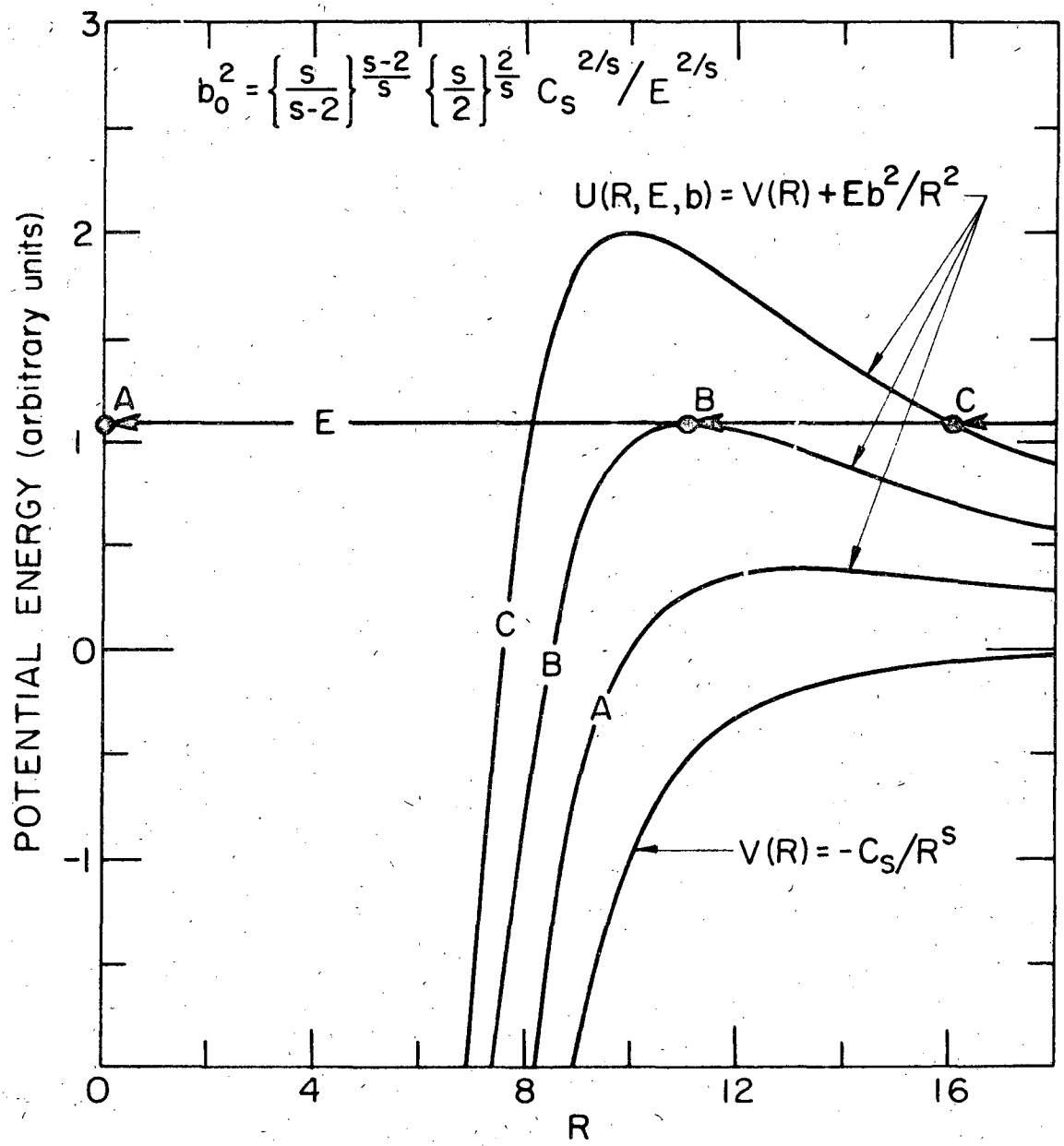

XBL 7110-7441

Fig. IV-2. The effect of the "centrifugal barrier" for collision energy $E = \mu g^2/2$ and various impact parameters, b. The orbiting impact parameter, b_o, corresponds to the turning point at B. Smaller impact parameters allow close approach (A), and larger impact parameters give turning points outside the position of the relative maximum in the effective potential (C).

Equating collision energy to the height of the barrier, provides an expression for b_o, the maximum impact parameter which will allow close approach at a given energy. This expression is given on Fig. IV-2. From it can be calculated directly the close approach cross section, Q_c, in terms of g and the potential power law constant, C_s.

$$Q_c(g) = K_s(\text{theor})/g^{4/s}$$

$$K_s(\text{theor}) = \pi[s/(s-2)]^{(s-2)/s}\,(s/\mu)^{2/s}\,C_s^{2/s}/g^{4/s} \qquad (36)$$

In applying this model to the investigation of the quenching cross sections, the implicit assumption is that "close approach" i.e., penetration to the repulsive wall of the potential or into some kind of trajectory sink, is necessary for a quenching collision to occur. It is further assumed that a constant fraction, w, of trajectories which achieve close approach lead to quenching, thus Q_q should depend on g in the same way as does Q_c. The orbiting model provides a very convenient method of parameterizing the energy dependence of the cross sections, and of comparing quenching efficiencies of various molecules, although it is to be emphasized that it is a highly simplified picture of a process which, in full physical reality, must be very complicated indeed.

In cases where k_q values were measured at several different energies, the form of $Q_q(g)$ was investigated by letting s = 4, 5 or 6, and finding the value of the coefficient $K_s(\text{exp})$, which gave the best fit to the experimental data when $K_s(\text{exp})/g^{4/s}$ was put into Eq. (33) and integrated over the appropriate relative speed distributions. This cross section constant can be compared to the theoretical close

approach cross section constant, K_s(theor). In particular, $K_s(\text{exp})/K_s(\text{theor}) = w$, and this ratio can be considered as a possible measure of quenching efficiency, as it gives the fraction of close collisions which lead to quenching.

For cases in which a rate constant was measured at only one energy, less information about Q_q vs g could be determined. One could only assume a value of s, and then find the value of K_s(exp) which corresponded to the experimental rate constant. Mostly, these were thermal cases, for which the integral in Eq. (33) can be evaluated analytically to give

$$k_q(\text{thermal}) = 2\pi^{-1/2} \, (\mu/2kT)^{(4-s)/2s} \, (s-2/2) \, \Gamma(s-2/2) \, K_s(\text{exp}) \qquad (37)$$

where $\Gamma(x)$ is the gamma function.[12] As before, the ratio $K_s(\text{exp})/K_s(\text{theor}) = w$ provides, within this model, a measure of the quenching efficiency.

Of course, the orbiting model is not the only approach to analyzing the energy dependence of cross sections. As already indicated, the close approach cross section, Q_c, includes all trajectories which get past the centrifugal barrier and penetrate to the inner repulsive wall of the effective potential. Especially for high values of collision energy, corresponding to small orbiting distances, from Eq. (34), this requirement may be too strict. In particular, one might wish to specify some minimum distance of closest approach, r_m, which is regarded as necessary to the possibility of a quenching collision. The expression for the turning point of a trajectory, which again is directly from conservation of energy, yields, for the cross section as a function of energy in this case,[10]

$$Q_m = r_m^2(1 - V(r_m)/E) \tag{38}$$

References 13 and 14 have, in fact used this idea in interpreting the energy dependence of the quenching of $Na^*(3p^2P)$ by N_2. In particular, they have attempted to introduce energy dependence into some theoretical calculations on this system, which will be discussed in the Quenching Theory section of this chapter.

Referring again to Fig. IV-2, it can be seen that if $r_m > r_o$ for a given E, the value of the impact parameter, b_m, which gives a turning point at r_m, and which corresponds to the critical trajectory in this case, will be greater than b_o: $b_m > b_o$, therefore $Q_m > Q_c$. However, for a given E, if $r_m < r_o$, there is no turning point short of the repulsive wall, so here orbiting must apply. In fact, the expression for the turning point yields complex values in this region, so Eq. (38) is strictly invalid. Thus, if one wishes to specify r_m as a basis for analyzing energy dependence, one should use Eq. (38) for energies such that $r_o(E) < r_m$, and Eq. (36) for energies such that $r_o(E) > r_m$. The energy, E_c, at which the orbiting and minimum distance models must coincide is clearly that for which $r_o = r_m$, and this gives, from Eq. (34)

$$E_c = (s - 2)\ C_s/2r_m^2 \tag{39}$$

and the value of the cross section at this energy is

$$Q_c(E_c) = Q_m(E_c) = \pi r_m^2 [s/(s - 2)] \tag{40}$$

The primary difficulty with the minimum distance model is the necessity of specifying r_m. As quenching of excited alkali atoms is generally considered to proceed via the transfer of the M* electron

to the quenching molecule, one choice would be the distance at which the excited covalent potential curve (for $M^* + A$) crosses the ionic potential curve (for $M^+ + A^-$). The use of this curve-crossing distance for the value of r_m would then yield a theoretical expression for the cross section as a function of energy which would have to be mated to the close approach cross section of the orbiting model at E_c, from Eq. (39) to get the overall theoretical dependence of the cross section on energy. If one then wished to fit experimental results to this combined model, one would be required in general to specify two parameters, rather than the single K_s(exp) of the orbiting model. Referring to Eq. (38) for Q_m, one can see that the two parameters would be a value for the energy independent term, which might be obtained from high energy extrapolation of the data, and a value for the coefficient of the energy term, which would, in general, be independent of the first parameter for the experimental cross sections. Any interpretation in terms of quenching efficiency would become rather cloudy. Moreover, analysis in terms of the orbiting model provides some insight into quenching efficiency even in those cases where the model is not expected to apply. Some such cases arise when the electron affinity of the quenching gas is large enough that the distance at which the ionic and covalent potential terms cross, which is where electron transfer should be most likely, is well outside the range of orbiting distances which occur in these experiments (~3.5-5 Å for the for the first resonance states). This is true for SO_2, I_2 and Br_2, and the result is that, in terms of the orbiting model, these gases are "super-efficient" quenchers, i.e., $w > 1$. However, even here, the energy dependence of the cross sections

is such that the orbiting model provides a very convenient method of deconvoluting the experimental data.

With $K^*(5p\,^2P)$, for which most measurements were done under thermal conditions, the orbiting distance at the energy corresponding to the most probable thermal speed in a collision with a typical gas (polarizability ~5Å^3) is ~6.5 Å, and the crossing distances for gases with small positive or negative electron affinities are ~10Å. Furthermore, if the polarizability of 1100Å^3 (Ref. 15) is regarded, roughly, as representing the effective volume occupied by the excited electron, then the corresponding radius is ~7Å, and it might be expected that if the collision penetrates to this distance, the interaction would be altered greatly and the orbiting model might lose its significance. Even here, however, quenching efficiencies will be discussed in terms of the orbiting model, for the reasons indicated above, as well as for the fact that it provides, a posteriori, quite interesting and seemingly reasonable comparisons to quenching efficiencies for the first reasonance states.

In Chapter V, then, the orbiting model will be used to fit the energy dependence of the experimental results and to investigate efficiencies for all quenchers studied. For the three superefficient quenchers, rough estimates in terms of a minimum distance model will also be made. This is done with the awareness of the limitations of models, particularly of the orbiting model in the case of $K^*(5p\,^2P)$.

3. Decay of the Speed Distributions

The $P_{T,\lambda}(g)$ distributions used in analyzing the non-thermal data involve the nascient $P_{T,\lambda}(V)$ distributions, derived in Chapter III. The latter are idealized, as the real steady-state speed distributions for the excited atoms will vary at least slightly from them, due to perturbations deriving from interaction with other species present in the fluorescence cell. The problem of just how $P_{T,\lambda}(V)$ relaxes is a complicated one, and here it will suffice to indicate approximately to what extent one might expect this distribution to be perturbed under a given set of experimental conditions.[8c]

The time interval of concern is simply the lifetime of the excited population, so it is instructive to consider what values of impact parameters, b_r, for elastic collisions will lead to a rate for such collisions equal to the rate of decay of the excited population, and to discern approximately what effect collisions at such impact parameters will have on the speed of the excited atom. In the regime of low quenching gas pressure, the lifetime of the excited population is approximately given by the natural radiative lifetime, so the rate of decay for $K^*(4p^2P)$ or $Na^*(3p^2P)$ will be approximately 5×10^7 sec^{-1}. If the elastic collision rate, $k_r N_A = g\pi b_r^2 N_A$, is to equal this at a pressure of A of, say, 1 Torr, $b_r \approx 10$ -14Å. At such large impact parameters, collisions will be quite soft, and the small angle formula for the classical angle of deflection, χ, can be used.

$$\chi \approx 15\pi C_6/8\mu g^2 b^6 \tag{41}$$

C_6 is just the potential power law constant for the dispersion attraction, which will be discussed in the next section. Taking, for the present, a value of 10^{-57} erg-cm^6, a typical value for K*(4p^{2}P) or Na*(3p^{2}P) with one of the quenching gases studied here, χ is found to be <0.5° for these collisions. In order to assess the effect of such collisions on the speed of the excited atom, one can assume that the two velocities intersect at right angles and assign to the quenching gas its most probable thermal speed. Then, for small deflection angles, the fractional perturbation in V can be expressed approximately as

$$|\Delta V/V| = \chi[m_A/(m_A + m_M)](\bar{v}_A/V) \tag{42}$$

and this relation gives perturbations of less than 0.5% for the soft collisions under consideration.

At higher quenching gas pressures, larger perturbations will be expected. Considering the lifetime of the excited population here to be dominated by the quenching term, $k_q N_A$, the requirement that the rate of elastic collisions be equal to this can be expressed as $Q_r = Q_q$, where Q_r is an elastic cross section. Taking the maximum quenching impact parameter, b_q, as $Q_q = \pi b_q^2$, and reserving impact parameters smaller than this for inelastic collisions, it is found that $b_r = \sqrt{2} b_q$ will satisfy $Q_r = Q_q$. Taking a value of $Q_q = 75$ Å^2 as exemplary, the approximate formulas of Eqs. (41) and (42) suggest $\chi \approx 3°$ and $|\Delta V/V| \approx 1$-2%.

Of course, in either the high or low pressure regime, M* atoms will suffer elastic collisions at impact parameters both larger and smaller than those discussed here. The probability of suffering a collision at an impact parameter b_r varies as b_r^2. Thus, the smaller impact parameters, which would perturb V more seriously, become rapidly

less probable, and are also more likely to result in quenching collisions. Likewise, larger impact parameter collisions become rapidly more probable but also have a much smaller effect on V, so the typical values which were quoted probably give a good idea of the extent to which V will be perturbed. However, even if these estimates are off by a factor of 2 or 3, the uncertainty in the speed distributions will be no greater than the uncertainty in the experimental results. These arguments do indicate that for gases such as CH_3OH, with quenching cross sections $\lesssim 20Å^2$, very considerable relaxation of the speed distributions will probably occur at gas pressures high enough to produce significant quenching.

4. Long-Range Forces

As mentioned above, values of the potential power law exponent s, of 4, 5 and 6 were considered. These values correspond to various interactions between the excited atoms and quenching molecules which might be important here. A value of s = 4 corresponds to the electrostatic dipole-quadrupole interaction. The orientation average of this interaction would be zero however, except with molecules possessing permanent dipole moments with respect to a lab coordinate system, namely symmetric top molecules with rotation about the symmetry axis excited. The only polar symmetric top molecules studied were CF_3Cl and CH_3CN. Of these two species, only CH_3CN showed quenching behavior which might suggest the importance of the r^{-4} interaction. From Eq. (33), it is seen that if $Q \propto g^{-1}$, corresponding

to s = 4, k_q will be independent of energy, and this seemed to be the case for CH_3CN. As s goes to larger values, the tendency of k_q to decrease with increasing collision energy becomes more pronounced, and CF_3Cl, like most of the quenchers, showed a decrease of k_q with increasing collision energy. This is somewhat surprising, as CH_3CN, though it does possess the largest dipole moment of any quencher studied, is so prolate that extremely high rotational energies would be required to maintain a space-fixed dipole moment.

A value of s = 5 corresponds to the quadrupole-quadrupole interaction, and most of the quenching gases studied here have quadrupole moments, so this term would be expected to contribute to the potential energy.

A value of s = 6 corresponds to the classical dipole-induced dipole interaction, and to the non-classical dispersion interaction. For all quenchers considered here, the second of these two interactions is considerably larger than the first, so the r^{-6} interaction between the excited atoms and quenching gas molecules will be discussed in terms of dispersion forces. The notable cases in which the inductive interactions are greater than the dispersion interactions are the M*-MX pairs. The inductive term goes as the square of the dipole moment, and the very large dipole moments of the alkali halides make this term dominant, with the result that the orbiting model suggests that the cross section for MX quenching M* is generally somewhat greater than quenching cross sections for other molecules. Thus it is necessary to maintain low alkali halide vapor pressures if such "self-quenching" is to be avoided.

In order to obtain a comparison between K_s(exp) and K_s(theor) for a given case, it is necessary to calculate K_s(theor), via C_s, the potential power law constant. This involves, in the case of the electrostatic interaction which might be of general interest here, a knowledge of the quadrupole moment of the excited atom, or at least of the value of $\langle r^2 \rangle$. Such information is not readily available, although, as indicated below, it might be susceptible to fairly accurate calculation. If it were obtained, however, it would still be a non-trivial problem to evaluate the interaction in terms of the atomic and molecular moments in a given case.

The situation in the case of the dispersion interaction is somewhat brighter. There are several well-known approximations which give simple expressions for C_6 in terms of the polarizabilities of the interacting species, perhaps the most successful of which is that due to Slater and Kirkwood,[16,17] which is used throughout this study. According to this approximation

$$C_6 = (3e\hbar/2m_e)\ \alpha_1\alpha_2/[(\alpha_1/N_1)^{1/2} + (\alpha_2/N_2)^{1/2}] \qquad (43)$$

where α_1 and α_2 are the polarizabilities, N_1 and N_2 are the numbers of electrons in the outermost shells, and e, $\hbar$, and m_e are the obvious physical constants. Furthermore, an excellent compilation of the polarizabilities of alkali metal atoms in their ^2P states has been provided by Schmieder, et al.[15] They used the method developed by Bates and Damgaard[18] to evaluate the necessary r-integrals for S-P and P-D transitions. This method uses the notion that the important contribution to the integral comes at distances large enough that the

potential energy on the p-electron has its asymptotic coulomb form. This potential is put into the Shroedinger equation, and the asymptotic solutions for the radial wavefunctions are used to evaluate the integrals. Bates and Damgaard applied this method to the calculation of transition probabilities, obtaining quite good agreement with experimental values for alkali metals. Likewise, the results of Ref. 15 for polarizabilities generally agree very well with the experimental values, where the latter are available. The polarizability is expressed as a sum of scalar and tensor components

$$\alpha(m_J) = \alpha_0 + \alpha_2[3m_J^2 - J(J + 1)]/J(2J + 1) \tag{44}$$

and a table of values of the α_0's and α_1's is given. As the former is approximately 10 times greater than the latter for a given case, the tensor component and the resulting slight anisotropies in the total polarizabilities have been neglected here, and the values of α_0 have been used as the polarizabilities of the excited atoms.

One very interesting fact arises from these results. In examining the table in Ref. 15 of contributions to the polarizability (r-integrals divided by energy separations), it is apparent that the value of the polarizability in a given case is usually dominated by a single contribution corresponding to a transition to the closest-lying D state. In the case of Na*($4p^2P$), the 3d state lies just below the 4p, so the polarizability takes on a large negative value. This should lead to a repulsive dispersion interaction, and attempts were made to do experiments on this state to try to see effects attributable to this. Unfortunately, these attempts did not meet with success, as the

oft-mentioned problem of uv intensity at low wavelengths once again came to the fore.

Given the values for the polarizabilities of the excited atoms, it is straightforward to calculate C_6, and hence K_6(theor). It would be nice to be able to at least get an idea of the magnitude of the magnitude of C_5, so that the two contributions to the potential energy could be compared. Since the method of Bates and Damgaard works so well for integrals involving the first power of r, it would presumably provide an excellent approximation for those involving the second power of r, or of its components. In particular, it should be very good for calculating $\langle 3Z^2 - r^2 \rangle$, the quadrupole moment of the atom.[19] However, as there are no experimental values with which the results of such calculations might be compared, there has apparently not been sufficient incentive to do them. Also, as mentioned, evaluation of the interaction energy, given the quadrupole moments, is a fairly complicated problem. Knipp,[20] for example, has treated the case of two atoms. The interaction vanishes in zero order, i.e., the trace of the interaction matrix is zero, corresponding to a zero orientation average. However, consideration of the off-diagonal elements via first-order perturbation theory leads to expressions for the interaction energy which differ according to the magnitudes of the l-s coupling in the two atoms, and which involve three "parts," two atomic coefficients, the root of a secular determinant, and values of $\langle r^2 \rangle$ for the two atoms. His results are tabulated for several cases and are also found in Hirschfelder, Curtis and Bird.[19] He finds interaction energies for ground state atoms of ~0.1-0.6 eV at separations equal to twice the

sum of the atomic radii. Use of the atomic polarizabilities from Ref. 21 and the Slater-Kirkwood approximation gives values of the dispersion energy a bit larger than those of the quadrupole interaction calculated by Knipp at the same distances. For example, Knipp's values for O-O at 1.8Å, F-F at 1.54Å, and O-F at 1.67Å are: -0.34 eV, -0.4 eV and -0.55 eV, respectively, while the corresponding dispersion energies are approximately -0.4 eV, -0.7 eV and -0.6 eV. Admittedly the dispersion interaction falls off more rapidly for larger distances than does the quadrupole-quadrupole interaction. It might be noted that the weakest point of Knipp's results are the values of $\langle r^2 \rangle$, and these values are just what one might be able to obtain quite accurately for excited alkalis.

Margenau[22] has indicated that for excited atoms or molecules the dispersion energy is considerably greater than the quadrupole energy. For the experimental cases here, an attempt was made to estimate some quadrupole interactions by using M* quadrupole moments calculated from the hydrogen atom formula using an effective nuclear charge derived from Slater's rules. The result indicated a value for the quadrupole moment of $Na^*(3p^2P)$ of $\sim 20\times10^{-26}$ esu-cm^2. This, combined with a typical molecular value of $\sim 3\times10^{-26}$ esu-cm^2, allowed a very rough estimate of the magnitude of the quadrupole-quadrupole interaction as simply the product of these values divided by the fifth power of the separation. The values thus obtained were compared to dispersion energies for $Na^*(3p^2P)$ with a gas of polarizability 5Å^3. The result was that the two energies were approximately equal at a separation of ~20Å, so the dispersion interaction was greater inside this distance.

The same process for $K^*(4p^2P)$ yielded a quadrupole moment of $\sim 50\times10^{-26}$ esu-cm^2. As the polarizability increased only by a factor of two, and the dispersion energy as the square root of this, it appeared that the quadrupole energy would dominate at distances greater than ~10 Å. It should be mentioned that the relationship of values for the quadrupole energy indicated here to the true interaction energy is not really clear. The relative magnitudes for $Na^*(3p^2P)$ and $K^*(4p^2P)$ should be reasonable, but the absolute magnitudes may differ considerably from reality.

Finally, in considering this comparison, if the results of Chapter V may be anticipated, it might be noted that for the quenching of $Na^*(3p^2P)$, for which the most reliable results were obtained, the best fit to the data was generally obtained with s = 6, except for the case of CH_3CN, as previously noted. This should be regarded cautiously, however, as the s = 5 fits were usually adequate, though not quite as good.

Summarizing the considerations of long-range forces in this study: The r^{-4} contribution might arise in a few cases, and may have experimental support in one case. Values of K_4(exp) will be found for all energy-dependent measurements, however. The r^{-5} contribution is likely comparable to or smaller than the dispersion contribution, but the only consideration given it will be to find values of K_5(exp) for the energy-dependent results, as its accurate treatment is felt to be beyond the scope of this work. The r^{-6} dispersion interaction will be assumed to dominate the scene, and comparisons will be made between K_6(exp) and K_6(theor) to investigate quenching efficiency in terms of the orbiting model.

C. Theory of Quenching

If long-range forces are considered in this study as dominating the energy dependence of cross sections, which is relatively easily measured, the "efficiency" of quenching by a given species, which is harder to get a handle on experimentally, is determined by what occurs after the excited atom and quenching molecule reach "close approach." That is, there must exist a mechanism for dissipating the excitation energy if quenching is to occur. This mechanism, in the case of alkali atoms, has generally been considered to involve an ionic intermediate which couples the initial and final covalent states of the atom-molecule system, providing a path by which the system goes from the excited to the ground (quenched) state. Among the first to recognize the importance of this mechanism was Laidler,[23] who applied the idea to quenching of $Na^*(3p^2P)$ by H_2 and halogens. The schematic potential curves of Fig. IV-3 illustrate the process. (Such curves are, in fact, appropriate to atom-atom encounters.) M* and A approach along the upper covalent curve, and at the outer crossing point R_o, may make a transition to the ionic curve, the possibility of which is indicated by the dashed lines, whence they proceed as $M^+ + A^-$ to the inner crossing point R_i. Here another transition may occur or not, and in either case the pair may oscillate in the well until eventually separating along the M + A curve (quenching collision) or the M* + A curve (elastic collision). For very highly excited states, and collisions of sufficient energy, separation into ions would also have to be considered, but will not be discussed further here. The solid

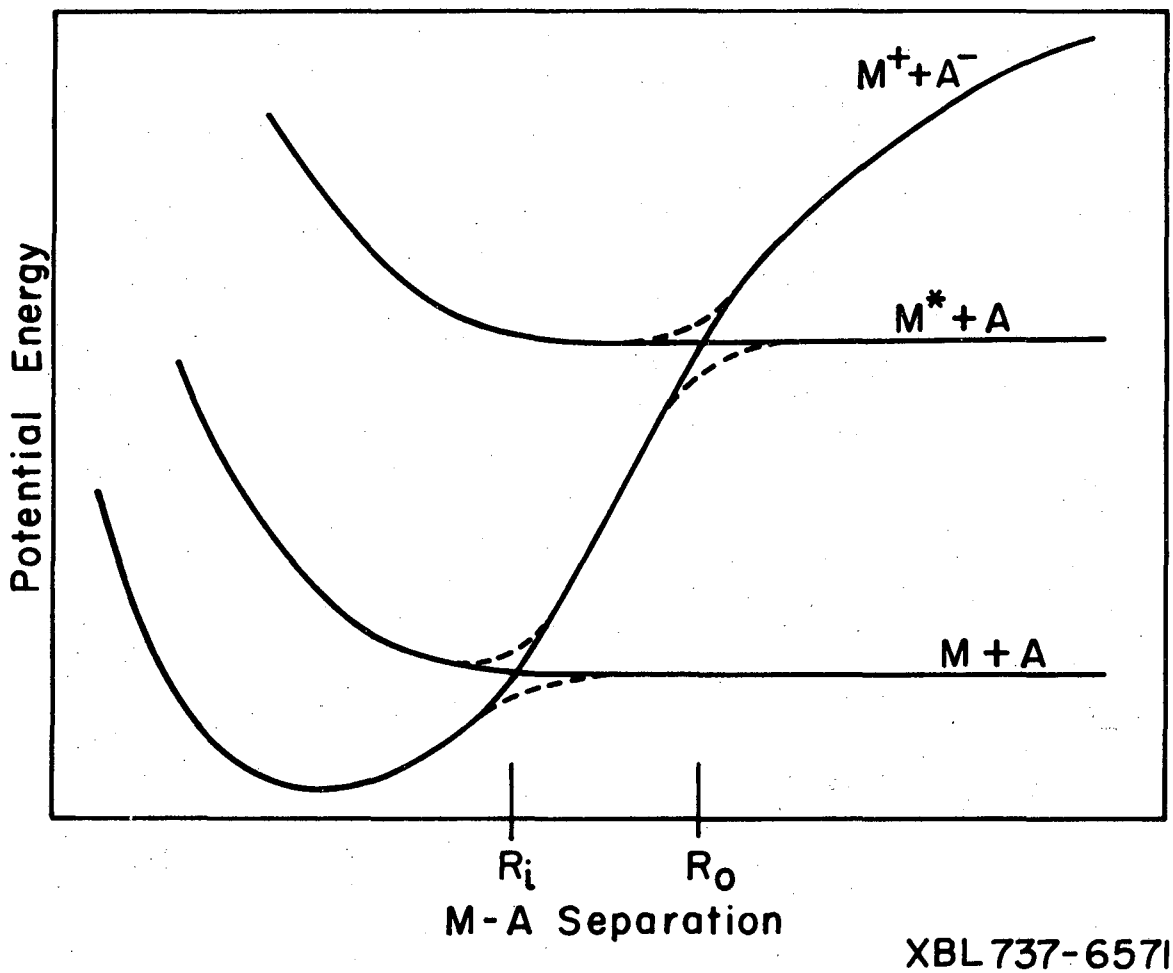

Fig. IV-3. Schematic potential curves illustrating the covalent-ionic curve-crossing picture of quenching. The solid lines represent the diabatic covalent or ionic curves. The dashed lines represent adiabatic transitions from covalent to ionic or vice versa, which arise because of interaction between the diabatic terms.

curves displayed in Fig. IV-3 are the zero-order diabatic curves, that is, the interaction between electronic terms is neglected. It is just this interaction which couples the curves, allowing for the possibility of "adiabatic" transitions from one curve to another.

The problems involved in doing decent calculations on this kind of process are certainly considerable, and, indeed, may even be greater than the problems involved in doing the experiments. The approach which has been taken in recent years in attempts to generate quantitatively acceptable results is to calculate classical trajectories along the diabatic electronic terms, while using the Landau-Zener formula or some more sophisticated relative[24] in order to calculate the probabilities of transitions from one term to another at or near the crossing points.

Calculations on quenching (or, more precisely, lack of quenching) by noble gases are, in this method, fairly simple, but are not very interesting because of the essentially negative nature of the results. Calculations on quenching by molecules are necessarily more complicated than curves such as those of Fig. IV-3 can indicate. In the most realistic case, one must consider three-dimensional potential surfaces. Nikitin and Bjerre[25] have done calculations on quenching of $Na^*(3p\,^2P)$ by N_2 using three such surfaces, two covalent and one ionic, and estimating the transition matrix elements from experimental data on resonance scattering of slow electrons from N_2. These matrix elements were plugged into the Landau-Zener formula to calculate crossing probabilities. As the outer crossing distance was adjusted to match the experimental quenching cross section, the results of interest are in terms of partial cross sections for each vibrational level of the outgoing N_2

molecule. These indicated high populations in v = 2 and v = 3, which is significant, if correct, as it would indicate that electronic-vibrational resonance is not important in the quenching process, the excitation energy of $Na^*(3p^2P)$ being sufficient to excite v = 8.

A series of calculations which seem more satisfying in that the adjustability of the quenching cross-sections is somewhat restricted have been done in recent years by Fisher and Bauer and their co-workers[26] on quenching of several excited alkalis by N_2 and of $Na^*(3p^2P)$ by CO and O_2 as well. They have restricted their calculations to two dimensions, however, by averaging the M*-A interactions over orientations of the diatomic, so that the trajectories proceed on curves rather than surfaces. To account for vibrational excitation of the diatomic, the ionic and lower covalent curves were each replaced by a family of curves generated by displacements of the v = 0 curves by amounts equal to vibrational quanta of the diatomic. This introduced a complex series of crossings, and at each point the adiabatic transition probability was calculated by inserting into the Landau-Zener formula a transition matrix element which was a product of an electronic term and a vibrational term (Franck-Condon factor). The electronic terms were taken from a correlation, due to Hasted and Chong,[27] between the value of the transition matrix element and the distance of crossing, and the Franck-Condon factors were derived from spectroscopic data. Using these transition probabilities, summation over all possible paths along the network of curves was done in order to generate partial cross sections for each vibrational level of the outgoing diatomic molecule.

The covalent potentials were taken from the O + N_2 interaction and

were simple exponential repulsive terms. The ionic curves were taken as sums of a coulomb term plus a polarizability term, $-e^2\alpha/2R^4$, where α is the polarizability of the ionic complex. This quantity was the one arbitrary parameter in the calculations. It was generally adjusted to fit experimental values, but over a reasonable range it did not make a drastic difference in the results. In the $Na^*(3p^2P) - N_2$ case, for example, $\alpha = 10Å^3$ gave $Q_q = 26Å^2$,[26a] and $\alpha = 40Å^3$ gave $Q_q = 40Å^2$.[26b] Experimental results generally fall in the range bracketed by these two values, although favoring the smaller side.

The calculations of partial cross sections indicated, as did those of Nikitin, a lack of importance of electronic-vibrational resonance. For instance, in the $Na^*(3p^2P) - N_2$ case the greatest vibrational populations in the outgoing channel were in v = 3, 4, 5 and 6. However, the vibrational excitation is considered as being produced solely by the electronic-vibrational coupling introduced by the inclusion of the Franck-Condon factors in the transition matrix elements, and possible effects of translational-vibrational energy transfer are neglected. For a system which comes together on a very steep ionic curve and slams into the repulsive wall with relative translational energy up to ~2 eV, translational-vibrational energy transfer might well be significant. In fact, the calculations of Nikitin and Bjerre indicate this, as they contained no <u>ad hoc</u> electronic-vibrational coupling, and yet produced significant vibrational excitation.

The Fisher-Bauer calculations were done for collision energies corresponding to temperatures achieved in flame studies, and their results generally agree quite well with experimental quenching cross

sections, although there is apparently no data on vibrational populations in molecules following quenching. The importance of electronic-vibrational coupling in the $Na^*(3p^2P) - N_2$ system has been demonstrated, however, for the "inverse" process of excitation of sodium atoms by vibrationally hot N_2.[28] The values of total quenching cross sections are predominantly a function of the outer crossing distances, as the probability that a trajectory which reaches the outer crossing distance on the incoming path will lead to quenching, which might be regarded as a quenching efficiency, is generally in the range 0.7-0.8. Thus the value of the quenching cross section depends primarily on the choice for the electron affinity of the diatomic, and secondarily on the fitting parameter, α. Given a value for the electron affinity of N_2 of -1.89 eV, which is what was used, the outer crossing distance for $\alpha = 10Å^2$, is at about 3.3Å, and this alone would indicate a cross section for reaching this distance in the absence of any attractive forces of $35Å^2$, which would lead to the expectation of Q_q being perhaps $20-25Å^2$, not at all in bad agreement with experimental results. If attractive forces were introduced, larger Q_q values would be calculated.

The neglect of attractive forces leads to one result which is in contrast to experimental evidence on most systems. This is that the calculated cross sections are essentially independent of initial collision energy. This lack is just what Refs. 13 and 14 have attempted to remedy, as mentioned earlier, by introducing an attractive potential in a minimum distance model. Reference 14, using $r_m = \sim 3.5Å$, and extrapolating the Fischer-Bauer results to lower energies, achieves a good fit to the experimental cross-sections over a wide energy range.

It should be emphasized that neither Reference 13 or 14 employed the attractive forces directly in doing trajectory calculations, but merely tried to correct the Fischer-Bauer results by assuming that they were essentially correct for high energies and using the attractive forces after the fact to achieve agreement for lower energies. What one would like to see is a full trajectory calculation with the attractive forces introduced in the construction of the initial potential curves or surfaces. Since these calculations were not really for extremely high collision energies (values between 0.1 and 0.2 eV were used), one would expect that this would lead to considerably larger calculated cross sections.

This hopefully describes briefly the present state of calculations on quenching of alkali atoms. There are many effects which might be regarded as influencing quenching efficiency for which calculations have not been done and, indeed, may not be currently feasible. This model of the quenching process, however, provides a good basis for discussing some of these effects, and indeed, the calculations described point the way in a couple of instances.

One thing which might enhance the quenching efficiency of a given molecule is the availability of more than one channel corresponding to quenching. The calculations on $Na^*(3p^2P) - O_2$ indicate this rather strongly. O_2 has three electronic states which are energetically accessible in the quenching process, and which can be reached via two intermediate $Na^+O_2^-$ states, all six paths being spin-allowed. Thus there would appear on a simplified potential curve diagram such as Fig. IV-3 two ionic curves and three outgoing covalent curves. These

excited electronic states of the quenching molecule not only provide a very convenient means of dissipating the excitation energy but also provide additional paths to quenching , so they should provide both energetic and statistical enhancement of the quenching efficiency. Preliminary calculations which accounted for only one quenching path yielded a value for the quenching cross sections ~4 times smaller than the experimental value.[26a]

A similar situation which would provide an additional quenched channel is chemical reaction. That is, if the quenching molecule is represented as AB, there would be two outgoing covalent curves, one for M + AB, and one for MB + A. This would again provide an extremely efficient mechanism for dissipation of the excitation energy, and would presumably become more probable as the asymptotic energy separation between the M* + AB curve and the MB + A curve, i.e., the reaction exoergicity, became larger. The idea that the large exoergicity for some such processes would lead to reaction with low activation energy, corresponding to high reaction probability and thus to large quenching efficiency, has been advanced previously,[8c,29] and will be considered for several of the quenching processes to be discussed in Chapter V.

The effect of Franck-Condon factors on quenching efficiency will also be considered in interpreting the results presented in Chapter V, namely cross sections for quenching by hydrogen and hydrides vs deuterium and deuterides. In particular, the larger vibrational amplitudes of the hydrogen-containing species should lead to more favorable overlap between the vibrational wavefunctions of the neutral molecule and the negative molecular ion, making an adiabatic transition more probable.

There are various factors which might be regarded as playing a role in quenching efficiency via their effect on the electron affinity of the molecule, which plays a crucial part in getting the colliding pair into an ionic intermediate. A classic example is the contrast, discovered very early in $Na^*(3p^2P)$ quenching studies, between the quenching behavior of saturated and unsaturated organic molecules. The former are very inefficient in quenching this species, and for that matter, first resonance states of other alkalis, presumably because their lowest unfilled molecular orbitals are at such high energies that they are extremely reluctant to accept an electron. On the other hand, the unsaturated molecules, possessing relatively low lying unfilled molecular orbitals, as is the case for ethylene and benzene, to name but two examples, should accept an electron quite easily, thus making the ionic intermediate readily accessible.

REFERENCES

1. O. Stern and M. Vollmer, Phys. Zeit. 20, 183 (1919).
2. (a) D. A. McGillis and L. Krause, Phys. Rev. 153, 44 (1967).
   (b) D. A. McGillis and L. Krause, Cana. J. Phys. 46, 1051 (1968).
3. H. P. Hommayers and P. L. Lijnse, J. Quant. Spectrosc. Radiat. Transfer 9, 995 (1969).
4. N. F. Mott and H. S. W. Massey, The Theory of Atomic Collisions (Clarendon Press, Oxford, 1965), p. 371.
5. F. Masnou-Seeuws and E. Roueff, Chem. Phys. Letters 16, 593 (1962).
6. (a) M. B. Hidalgo and S. Geltman, J. Phys. B: Atom. Molec. Phys. 5, 265 (1972).
   (b) J. F. Papp and F. A. Franz, Phys. Rev. A 5, 1763 (1972).
7. L. B. Loeb, The Kinetic Theory of Gases (McGraw-Hill Book Co., Inc., New York, 1934), p. 102.
8. (a) H. G. Hanson, J. Chem. Phys. 23, 1391 (1955).
   (b) L. E. Brus, J. Chem. Phys. 52, 1716 (1970).
   (c) B. L. Earl, R. R. Herm, S-M. Lin, and C. A. Mims, J. Chem. Phys. 56, 867 (1972).
9. J. L. Kinsey, MTP International Review of Science, Phys. Chem. Series One, Chemical Kinetics, J. C. Polanyi, ed. (Butterworths, London, 1972), Vol. 9, Chap. 6, reviews molecular beam work.
10. H. S. Johnston, Gas Phase Reaction Rate Theory (The Ronald Press Company, New York, 1966), Chapter 7 and 8.
11. A. Henglein, Proceedings of the International School of Physics Enrico Fermi, Course XLIV, Molecular Beams and Reaction Kinetics, Ch. Schlier, ed. (Academic Press, New York, 1970), p. 139.

12. I. S. Gradshteyn and I. M. Ryzhik, Table of Integrals, Series and Products (Academic Press, New York, 1965), p. 935.

13. J. R. Barker and R. E. Weston, Jr., Chem. Phys. Letters 19, 235 (1973).

14. P. L. Lijnse, Chem. Phys. Letters 18, 73 (1973).

15. R. W. Schmieder, A. Lurio and W. Happer, Phys. Rev. A 3, 1209 (1971).

16. (a) J. C. Slater and J. G. Kirkwood, Phys. Rev. 37, 682 (1931).
(b) J. G. Kirkwood, Phys. Zeit. 33, 57 (1932).

17. H. K. Kramer and D. R. Herschbach, J. Chem. Phys. 53, 2792 (1970).

18. D. R. Bates and A. Damgaard, Phil. Trans. Roy. Soc. London 242, 101 (1949).

19. O. Hirschfelder, C. F. Curtiss and R. B. Bird, Molecular Theory of Gases and Liquids (John Wiley and Sons, Inc., New York, 1964), Chapter 13.

20. Julian K. Knipp, Phys. Rev. 53, 734 (1938).

21. A. Dalgarno, Advan. Phys. 11, 281 (1962).

22. H. Margenau, Rev. Mod. Phys. 11, 1 (1939).

23. K. J. Laidler, J. Chem. Phys. 10, 34 (1942).

24. E. E. Nikitin, Disc. Far. Soc. 33, 14 (1962).

25. E. E. Nikitin, Fast Reactions and Primary Processes in Chemical Kinetics, S. Claesson, ed. (Interscience, New York, 1967), p. 165.

26. (a) E. Bauer, E. R. Fisher and F. R. Gilmore, J. Chem. Phys. 51, 4173 (1969).
(b) E. R. Fisher and G. K. Smith, App. Opt. 10, 1803 (1971).
(c) E. R. Fisher and G. K. Smith, Chem. Phys. Letters 13, 448 (1972).

27. J. B. Hasted and A. Y. J. Chong, Proc. Phys. Soc. 80, 441 (1962).

0 0 0 0 3 9 0 7 2 9 9

28. J. E. Mentall, H. F. Krause and W. L. Fite, Disc. Far. Soc. 44, 157 (1967).

29. D. J. Dowling, G. R. H. Jones and E. Warhurst, Trans. Far. Soc. 55, 537 (1959).

V. QUENCHING OF EXCITED ALKALI METALS

A. Introduction

As indicated in Chapter I, one goal of this work was to attempt to develop a general feeling for the type of quenching behavior which might be expected if a given excited alkali atom is exposed to a given quenching gas. Initially, this involved studies on $Na^*(3p\,^2P)$ from NaI. This excited state has been the principle subject of quenching studies among the alkali metals over the years. Still, most of these studies concentrated on small molecules (e.g., H_2, first row diatomics and noble gases). Notable exceptions were the atomic vapor studies of Norrish and Smith,[1] who, in 1940, investigated an impressive variety of organic molecules, and the photodissociation studies of Dowling, et al.[2] Aside from these, there have been photodissociation studies on quenching by I_2 and Br_2.[3]

Still, it was felt that the picture could be clarified by investigation of a few more molecules of "chemical" interest. In this spirit, species which quenched only slightly were not investigated at length, as cross sections of the order of $1Å^2$ were not regarded as interesting, except as a basis for comparison to larger values. Combination of the results on $Na^*(3p\,^2P)$ from NaI led to a tentative separation of prospective quenchers into four classes.[4] Class A included molecules which provided no possibility of a highly exoergic reaction (which might be expected to proceed with low activation energy) with the excited atom, and which possessed large negative electron affinities due to their lowest unfilled molecular orbitals being at very high energies. Examples would be saturated hydrocarbons, CF_4, and possibly H_2O, all very inefficient

quenchers of $Na^*(3p^2P)$. For this class, w, the ratio $K_6(exp)/K_6(theor)$, would be in the range 0-~0.05. Class B included molecules which could not react with $Na^*(3p^2P)$, but which did possess relatively low-lying unfilled molecular orbitals, placing their electron affinities in a range which made electron transfer more favorable than with class A molecules. Molecules in this class, examples of which would be CO_2, C_2H_4 and C_6H_6, were characterized as having quenching efficiencies, w, in the range ~0.2-1.0. Since no exoergic reaction channel was available, the excitation energy in a quenching collision would have to be dissipated as internal excitation of the molecule or as translational energy of separation. In class C were included molecules which, though not highly electronegative, afforded a very exoergic reaction channel. The two examples studied, CF_3Cl and CH_3CN, indicated that w values near unity might be expected for molecules in this class. Finally, the proposed class D included molecules with large positive electron affinities, such as SO_2 and I_2, which might be denoted as super-efficient, since w values larger than one indicated that the orbiting-dispersion forces model failed to account for their quenching ability.

Following the NaI studies, it was desired to extend measurements to other alkali metals, and $K^*(4p^2P)$ from KI proved accessible. Previous studies had provided extensive data on quenching of this atomic state by H_2 and D_2,[5-9] but very little on larger molecules.[10] Quenching by three gases which had been used in the NaI work was studied as a function of energy. These gases represented the last three of the four groups proposed above, and the results seemed to indicate behavior similar to that toward $Na^*(3p^2P)$.

The next experimental step was to go to more highly excited atomic states, on which only one previous study is known, that by the flame technique.[9] Results on quenching by molecules of classes B and C indicated only the expected increases in quenching cross sections. However, the only super-efficient quencher studied with this state and most of the inefficient quenchers provided interesting and sometimes quite unexpected contrasts to what had been observed with the first resonance states. I_2 became an only moderately efficiently quencher, and promotion of very inefficient quenchers to apparently quite efficient status led to considerable investigation of various effects in the quenching of $K^*(5p\,^2P)$.

The results of these studies are presented here, along with discussion on various factors which might influence quenching efficiency and comparisons to other work on quenching of atomic fluorescence.

B. Experiments and Results

1. Quenching of First Resonance States

The general experimental conditions and procedures have been set forth in Chapter II. Discussion of these matters in this chapter will be confined to specific problems relating to particular gases or to experimental checks which were made to investigate possible effects of factors such as polarization or self-quenching. These considerations will be presented following the results.

Figure V-1 and the upper panel of Fig. V-2 show experimental Stern-Vollmer plots for cases which are more or less typical of the quality of the data with the indicated excited atoms. The lines are the linear least-squares fits to the experimental points. Reference

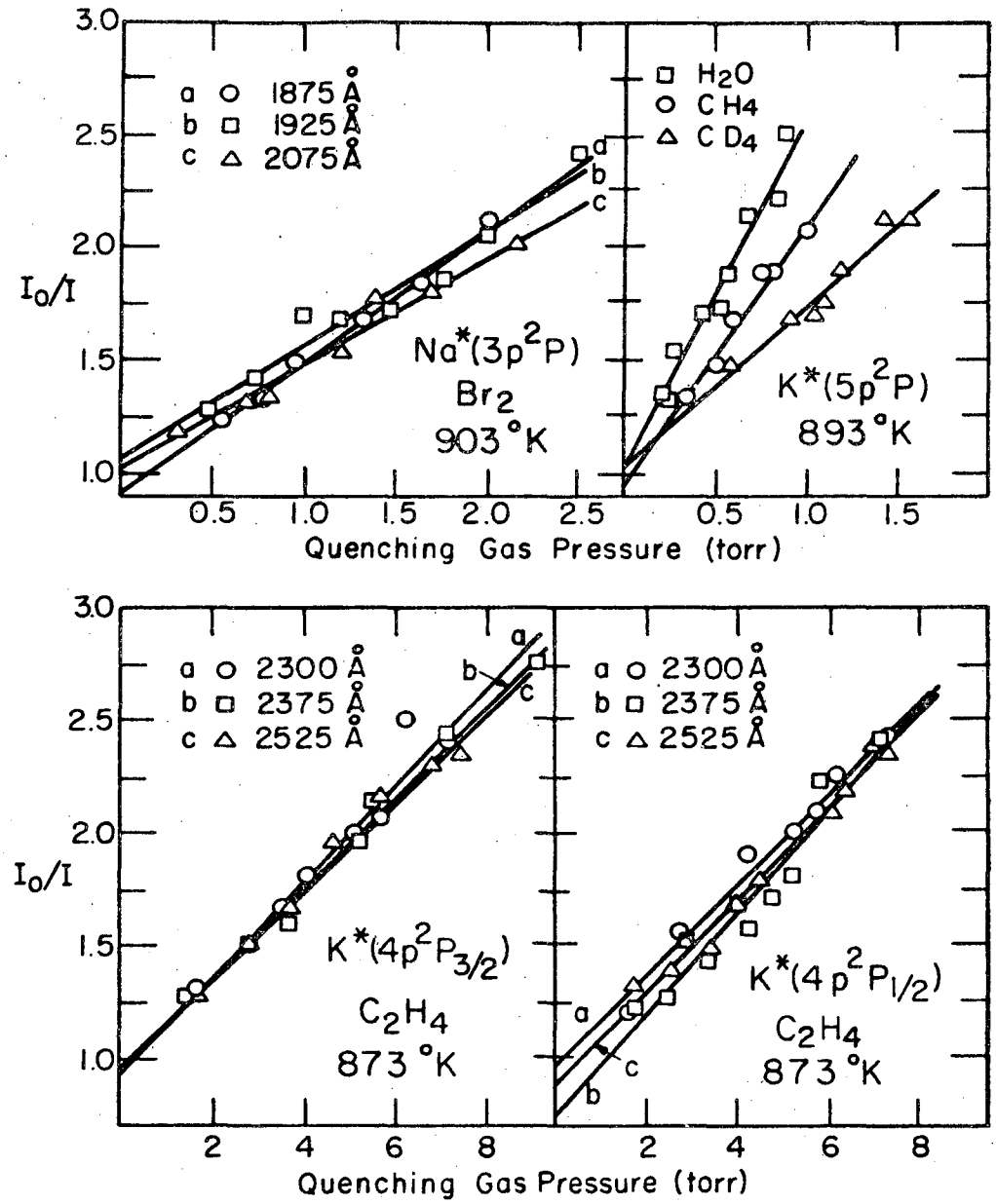

XBL738-1658

Fig. V-1. Stern-Vollmer plots typical of those obtained with $Na^*(3p^2P)$ from NaBr (upper left), $K^*(5p^2P)$ (upper right) and $K^*(4p^2P)$ (lower panels). The bandwidth in each case was 60Å (FWHM). With $K^*(5p^2P)$, the monochromator setting was 1925Å; others were as indicated. The CH_4 and CD_4 data were obtained using thermalization with high pressures of argon. The H_2O data were not thermalized.

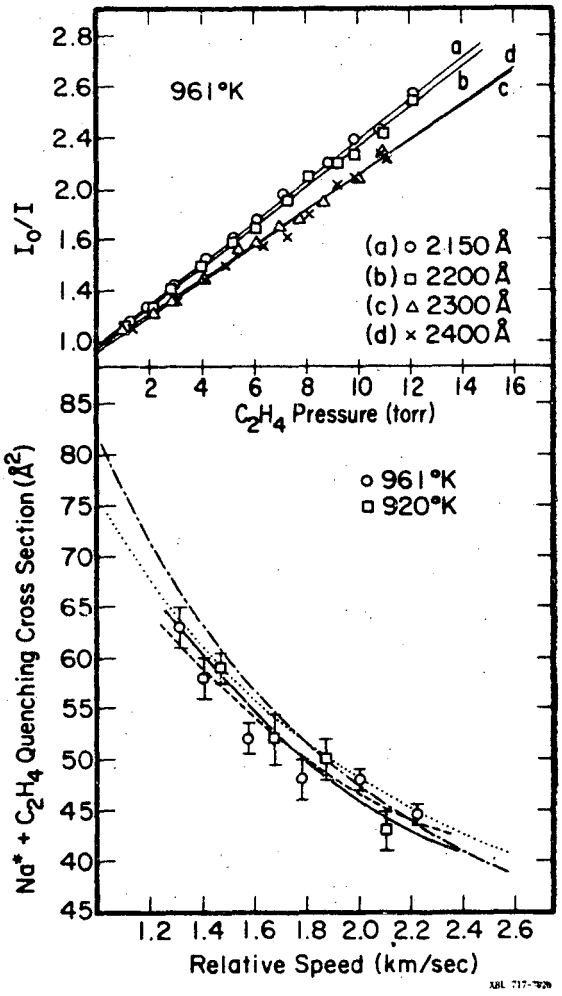

Fig. V-2. Quenching of $Na^*(3p\,^2P)$ from NaI by C_2H_4. The upper panel shows the Stern-Vollmer plots, quite typical of those obtained with this salt-excited atom system. The bandwidth was 48Å (FWHM). The lower panel shows: Quenching data represented by points as phenomenological cross sections, $\langle Q_q \rangle$, at characteristic relative collision speeds, $\langle g \rangle$, from the initial data analysis discussed in Chap. IV; deconvaluted $Q_q(g)$ curves which gave the best fits to the data, upon averaging over the relative speed distributions, if $Q_q(g)$ was assumed to vary as $K_5/g^{4/5}$ (dash-dot-dash) and $K_6/g^{2/3}$ (dot-dot-dot); the fits obtained from these $Q_q(g)$ curves from s = 5 (solid curve) and s = 6 (dashed curve).

to the Stern-Vollmer formula, Eq. (21a) of Chapter IV, indicates that the plots should have unit intercepts on the ordinate. There is generally some deviation from this, and this is one indication of the uncertainties in a given case. One case in Fig. V-1 displays a considerable deviation, and it is to be noted that the scatter of the points is quite large in this case, as well. Quenching rate constants were extracted from the Stern-Vollmer plots using the following values for excited-state lifetimes:[11] $Na^*(3p^2P)$, 1.61×10^{-8}; $K^*(4p^2P)$, 2.70×10^{-8}; $K^*(5p^2P)$, 1.40×10^{-7}, all in units of sec^{-1}.

The lower panel of Fig. V-2 and Figs. V-3 through V-6 display the results of the energy-dependent studies. The points are the phenomenological cross sections, $\langle Q_q \rangle$, at characteristic relative speeds, $\langle g \rangle$, from the first-order analysis of Chapter IV, Eqs. (30) and (31), with one modification of the usual first-order procedure: V_T, the characteristic lab speed of the excited atom as calculated from Eq. (29) of Chapter IV was replaced by the most probable speed as found from the calculated atomic speed distributions.

The error bars on the points represent one standard deviation in the least-squares slopes and do not represent all possible uncertainties in a given case. For instance, absorption of the uv by SO_2 and C_6H_6 in the lower ranges used with NaI added to the uncertainty in these cases. Also, in Fig. V-5, the two highest energy points for quenching of $Na^*(3p^2P)$ by Br_2 are subject to larger uncertainties than the others. This derives from possible ambiguities in the lower wavelength portion of the NaBr fluorescence efficiency curve, particularly from the assumption that only a single process contributed. As indicated in

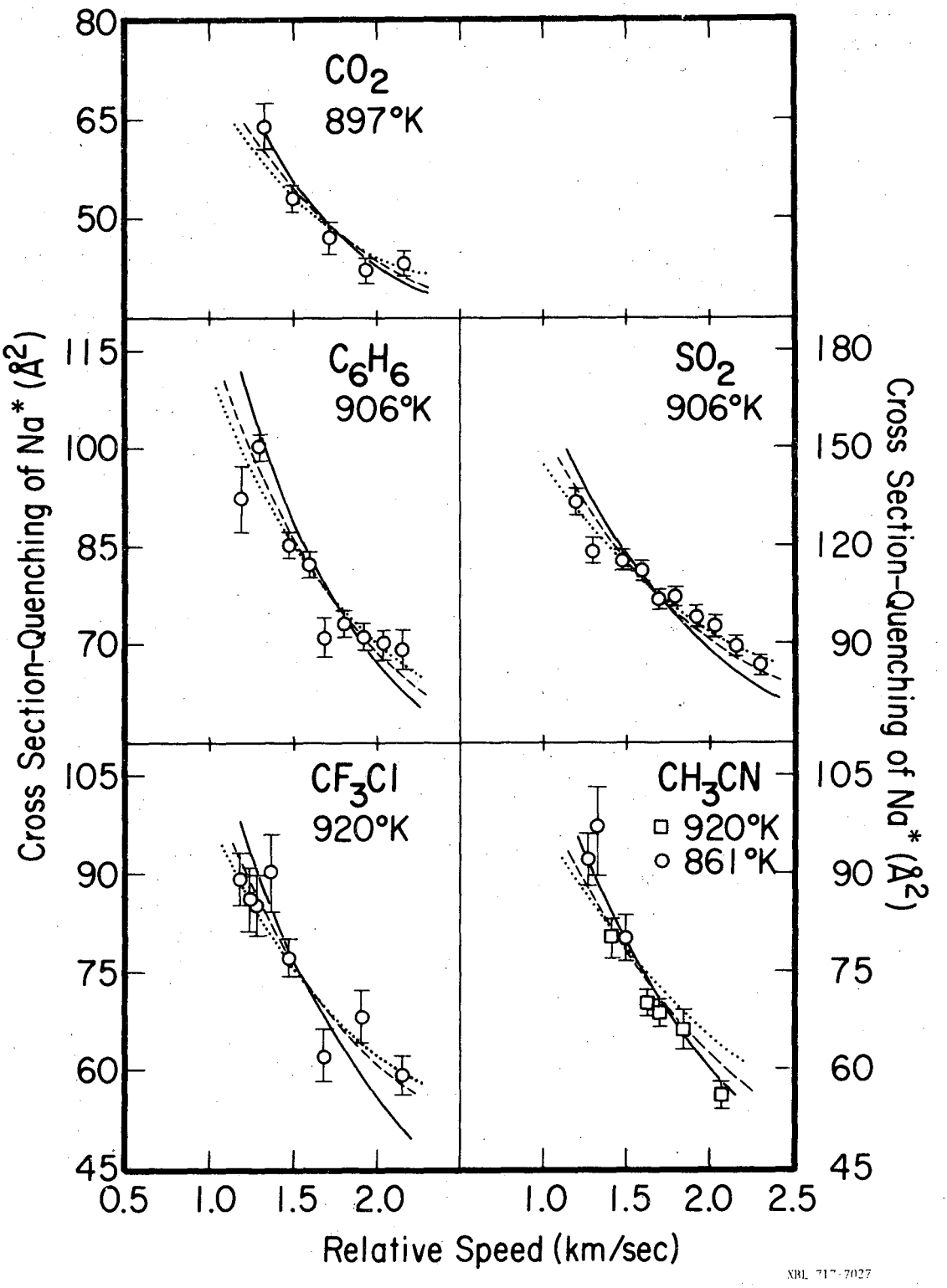

Fig. V-3. Cross sections for quenching of Na*($3p^2P$) as a function of relative speed. The points are the data represented as $\langle Q_q \rangle$ vs $\langle g \rangle$. The curves show the best fits to the data obtained by averaging cross sections of the form $Q_q(g) = K_s/g^{4/s}$ over the relative speed distributions: solid curve, s = 4; dashed curve, s = 5; dotted curve, s = 6.

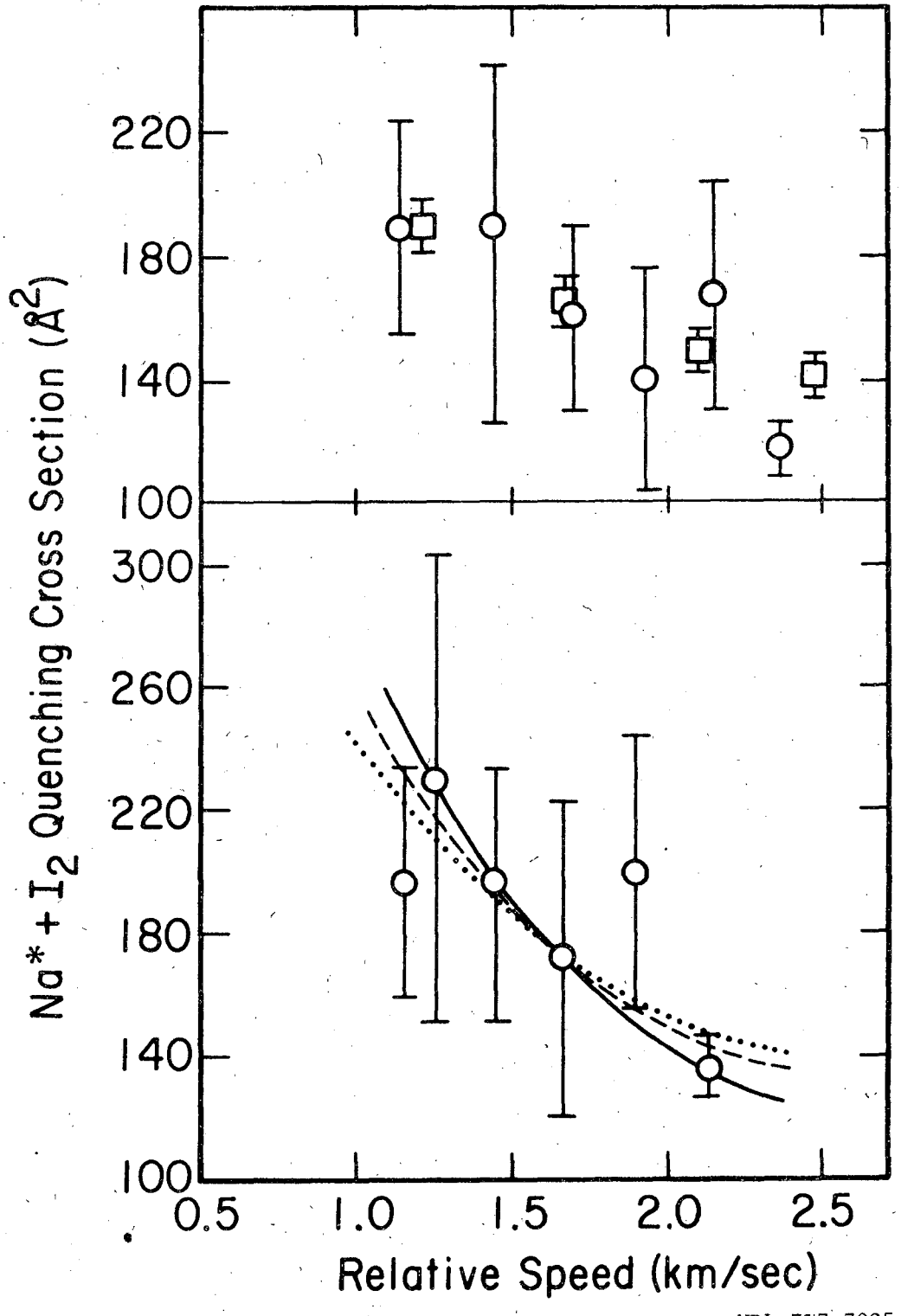

XBL 717-7025

Fig. V-4. Cross sections for quenching of $Na^*(3p^2P)$ by I_2 as function of relative speed. Upper panel: comparison of results of Ref. 3 (squares) with results of this work (circles), if the data collected here is analyzed as in Ref. 3. Lower panel: results of this work; conventions are as given for Fig. V-3.

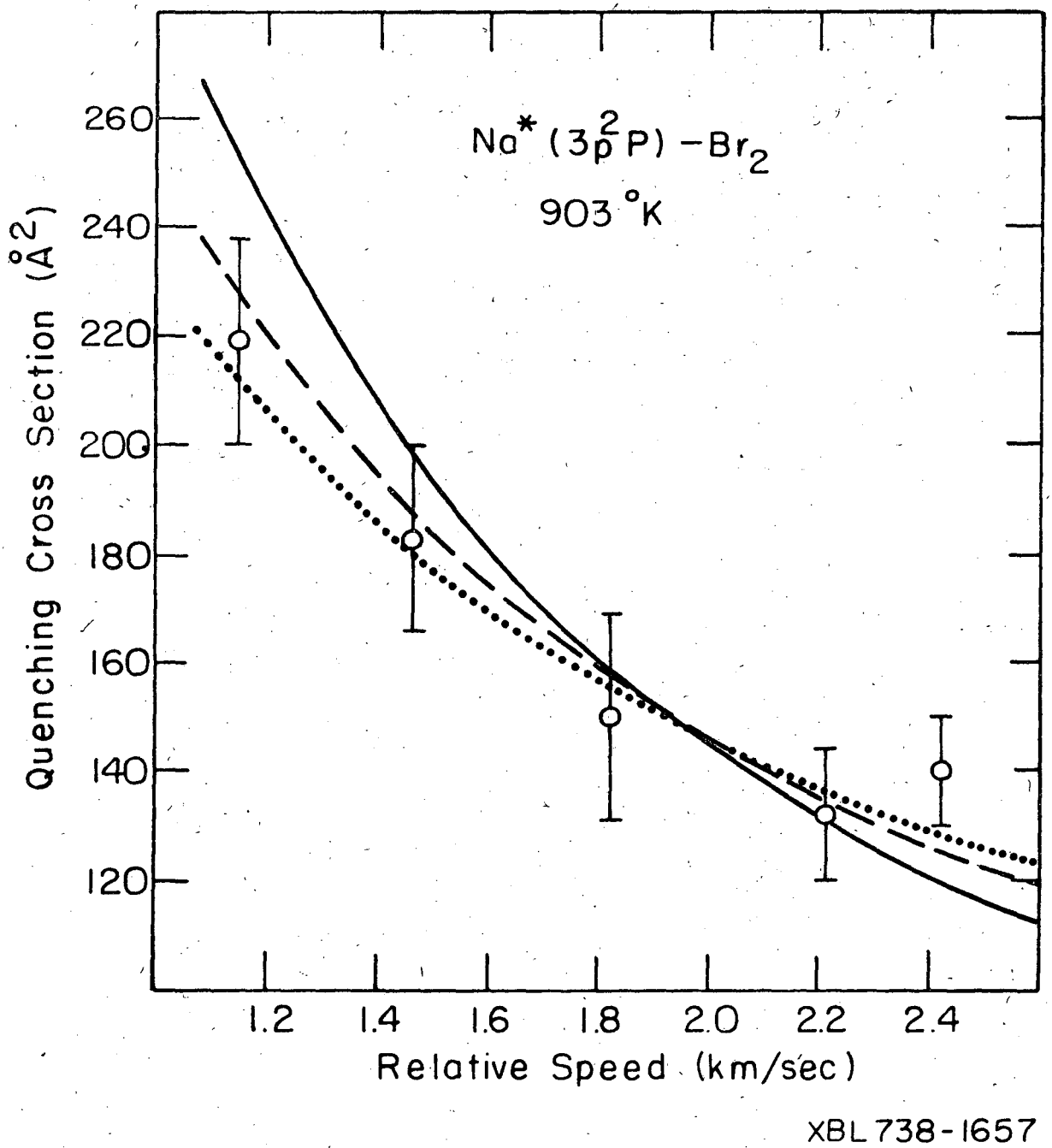

Fig. V-5. Cross sections for quenching of $Na^*(3p^2P)$ by Br_2 as a function of relative speed. Again the points are the data represented as $\langle Q_q \rangle$ vs $\langle g \rangle$. Here the curves are the deconvoluted $Q_q(g)$ curves which gave the best fits to the data when averaged over the relative speed distributions: solid curve, s = 4; dashed curve, s = 5; dotted curve, s = 6.

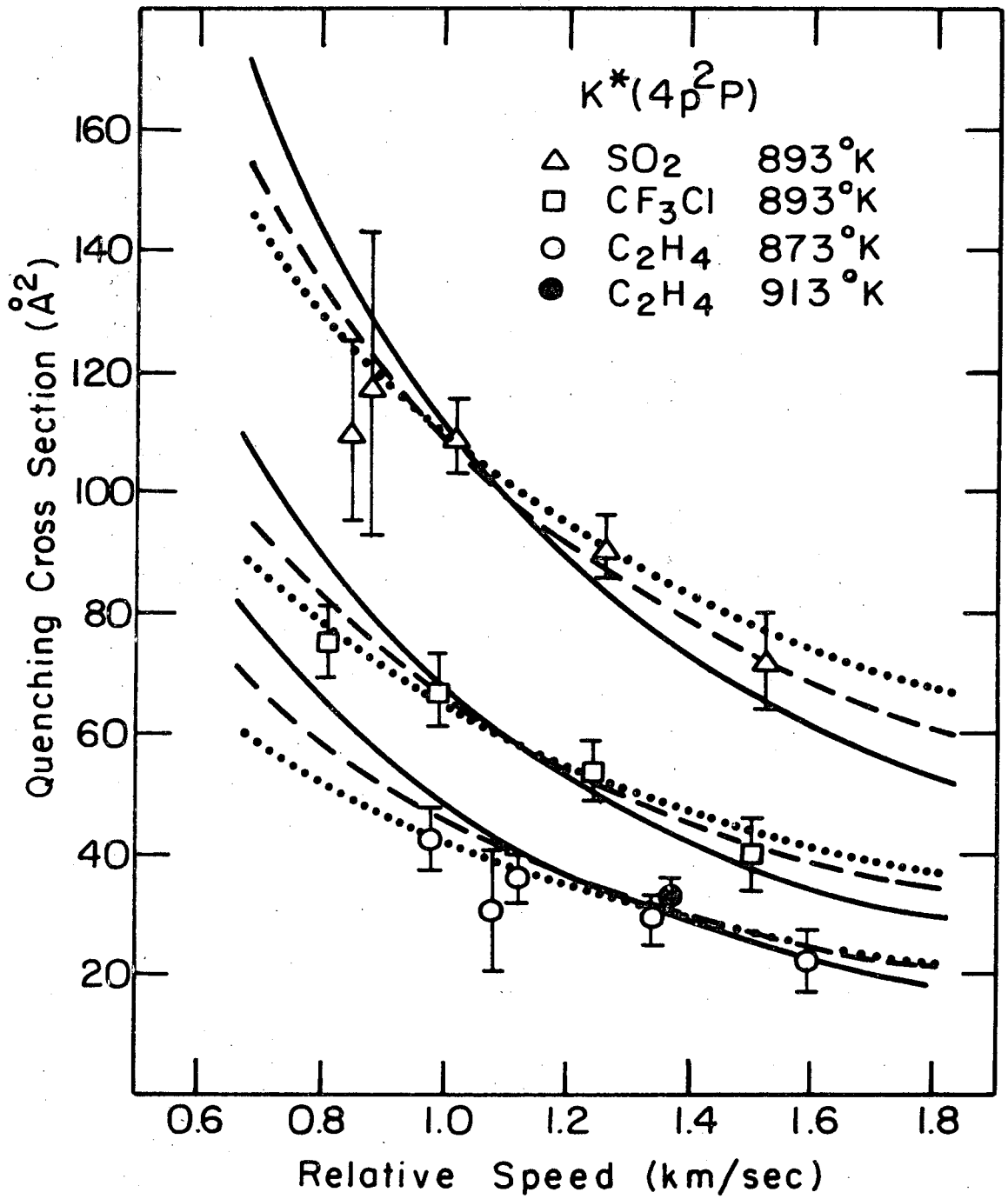

XBL 738-1656

Fig. V-6. Cross sections for quenching of $K^*(4p^2P)$ as a function of relative speed. Conventions are as described for Fig. V-5.

Chapter III, an adjacent process might be expected to peak at ~1840Å, and a small contribution could not be ruled out. If this is occurring these $Na^*(3p^2P)$ atoms would have much lower speeds than were used in analyzing the data taken at the affected wavelengths.

In Fig. IV-6, the points with the largest error bars for C_2H_4 and SO_2 were taken under thermal conditions, using high pressures of argon. The $\langle Q_q \rangle$ and $\langle g \rangle$ then came from Eq. (32) of Chapter IV, which applies in these cases. The increased uncertainties represent real added difficulties involved in taking the thermal data.

As indicated in Chapter IV in discussing the energy dependence of the cross sections, the "true" cross sections might, under certain assumptions, be expected to vary as $K_s(\exp)/g^{4/s}$, s = 4,5 or 6. Employing this idea, the energy dependence of the cross sections can be deconvoluted in terms of these functional dependences, which process is a convenient means even in cases in which the above-mentioned assumptions become questionable. This deconvolution yields values of $K_s(\exp)$ for each atom-gas system which provide the best fits to the experimental rate constants when integrated over the appropriate relative speed distributions, as per Eq. (33) of Chapter IV. Also, the fits to the data obtained for different values of s can be compared.

In the lower panel of Fig. V-2, four curves illustrating this process are shown. Two are the deconvoluted $Q_q(g)$ curves for s = 5, 6, and the other two represent the corresponding fits to the data. For purposes of constructing the latter two curves, the rate constants derived from the first two were subjected to the same first-order analysis as were the experimental rate constants. Comparison of the curves in

Fig. V-2 shows that there is a noticeable, though not great, difference between a $Q_q(g)$ curve and the corresponding $\langle Q_q \rangle$ vs $\langle g \rangle$ curve.

In each of Figs. V-3 through V-6, three curves are shown. In Figs. V-3 and V-4, these curves show the best fits to the data obtained by averaging the $Q_q(g) = K_s/g^{4/s}$ functions over the relative speed distributions. In Fig. V-5 and Fig. V-6, these curves are the deconvoluted $Q_q(g)$ curves which themselves gave the best fits to the data when averaged over the relative speed distributions. Tables I and II list the values of k_q, $\langle Q_q \rangle$ and $\langle g \rangle$ for each atom-gas system and Table III lists the values of $K_s(\exp)$ which gave the best fits to the data. It might be noted that there is, in general, a tendency of k_q to decrease with increasing energy, and, in fact, the s = 6 fits were generally best, in cases in which there seemed to be a real distinction. The one exception, as previously discussed, was CH_3CN, which seemed to show a predilection for s = 4. However, the data in no case allow a definite choice for a value of s.

Besides the energy-dependent results presented thus far, several gases were studied with the first resonance states with only single energy distributions, usually thermal. The results for these cases are presented in Table IV. The rate constants are given, again with the tolerances from the least-squares fits, along with $\langle Q_q \rangle$ and $\langle g \rangle$ values, as discussed for thermal conditions. For CH_3OH with $Na^*(3p^2P)$, non-thermal measurements at three wavelengths, 2150, 2300, and 2400Å, spanning the full energy range used in NaI quenching studies, failed to reveal a significant variation in the rate constants. The two longer wavelength values were essentially equal to the thermal value, and the

Table I. Energy dependent quenching of $Na^*(3p\,^2P)$.

System/Gas	Temp.* (°K)	Monochromator Setting (Å)**	$10^9\ k_q$ cm^3/sec-molec.	$\langle Q_q \rangle$ ($Å^2$)	$\langle g \rangle$ km/sec
$NaI \rightarrow Na^*(3p\,^2P)$					
C_2H_4	$\binom{961}{890}$	2150	1.04±0.02	44	2.22
		2200	0.98±0.02	48	2.00
		2250	0.89±0.03	48	1.78
		2300	0.85±0.02	52	1.57
		2350	0.84±0.03	56	1.40
		2400	0.87±0.03	63	1.31
	$\binom{920}{897}$	2175	0.92±0.05	43	2.10
		2225	0.97±0.04	50	1.87
		2275	0.89±0.05	52	1.67
		2325	0.91±0.03	59	1.46
CO_2	$\binom{897}{860}$	2150	0.94±0.03	43	2.18
		2200	0.83±0.04	42	1.78
		2250	0.83±0.05	47	1.72
		2300	0.82±0.03	53	1.92
		2350	0.88±0.04	64	1.33
C_6H_6	$\binom{906}{875}$	2150	1.49±0.07	69	2.15
		2175	1.42±0.03	70	2.04
		2200	1.37±0.03	72	1.92
		2225	1.32±0.04	73	1.80
		2250	1.21±0.05	71	1.69
		2275	1.31±0.03	82	1.59
		2300	1.26±0.03	85	1.47
		2350	1.31±0.03	100	1.29
		2400	1.11±0.06	92	1.19
SO_2	$\binom{906}{875}$	2125	1.95±0.06	83	2.30
		2150	1.96±0.06	89	2.16
		2175	1.97±0.03	94	2.04

Table I. Continued

System/Gas	Temp.* (°K)	Monochromator Setting (Å)**	10^9 k_q cm^3/sec-molec.	$\langle Q_q \rangle$ ($Å^2$)	$\langle g \rangle$ km/sec
SO_2		2200	1.91±0.03	98	1.92
		2225	1.93±0.05	104	1.80
		2250	1.80±0.05	103	1.70
		2275	1.84±0.03	112	1.60
		2300	1.75±0.04	115	1.48
		2350	1.59±0.06	118	1.30
		2400	1.65±0.05	132	1.20
CF_3Cl	(920/895)	2150	1.27±0.06	59	2.14
		2200	1.30±0.05	68	1.91
		2250	1.05±0.07	62	1.68
		2300	1.14±0.04	77	1.47
		2325	1.24±0.08	90	1.36
		2350	1.10±0.06	85	1.28
		2375	1.07±0.06	86	1.23
		2400	1.06±0.06	89	1.18
CH_3CN	(920/895)	2175	1.17±0.03	56	2.07
		2225	1.23±0.05	66	1.84
		2275	1.16±0.02	70	1.63
		2325	1.16±0.04	80	1.42
	(861/850)	2250	1.18±0.03	68	1.71
		2300	1.22±0.04	80	1.50
		2350	1.32±0.08	97	1.33
		2400	1.21±0.05	92	1.27
I_2	(906/875)	2150	2.87±0.20	136	2.13
		2200	3.25±0.65	199	1.89
		2250	2.83±0.90	171	1.66
		2300	2.83±0.55	196	1.44
		2350	2.84±0.95	227	1.25
		2400	2.24±0.40	196	1.15

Table I. Continued

System/Gas	Temp.* (°K)	Monochromator Setting (Å)**	10^9 k_q cm^3/sec-molec.	$\langle Q_q \rangle$ ($Å^2$)	$\langle g \rangle$ km/sec
NaBr→Na*($3p^2P$)					
Br_2	$\binom{903}{890}$	1875	3.40±0.30	140	2.40
		1925	2.91±0.26	132	2.21
		2000	2.73±0.33	150	1.82
		2075	2.70±0.25	183	1.46
		2125	2.53±0.23	219	1.15

*The lower temperature in each case is that of the salt, which determines the vapor pressure. The higher value is the temperature of the window region of the cell, which is involved in the speed distribution.

**For all the NaI data listed, the monochromator bandwidth was 48°Å (FWHM). For the NaBr work, it was 60Å.

Table II. Energy dependent quenching of $K^*(4p^2P)$.†

Gas	Temp.* (°K)	Monochromator Setting (Å)**	10^9 k_q cm^3/sec-molec.	$\langle Q_q \rangle$ ($Å^2$)	$\langle g \rangle$ km/sec
C_2H_4	873	2300	0.70±0.07	43	1.58
		2375	0.70±0.04	50	1.34
		2450	0.65±0.05	54	1.12
		2525	0.67±0.05	63	0.98
		2450 (Thermal)	0.54±0.11	51	1.08
	913	2375	0.76±0.04	53	1.37
SO_2	893	2300	1.42±0.12	92	1.52
		2375	1.42±0.06	111	1.26
		2450	1.37±0.05	130	1.02
		2525	1.16±0.13	130	0.85
		2450 (Thermal)	1.21±0.22	138	0.88
CF_3Cl	893	2300	0.92±0.09	60	1.50
		2375	0.93±0.07	74	1.24
		2450	0.87±0.06	87	0.99
		2525	0.80±0.06	95	0.81

†For every case, quenching measurements were made on each component separately, and the results combined as described in Chapter IV. No significant difference between the two was observed in any case.

*The temperature listed in the window temperature. The salt temperature was 20°K lower.

**The monochromator bandwidth was 60Å (FWHM) in each case.

Table III. Best-fit values of K_s(exp)* for energy-dependent quenching.

	Na*($3p^2P$) Quenching			K*($4p^2P$) Quenching		
Gas	10^9 K_4	10^{10} K_5	10^{11} K_6	10^9 K_4	10^{10} K_5	10^{11} K_6
C_2H_4	0.93	0.82	1.7	0.69	0.65	1.3
CO_2	0.88	0.78	1.6			
C_6H_6	1.3	1.2	2.4			
CF_3Cl	1.2	1.1	2.2	0.87	0.86	1.8
CH_3CN	1.2	1.1	2.3			
SO_2	1.8	1.6	3.3	1.3	1.3	2.8
I_2	2.9	2.6	6.0			
Br_2	2.9	2.5	5.0			

*K_s has units of cm^2-$(cm/sec)^{4/s}$.

Table IV. Quenching of $Na^*(3p^2P)$ and $K^*(4p^2P)$ at single energies.

Atom/Gas	T(°K) Monochromator Setting (Å)*	10^9 k_q cm^3/sec-molec.	$\langle Q_q \rangle$ ($Å^2$)	$\langle g \rangle$ (km/sec)	10^{11} K_6 $cm^2(cm/sec)^{2/3}$
$Na^*(3p^2P)$					
CH_3OH	873(t)	0.28±0.01	25.1	1.17	0.59
H_2	873	0.32±0.01	10.2	3.15	0.48
D_2	873	0.19±0.01	8.3	2.32	0.32
D_2 (polarized uv)	873	0.19±0.01	8.1	2.32	0.31
H_2O	820	0.04±0.01	3.0	1.31	0.08
D_2O	820	<0.01	<1.0	1.25	<0.01
CF_4	873	<0.01	<1.0	1.03	<0.01
CH_4	873	<0.01	<1.0	1.37	<0.01
C_2H_6	873	<0.01	<1.0	1.21	<0.01
$K^*(4p^2P)$					
CH_3OH	893(t)	0.25±0.2	24.0	1.04	0.55
H_2	893	0.098±0.009	3.0	3.14	0.15
D_2	893	0.073±0.007	3.0	2.28	0.12
H_2O	893	0.024±0.008	1.5	1.24	0.05
CF_4	893	<0.01	<1.0	0.84	<0.01
CH_4	893	<0.01	<1.0	1.29	<0.01
I_2	893/2450Å**	2.08±0.21	214.0	0.97	4.6

*The temperature given is that of the window region. The salt temperature was 20°K lower. The monochromator settings were 2250 or 2300Å for $Na^*(3p^2P)$ from NaI and 2450Å for $K^*(4p^2P)$ from KI. The symbol "(t)" indicates thermalization with argon. As indicated in the text, speed distributions may be assumed to be thermal in all other cases except for $K^*(4p^2P)$-I_2.

**The monochromator bandwidth for this measurement was 60Å (FWHM).

value obtained at 2150Å was only 8% higher. An absence of variation of k_q with energy may in some cases be interpreted as indicating that $Q_q(g) \propto 1/g$. This, however, assumes that the distributions in collision energies are significantly different for the various measurements of k_q. In the case of CH_3OH, it seems probable, in view of the small quenching cross section, that the lack of dependence of k_q on nominal energy is due to collisional relaxation of the speed distributions, which wipes out much of the energy selection.

For most thermal measurements listed in Table IV, argon at high pressures was used to thermalize the energy distributions (generally, the use of the term "thermalize" or "thermalization" indicates the forced relaxation of the speed distribution by this means). The exceptions were H_2 and D_2, whose small masses ensured that the relative speed distributions were essentially thermal, and the several gases which exhibited very small quenching cross sections, ~1Å^2, which ensured at least quite effective relaxation of the speed distributions in a time short compared to the quenching lifetime. At any rate, the precise character of the speed distributions was not of great consequence with the very inefficient quenchers.

The one non-thermal case presented in Table IV is for I_2 quenching $K^*(4p^2P)$ at 2450Å. This quenching process, though it is very interesting, was studied at only one wavelength, because of special difficulties encountered with this system.

As energy dependence was not studied for the cases of Table IV, it was assumed, for purposes of analysis, that s = 6 was appropriate, which is probably not too bad an assumption for most of these cases,

and values of K_6(exp) were calculated and are presented in Table IV along with the other results. With exception of the I_2 case, for which the appropriate non-thermal speed distribution was calculated and the integration to fit K_6(exp) to k_q done numerically, these K_6 values are just from the analytic expression, Eq. (37) of Chapter IV, which applies in thermal cases.

2. Quenching of $K^*(5p^2P)$

The initial plan of attack with this species was to investigate its quenching by the same gases which were investigated with energy dependence for $K^*(4p^2P)$, plus perhaps a few "basic" molecules such as H_2, D_2 or H_2O. However, the quenching behavior of some gases with this state seemed so unusual that finally a considerable number of gases were investigated. Results are presented in Table V as k_q, $\langle Q_q \rangle$, $\langle g \rangle$, and K_6(exp).

The tolerances again indicate the standard deviations in the least-squares fits. Here, there are more uncertainties in almost every respect than was true for the studies of the first resonance states. Self-quenching could be a more significant experimental problem, the presence of interfering states could affect the results, and interpretation is subject to greater uncertainty, due to less reliable values for the atomic transition probabilities.[11] Overall, it is estimated that the uncertainty in the results is probably ±20% here, as compared to ±10-20 with $Na^*(3p^2P)$ from NaBr and $K^*(4p^2P)$, and ±5-10% for $Na^*(3p^2P)$ from NaI (except for the case of I_2).

Table V. Quenching of $K^*(5p^2P)$.

Gas	T(°K) Monochromator Setting(Å)*	10^9 k_q cm^3/sec-molec.	$\langle Q_q \rangle$ ($Å^2$)	$\langle g \rangle$ (km/sec)	10^{11} K_6 cm^2 $(cm/sec)^{2/3}$
		THERMAL			
C_2H_4	893	0.83±0.10	77	1.08	1.8
C_2D_4	893	0.82±0.11	79	1.04	1.8
CF_3Cl	893	1.40±0.25	172	0.82	3.3
N_2	893	0.65±0.05	60	1.08	1.4
CH_3OH	893	1.16±0.18	112	1.04	2.5
CF_4	893	0.21±0.04	25	0.84	0.49
H_2	893	0.39±0.03	12	3.15	0.58
D_2	893	0.25±0.02	11	2.28	0.41
CH_4	893	0.77±0.06	60	1.29	1.6
CD_4	893	0.48±0.05	40	1.19	1.0
C_2H_6	893	1.03±0.05	98	1.05	2.2
C_2D_6	893	0.70±0.07	70	1.00	1.5
		NON-THERMAL**			
H_2O	893	1.04±0.10	84	1.24	2.1
D_2O	893	1.09±0.09	91	1.19	2.3
HCl	893/1925	1.12±0.06	102	1.03	2.4
DCl	893/1925	1.13±0.06	103	1.03	2.4
I_2	893/1925	0.39±0.04	43	0.90	0.87
CD_4	893/1925	0.44±0.04			
CH_4	893/1925	0.67±0.08			
CH_4	893/1950	0.70±0.09			
CH_4	893/1975	0.62±0.10			

*The temperature given is that of the window region. The salt temperature was 20°K lower. The symbol "(t)" indicates thermalization with argon. All the thermal measurements for which monochromator settings are not given were not done at 1925Å. As discussed in the text, the H_2O-D_2O cases were assumed to be thermal for purposes of analysis, and the HCl, DCl and I_2 were analyzed using speed distributions obtained for $K^*(4p^2P)$ from KI at 2475Å. The non-thermal measurements on methane are also discussed in the text in relation to the problem of possible interference from $K^*(6s^2S)$ and $K^*(4d^2D)$.

**The non-thermal measurements were done with monochromator bandwidths of 60Å(FWHM).

With the exceptions of H_2, D_2, H_2O, D_2O, HCl, DCl, I_2 and some special CH_4 and CD_4 runs, all the measurements were thermalized, and except for some of the special CH_4 and CD_4 runs, all were done at a monochromator setting of 1925Å. The speed distributions in the cases of H_2O, D_2O, HCl, DCl and I_2 could not be thermalized, due to experimental problems. In the cases of H_2O and D_2O, they were assumed to be thermal, for purposes of analysis, as the masses of these gases are fairly small. In the cases of CH_4 and CD_4, whose masses are nearly the same as those of H_2O and D_2O, the results of thermalized and non-thermalized measurements agreed within experimental uncertainty.

HCl, DCl and I_2 are a bit more problematical, as the assumption of full thermal character in the relative speed distributions would be quite suspect, especially in the I_2 case. The speed distributions used to analyze these cases were generated by assuming that one could obtain the potential curve for the photodissociation of KI to $K^*(5p^2P)$ simply by displacing the curve for the $K^*(4p^2P)$ process, and that one could then use the same transition probability factors in generating the speed distributions. These are essentially the assumptions made in analyzing the lower fluorescence processes in Chapter III, but are probably somewhat less plausible here. At any rate, they lead to the conclusion that the speed distribution for $K^*(5p^2P)$ at 1925Å would be about the same as for $K^*(4p^2P)$ at 2475Å, so the latter was found, convoluted with the thermal quenching gas distributions, and the results were applied to find values of K_6(exp). For HCl and DCl, analysis assuming thermal distributions was done for purposes of comparison, and it was found that the thermal values for K_6(exp) were ~5% larger

than the values obtained using the non-thermal distributions. This would indicate only a very small error in the assumption of thermal distributions for H_2O and D_2O.

As with the single-energy-distribution results on the first resonance states, it has been assumed here, for purposes of analysis, that s = 6 applies. It is probable that the quadrupole-quadrupole interaction energies here are considerably enhanced relative to the dispersion energies as compared to first resonance states, and in addition, there are considerable doubts concerning the applicability of the orbiting model here, even insofar as it applies to the first resonance states. Why, then, bother with K_6(exp). Certain dramatic differences in quenching behavior are obvious anyway. The answer lies in an interest in trying to obtain a better estimate of changes in quenching efficiency than can be got from simple comparisons of cross sections. If one wishes to do this in an amount of time small compared to a graduate career, the orbiting-dispersion forces model or some equally simple approach is the sort of thing one uses. One can partially dispense with the notion that increased quenching ability with $K^*(5p^2P)$ is due simply to much larger quadrupole forces by noting that C_2H_6 does not behave much differently than CH_4, but there are obviously many other matters to be considered as far as quenching efficiency goes, and some of these will be taken up at length in the Discussion. For purposes of convenience, this subject will often be considered in terms of w, the ratio K_6(exp)/K_6(theor), as discussed in Chapter IV. The quantitative validity of this may be in doubt, but the trends which are represented by significant changes in w are quite probably real, and need explanation.

3. Special Experimental Considerations

As has been indicated at several points, there were various problems and questions which had to be dealt with in the course of the experiments, and their consideration can no longer be deferred. First will be considerations involving particular quenching gases. The reader may refer to Table III of Chapter II for a capsule view of these. The mass spectral data referred to along the way will be presented and discussed in more detail later in this section.

I_2. The main source of the difficulty with this gas is that it has a low vapor pressure. Even at elevated room temperature (~90°F) only ~0.6 Torr can be obtained. To make it worse, it dissociates to a considerable extent at the experimental temperatures, so that at 0.6 Torr in the vacuum line, only ~0.3 Torr in the fluorescence cell is I_2. With NaI, it was possible to get results, even at such low I_2 pressures, as the signal-to-noise situation was quite good. This data has been presented in Fig. V-4, where it is compared in the upper panel to results obtained by the direct lifetime measurement method.[3] The large error bars on the results obtained here are due to the fact that only small deviations from unity could be induced in the I_o/I ratio at the low vapor pressures used. However, the general agreement with the results of Ref. 3 is quite satisfactory.

In studying the quenching of $K^*(4p^2P)$ and $K^*(5p^2P)$ by I_2, the signal-to-noise situation demanded considerably higher pressures if significant results were to be obtained. This was achieved by attaching a bulb containing I_2 to the vacuum line near the feed-through into the vacuum chamber, then heating this bulb with a water bath and heating

the exposed portion of the line with heating tape. It was known that the metal and quartz tubing inside the vacuum chamber became very hot during experiments, so they presented no problem as far as condensation of the I_2 was concerned. However, the feed-through flange itself had to be heated regularly with a heat gun. All this rendered the experiments somewhat bothersome, and the uncertainties in the vapor pressure values, taken from the water bath temperatures, somewhat larger than usual. The estimated uncertainties in the vapor pressures are $\leq \pm 10\%$. However, the validity of the comparison of the results on $K^*(4p^2P)$ and $K^*(5p^2P)$, which is what will be of greatest interest, is not seriously impaired by this added uncertainty.

That the quenching observed was due primarily not to I but to I_2, as Brus[3] has found for the $Na^*(3p^2P)$ case, was indicated by plotting I_o/I vs both P_{I_2} and P_I. The latter plots were distinctly non-linear, and if constrained to linear fits would have given I_o/I intercepts of $\lesssim 0.5$. The I_o/I vs P_{I_2} plots, on the other hand, were representative Stern-Vollmer plots with intercepts of ~ 0.9, so all the observed quenching was assigned to I_2. In theory, measurements of I_o/I for various values of $P_{I_2} + P_I$ could yield k_q values for both species. However, in these experiments, the uncertainties in the data, coupled with the probably relatively small quenching cross section[3] of I, made this impossible.

<u>C_6H_6 and SO_2</u>. The main problem with these two gases was absorption of the uv in the range used in the NaI experiments. Both absorbed only very slightly at 2400Å, but became progressively stronger absorbers as lower wavelengths were reached. In order to correct for this, it

was necessary to measure the uv transmitted through the cell and to estimate the fraction of the distance through the cell traversed by the uv beam before reaching the zone from which fluorescence was detected. This latter quantity became somewhat of a parameter in the analysis, and was finally estimated to be 0.6 for these experiments, which were done in the open air days when the geometry of the apparatus was not as tight as later. The difference between cross sections found using a value of 0.6, and those found using a value of 0.5, was, for both gases, ~10% at the lowest wavelength, ~5% at 2250Å, in the center of the spectrum, and negligible at 2400Å, where there was very little absorption. The absorption of the uv by the quenching gas indicates the production of electronically excited molecules and the possible effects of this were checked, in the case of SO_2, by measuring quenching of $Na^*(3p^2P)$ at different uv intensities. These experiments will be referred to again in connection with the possibility of radiation imprisonment. The result found was that a decrease by a factor of three in uv intensity produced no significant variation in the measured quenching cross section. This indicates either that the excited molecules exhibit quenching behavior similar to that of the ground state molecules, or, more probably, that excited molecules are being produced in negligible concentration. If the latter explanation is correct, the result would hold for C_6H_6 as well.

C_6H_6 was one of several gas studied which adsorbed to some extent on the surfaces of the vacuum system. With this gas, the tendency was not pronounced, though it did produce a measurable pressure drop during the taking of a fluorescence intensity reading. It was felt

that, due to the smallness of the effect, it could be assumed that it occurred mostly in the cold manifold, so the initial pressure was measured and then the cell was isolated. The constancy of the fluorescence signal during a measurement, and the fact that only a short time (~2 min) was required to establish the value of this signal lent acceptability to this procedure. The mass spectral results indicated good behavior. Mass spectral analysis was also done on SO_2.

CF_3Cl. With high pressures ($\gtrsim$6 Torr) of this gas in the cell, it was found that the quenched fluorescence signal would begin to drop slowly after a minute or two and would continue to do so until the CF_3Cl was pumped out. One possible, though not necessarily probable, explanation for this is that NaCl or KCl is formed by reaction of the excited species with the gas and, if the gas is present at higher pressures, enough of the chloride forms to begin to coat the cell windows slightly. It is also possible that a very slow reaction occurred with the KI or NaI, although the restoration of I_o on pumping out seems to make this unlikely. This gas presented no problem with $K^*(5p^2P)$, perhaps due to much lower excited atom concentrations, or perhaps directly to the lower CF_3Cl pressures required to produce quenching (larger cross section plus longer excited state lifetime). However, it did prevent thermal measurements with $K^*(4p^2P)$, presumably due to excessive signal deterioration in the time period (5-10 min) required to establish the fluorescence level after introducing the argon-CF_3Cl mixture. The mass spectrum of a 10 Torr sample exposed under experimental quenching conditions showed negligible changes from that of an unexposed sample.

CH_3CN. It was considered that significant isomerization of this compound to CH_3NC might occur at experimental temperatures. However, estimation of the equilibrium constant for the isomerization from data in Benson's fine little book[12] gave a value 1.7×10^{-3}, indicating no particular cause for concern. Mass spectral data were taken on this gas.

CH_3OH. The vapor of this compound again showed a tendency to adsorb on glass, similar to that discussed for benzene, but slightly more pronounced, so as before, no good pressure checks could be done. The behavior of the fluorescence and the mass spectral data indicated that no significant problem was occurring the fluorescence cell.

CF_3H. This seems to be a very strange species. With $Na^*(3p^2P)$ it enhanced the fluorescence regularly to pressures up to 50 Torr. With $K^*(5p^2P)$, it appeared to be a fairly strong quencher, but with $K^*(4p^2P)$, its introduction into the cell at pressures $\gtrsim$10 Torr brought about a translucent coating of the inner surface of the cell, which could not be removed with H_2O or hot chromic acid cleaning solution, but which did come out fairly well with 50% HF. This was the last time this gas was looked at.

H_2O and D_2O. These gases are apparently well known as strong adsorbers on vacuum system surfaces, and this made it necessary to study them by maintaining at least approximate equilibrium with a reservoir at a temperature corresponding to the desired vapor pressure. Thus they could not be studied in argon mixtures. A further problem arose in the study of quenching of $K^*(5p^2P)$ by D_2O. As this involved low D_2O pressures in a vacuum system constantly exposed to H_2O, albeit at low

pressures, there was some concern as to the composition of the gas which was doing the quenching. Investigation by mass spectrometry was complicated by the well known tendency of mass spectrometers to give H_2O and HDO peaks when fed "pure" D_2O, as well as by the tendency of mass spectrometer operators to resist introduction of water in any form into their instruments.

Analysis of some D_2O samples was finally done by mass spectrometry. As the problem and the nature of the results is a bit more complicated than with the other mass spectra used, this operation will be discussed in some detail, and the data will not be presented in tabular form. Due to the scrambling introduced by the mass spectrometer, some artifice had to be used to get the desired information. What was done was to compare the ratios of the $20(D_2O^+)$ and $17(OH^+)$ peaks in four separate samples. These were (1) a sample of pure D_2O put directly onto the mass spectrometer vacuum line, degassed briefly, and run, (2) a sample of nominal D_2O which had been exposed to the experimental vacuum line but not to conditions of a quenching experiment, (3) a sample of nominal D_2O which had been used in a quenching experiment, and (4) a sample consisting of equal pressures of sample (3) and pure H_2O. The 20/17 ratios were, respectively, 3.5,2.5,2.5, and 0.5. It can be seen that a D_2O/H_2O pressure ratio in (3) of 3:1 would give such a ratio in (4) of 3:5, which values are consistent with the intensity ratios of the mass peaks, indicating a value of ~25% H_2O in (3), which would clearly hold for (2) as well. However, if one then assumes that all the OH^+ peak in (1) is due to the mass spectrometer, one comes up with the result that the most probable value for contamination due to the quenching

experiment or the experimental vacuum system is ~5%. Thus the analysis yields the result that the H_2O content of (2) or (3) is less than ~25%, and probably ~5%. This result, though subject to considerable uncertainty, leads to the conclusion that the quenching observed with the nominal "D_2O" sample was, at least predominantly, due to D_2O.

SF_6. This gas exhibited strange behavior in several respects. The apparent quenching cross sections with $Na^*(3p^2P)$ were in the range 800-1200Å^2. The pressure and fluorescence intensity fluctuated in such a way as to indicate possible decomposition, and the mass spectra of exposed samples showed a discrete infinity of peaks which were not assignable directly to SF_6, although these were small compared to the assignable peaks. Reference 2b also observed anomalously large quenching with this gas, and surmised that it might have been due to reaction with NaI, liberating significant quantities of I_2.

Br_2. This gas exhibited a behavior similar to H_2O and D_2O as far as pressure instability was concerned. It was felt that it probably reacted with stopcock grease. It was not convenient to maintain pressure in equilibrium with a reservoir, as only quite low pressures were needed, so a procedure was adopted which involved initially exposing the entire vacuum manifold and cell to a relatively high pressure of Br_2 for several hours before and during heating to the experimental temperature. This Br_2 was then pumped out, and any pressure deterioration which occurred when Br_2 was admitted to line for quenching measurements was controlled by admitting additional small doses as required to maintain the pressure within ~0.05 Torr of the nominal value. This problem certainly introduced some additional

uncertainty into the results, and would perhaps have led to abandonment of a less interesting quencher. However, the experiments on NaBr, including the fluorescence efficiency measurements, were done with the main idea of studying quenching by Br_2, as it was regarded as very interesting, so persistence overcame recalcitrance, and quenching cross sections were obtained. Comparison of these results to direct lifetime measurements by Brus,[3] which gave a cross section of ~180Å^2 at a nominal speed of 1.4 km/sec, using excitation over the entire range available from an H_2 lamp in air, indicates that the results obtained here are probably fairly reliable.

HCl and DCl. These gases again adsorb on or react with some component of the vacuum system. Impregnation of the system with a particular gas was done here as with Br_2, but with somewhat different results. First of all, the pressure dropped quite sharply as the cell was heated up, indicating that probably the gas was reacting with the metal tubing inside the vacuum chamber. Secondly, better, though not complete, stabilization of pressures during subsequent measurements was achieved by this impregnation, so that experiments on $K^*(5p\,^2P)$ proceeded fairly easily. However, at the considerably higher pressures needed to do quenching of $K^*(4p\,^2P)$, the pressure instability was a sufficiently serious problem that experiments were not done.

Mass Spectra. The mass spectral data which have been referred to in the preceeding section are shown in Table VI, with the exception of the SF_6 data, along with similar data on C_2H_6. Given in each case is a standard spectrum, a spectrum of a reagent sample which was not exposed in a quenching experiment, and a spectrum of a sample

Table VI. Mass Spectral Data

Peak	Standard*	Unexposed	Exposed	Comment
	Peak Intensities Scaled to 100			
		C_2H_4		
12	0.5	1.0	<0.5	
13	1.0	2.0	1.0	
14	2.0	5.0	2.0	
15	0.3	0.5	b**	
24	2.0	3.0	2.0	
25	8.0	12.0	8.0	
26	52.0	56.0	40.0	
27	59.0	60.0	50.0	
28	100.0	100.0	100.0	
29	3.0	1.5	2.0	
		C_6H_6		
17	0.0	0.1	0.1	Impurity
18	0.0	0.5	0.5	Impurity
25	0.5	0.1	0.1	
26	3.0	1.0	1.0	
27	3.0	1.0	1.0	
28	0.5	b	b	
36	0.5	0.2	0.2	
37	4.0	1.0	1.0	
38	6.0	2.0	2.0	
39	14.0	5.0	6.0	
43	0.0	1.0	0.2	Impurity

Table VI. Continued

Peak Intensities Scaled to 100				
Peak	Standard*	Unexposed	Exposed	Comment
		C_6H_6		
49	3.0	2.0	1.0	
50	16.0	12.0	12.0	
51	19.0	15.0	14.0	
52	19.0	16.0	15.0	
53	1.0	1.0	0.5	
58	0.0	0.2	<0.1	Impurity
59	0.0	0.3	0.0	Impurity
61	0.5	0.5	0.5	
62	0.5	0.5	0.5	
63	3.0	2.0	2.0	
64	0.0	0.2	0.1	Impurity
65	0.0	0.1	<0.1	Impurity
66	0.0	0.2	<0.1	Impurity
73	1.0	1.0	2.0	
74	5.0	5.0	5.0	
75	2.0	2.0	2.0	
76	6.0	5.0	4.0	
77	14.0	16.0	18.0	
78	100.0	100.0	100.0	
79	6.0	8.0	7.0	
		SO_2		
17	0.0	0.0	1.0	Impurity
18	0.0	0.3	5.0	Impurity
24	1.0	0.2	0.1	
32	10.0	4.0	4.0	
43	0.0	0.1	0.2	
44	0.0	0.2	2.0	Impurity

Table VI. Continued.

Peak Intensities Scaled to 100				
Peak	Standard*	Unexposed	Exposed	Comment
		SO_2		
48	50.0	48.0	45.0	
49	0.5	0.3	0.5	
50	2.0	2.0	2.0	
64	100.0	100.0	100.0	
65	1.0	1.0	1.0	
66	5.0	5.0	5.0	
		CH_3CN		
12	5.0	1.0	1.0	
13	3.0	1.0	1.0	
14	11.0	3.0	3.0	
15	2.0	1.0	1.0	
16	0.0	0.0	0.5	Impurity
17	0.0	0.0	0.5	Impurity
18	0.0	0.1	3.0	Impurity
20	1.0	0.3	0.5	
24	1.0	1.0	1.0	
25	3.0	1.0	2.0	
26	5.0	2.0	3.0	
27	2.0	1.0	2.0	
28	3.0	2.0	b	
38	11.0	11.0	10.0	
39	19.0	18.0	20.0	
40	52.0	52.0	55.0	
41	100.0	100.0	100.0	
42	3.0	3.0	4.0	
44	0.0	0.0	0.1	Impurity
52	0.0	0.1	0.1	Impurity
53	0.0	0.1	0.1	Impurity
54	0.0	0.2	0.0	Impurity

Table VI. Continued.

Peak	Standard*	Unexposed	Exposed	Comment
	Peak Intensities Scaled to 100			
		CF_3Cl		
19	Not Given	2.0	2.0	F^+
31	2.0	2.0	1.0	
35	3.0	2.0	2.0	
37	1.0	0.5	0.5	
43		0.5	0.3	Impurity
50	6.0	6.0	5.0	
69	100.0	100.0	100.0	
70	1.0	1.0	0.5	
85	18.0	20.0	20.0	
87	6.0	7.0	8.0	
104	1.0	0.5	0.5	
		CH_3OH		
12	Not Given	1.0	1.0	C^+
13	"	2.0	2.0	CH^+
14	"	5.0	5.0	CH_2^+
15	"	31.0	28.0	CH_3^+
15.5	"	0.2	0.0	CH_3O^{++}
16	"	0.5	3.0	$CH_3OH^{++}(O_2^{++})$
17	"	1.0	1.0	OH^+
18	"	1.0	2.0	H_2O^+
19	0.0	0.5	0.0	Impurity
29	42.0	66.0	60.0	
30	8.0	10.0	8.0	
31	100.0	100.0	100.0	
32	72.0	90.0	80.0	
33	1.0	2.0	2.0	

Table VI. Continued.

Peak Intensities Scaled to 100				
Peak	Standard*	Unexposed	Exposed	Comment
		C_2H_6		
14	3	100	100	
15	4	10	9	
16	1	40	43	
25	4	2	2	
26	23	26	23	
27	33	40	34	
28	100	b	b	
29	22	26	21	
30	26	29	23	

**b indicates interference from a background peak, due either to mass spectrometer background or air leakage into the sample.

*Standard spectra from Ref. 13, except for CF_3Cl, from Ref. 14.

which was used in a quenching experiment, denoted by "exposed" in the table. The spectrum of the unexposed sample compared to that of the standard serves as a check on the purity of the reagent, and comparison of the spectra of the exposed and unexposed samples provides a check on possible decomposition. It should be noted that what would be of primary concern is evidence of significant changes in composition during the typical exposure time in a quenching experiment (2-10 min).

For purposes of comparing intensities to those of peaks in the standard spectra, these latter were neglected if their intensities were less than 0.5/100. However, peaks in either of the experimental samples which did not correspond to standard peaks have been noted even if considerably smaller than this. Exceptions occur in the cases of CF_3Cl and CH_3OH, for which the lower mass portions of the standard spectra were not given. This is apparently not uncommon, and consultation with an expert[15] lent assurance that, indeed, peaks in the 12-17 range were to be expected in the case of CH_3OH, and that even an 18 peak might be expected, from rearrangement. Armed with this assurance, the assignments indicated were made just to be clear that these peaks were not due to impurities, at least for the most part. It is to be noted that the behavior of the peak at 16 is slightly suspicious. In the CF_3Cl case, assignment of the peak at 19 to F^+ seems quite obvious.

In the case of C_2H_6, the locations of the peaks can be compared with the standard spectrum, but intensities cannot be compared, as the two samples were run on a quadrupole instrument which gave very different intensities from those obtained on the magnetic instrument on which the other samples were run. Of course, quantitative peak-height

comparisons are not necessarily to be expected in mass spectra, and some fairly sizeable deviations of other samples from the standards, especially in the low mass region, are probably not significant.

The results of spectral comparisons are generally quite satisfactory. A few small "impurity" peaks have been noted in the reagents. In addition, noticeable increases in intensities of "impurity" peaks appeared in the exposed samples of SO_2, at 18 and 44, of CH_3CN, and 16, 17 and 18, and of CH_3OH, at 16. The last of these, as has been mentioned, is probably not entirely impurity, but the growth indicates the addition of some impurity, possibly O_2^{2+}. The peak at 18 also appeared as an impurity in other cases, and may be due to H_2O, particularly as it nearly always appeared in combination with a smaller peak at 17. H_2O could have been introduced either from atmospheric leakage or exposure to the experimental vacuum system.

As the electron-impact ionization cross section for 75V electrons has been found to vary in an approximately linear fashion with the polarizability of the species to be ionized,[16] and as any imagineable impurities in the reagents used in these experiments would not be expected to possess polarizabilities largely different from those of the reagents, the intensities of the impurity peaks may be taken as approximately indicating the amount of impurity present. Since the quenching cross sections measured are generally quite large, any contaminant present in small amounts would have to quench with a ridiculously large cross section in order to affect the results noticeably. Thus it is felt that these mass spectra indicate reagent purities more than sufficient for the purposes of this study.

Mass spectra were also run to check the isotopic purity of unexposed samples of CD_4, C_2D_6, and C_2D_4, with fully satisfactory results. It was assumed that if the hydrogen-containing counterparts behaved themselves in the fluorescence cell, the deuterated species would do likewise, so no spectra were run on exposed samples. Some mass spectral studies of CH_4-CD_4 mixtures were done, but they will be gone over in the Discussion.

Absorption of uv. In doing quenching experiments on $K^*(5p^2P)$, CF_3Cl, C_2D_6, H_2O, CH_3OH and C_2H_4 were checked to see if they absorbed uv at a monochromator setting of 1925Å. As expected, Only C_2H_4 showed any absorption, and this was so slight as to be negligible in the quenching experiments. Comparison of measured spectra[17] indicates that C_2D_4 would absorb no more than C_2H_4 around 1925Å.

Self-Quenching and Radiation Imprisonment. The validity of rate constants derived from Stern-Vollmer analysis depends on, among other things, the use of the correct value for the lifetime of the excited state. Two factors which might cause this value to vary from the natural radiative lifetime are radiation imprisonment and "self-quenching". The first of these is generally not regarded as a problem in photodissociation experiments, due to the very small concentrations of ground state atoms produced. An experimental check was run by measuring quenching of $Na^*(3p^2P)$ by SO_2 at monochromator bandwidths corresponding to 1/2 and 1/3 the usual uv intensity. Comparison of the results of these measurements to the "full-intensity" results showed no significant variation. As radiation imprisonment would scale with uv intensity, if it did occur, and as it would cause the

apparent quenching to be fictitiously large, this was taken to indicate that it was not a problem.

Self quenching, however, could present real difficulty. The problem is the possible quenching of the excited atoms by the parent salt vapor. If such quenching occurs at a rate which is not negligible compared to the natural decay rate, the lifetime of the excited population in the absence of any foreign gas would be shortened, with the result that the apparent quenching rate constant for foreign gases would be fictitiously small.

As was indicated in Chapter IV, the very large dipole moments of the alkali halides,[18] coupled with the very large polarizabilities of the excited atoms, give rise to a dipole-induced dipole interaction which varies as r^{-6}, and which is much stronger than the corresponding dispersion interaction. If C_6^D represents the dispersion potential constant, and C_6^I the induction potential constant, then for $Na^*(3p^2P)$-NaI, $C_6^D = 1.8\times10^4$ and $C_6^I = 6\times10^4$, and for $K^*(4p^2P)$-KI, $C_6^D = 2.5\times10^4$ and $C_6^I = 1.7\times10^5$, all in units of kcal/mole $Å^6$. The C_6^D values are about the same as those for typical quenching gases, so the total r^{-6} interaction should be much stronger for M*-MX than for M*-quenching gas cases. In terms of the close-approach cross section of the orbiting model, which varies as $C_6^{1/3}$, one might expect cross sections for the $Na^*(3p^2P)$-NaI case to be ~2 times larger than the cross sections for typical efficient quenchers such as CF_3Cl, and for $K^*(4p^2P)$-KI one might expect cross sections ~2.5 greater than for such quenchers.

If the quenching cross sections reflect this comparison, these values could lead to a 5% change in the lifetime of the excited population

at MX pressures of ~100-150 mTorr. It has already been stated that MX pressures were usually maintained at less than ~30 mTorr, so no significant error would be expected from this effect. An experimental check was made in the case of $K^*(4p^2P)$ by measuring quenching by C_2H_4 at 630°C (salt temperature) and comparing the result to the measurements at 580°C, which comparison can be seen in Fig. V-6 or Table II. The vapor pressure of KI at 630°C is 66 mTorr, and at 580°C is 16 mTorr.

In the case of $K^*(5p^2P)$, the increased polarizability of the excited atom would lead to an estimate of a possible 5% error at ~40 mTorr KI pressure. Most of the experiments on this state were done at vapor pressures around 30 mTorr, so a small uncertainty might arise from this effect.

It should be noted that Brus[3] has estimated a maximum cross section for quenching of $Na^*(3p^2P)$ by NaI of ~15Å^2. This estimate was based on the failure to observe any deviation from the natural lifetime of the $Na^*(3p^2P)$ population at NaI temperatures up to 640°C. However, the value of the NaI vapor pressure which he used was ~8 times larger than the value derived from the data of Margrave,[19] which agrees quite well with that of Stull.[20] Thus there is room for a cross section of ~120Å^2, which would be quite compatible with the estimate made above.

Polarization. In order to check possible effects of polarization on quenching measurements, an experiment was done with a partial polarizer in the uv beam, using D_2 as a quenching gas. A pile-of-plates polarizer[21] was constructed using 6 suprasil plates arranged in two piles of three each and put into a "V" configuration to eliminate displacement of the uv beam. This polarizer was found to have a polarization of ~60%

at 4860Å, according to the usual definition of polarization as the difference of the intensities of the two perpendicular components divided by their sum. In accordance with literature on gratings,[22] it was found that, at 4860Å, the polarization of the monochromator (grating blazed for 1900Å) was 33% favoring the orientation perpendicular to the grating rulings. The polarization of the monochromator is probably somewhat less at lower wavelengths, while that of the pile-of-plates polarizer should have peaked at 2250Å, as it was constructed to do so. However, the construction was not particularly fine. The results of the quenching measurements on D_2 with and without the polarizer have been listed in Table III, and there is clearly no significant difference.

Interfering States. Another problem which has been referred to previously is the possibility of interference from the $4d^2D$ and $6s^2S$ states of potassium in the $K^*(5p^2P)$ experiments. The 4d state would present the greatest problem in quenching experiments, if it is produced in significant quantities, as it decays almost exclusively to the 5p state and as its lifetime is ~2.5 times greater than that of the 5p state.[11] These two factors would presumably lead to fictitiously large quenching rate constants if all the observed quenching were then analyzed assuming the lifetime of the unquenched excited atom population to be that of $K^*(5p^2P)$. It was estimated that perhaps 5% of the fluorescence observed from $K^*(5p^2P)$ with a monochromator setting of 1925Å could be originating from production of $K^*(4d^2D)$. Naturally, the amount of the latter produced would decrease at longer wavelengths, so experiments were done to compare non-thermal quenching of $K^*(5p^2P)$

by CH_4 at 1925, 1950 and 1975Å, in order to see if a noticeable decrease in the quenching rate constants appeared at the longer wavelengths. Non-thermalized conditions were employed as better data could be collected, and it was only desired to compare the rate constants. The measured values have been listed in Table V, and it can be seen that there is not significant deviation among them. The comparison of the non-thermal rate constant at 1925Å to the thermal rate constant is a bit surprising, as the latter is ~15% larger. This is not thought to be a real difference, and is probably reflective of the overall quality of the $K^*(5p^2P)$ results, and particularly of the results of thermalized measurements.

Enhancement. The observation of an increase in the intensity of fluorescence from excited atoms upon exposure to a foreign gas has been previously reported for the fluorescence of $Na^*(3p^2P)$ from NaI, for which the enhancing agent was H_2,[23] and for the fluorescence of $Tl(7s^2S)$ from TlI, for which the enhancing agent was NH_3.[24] In the present experiments, enhancement of fluorescence of $Na^*(3p^2P)$ from NaI was observed with H_2, H_2O, D_2O and CF_3H. Enhancement was not observed with any other fluorescence system studied, but this may have been at least partially due to poorer signal-to-noise, as enhancement is generally small, $\lesssim$10%. Additionally, with $Na^*(3p^2P)$ from NaBr, the only foreign gas examined was Br_2, which, being a very strong quencher, would not be expected to produce any enhancement.

The one case in which enhancement was very pronounced was with CF_3H, which produced increases in the fluorescence intensity of up to 30% at 50 Torr, with smaller increases at smaller pressures. In this

case, the effect did seem to deteriorate with time in a given experimental run. Attempts to investigate this gas with the potassium states met with a somewhat disastrous end, as previously discussed, but preliminary results on $K^*(5p^2P)$ indicated that it quenched quite strongly, comparably to HCl. In the brief exposure of $K^*(4p^2P)$ to CF_3H, there were no clear indications of enhancement, though the behavior of the gas did not allow for a clear interpretation of this fact. Definite, though much smaller, enhancement effects were also observed with H_2, H_2O and D_2O with $Na^*(3p^2P)$. Hanson[23] studied the first of these cases quite thoroughly, and no attempt was made to do more than observe it here. Enhancement by H_2O seemed to be temperature dependent. At 800°K, salt temperature (820°K, window temperature), none was observable, and quenching, albeit slight, was measured at H_2O pressures from ~10 to ~20 Torr. At 900°K (920°K), no clear quenching was measurable even at 20 Torr, and lower pressures produced varying degrees of enhancement. At 850°K (870°K), no quenching was observable at 10 Torr, but quenching could be seen at 20 Torr. D_2O seemed to produce some enhancement over a like range of temperatures, with no clearly discernible quenching at any temperature. With both these gases, the enhancement seemed to be somewhat irregular. These results certainly indicate a good deal of uncertainty concerning the value of k_q reported for H_2O in Table IV, which was obtained from the 800°K (820°K) measurements, and the other numbers derived from it.

When enhancement occurs at very low pressures with a gas which quenches at higher pressures, the effect on the Stern-Vollmer plots should be to depress the I_o/I intercepts, as quenching is occurring

with respect to an enhanced I_0 value, but the smaller value seen with no gas present is assumed. In these experiments, the Stern-Vollmer plots generally exhibited intercepts between 0.9 and 1.1, with values less than unity being much more common than those greater than unity. However, in all but possibly three cases, the deviations in the intercepts were regarded as being within the experimental uncertainties. These three cases were quenching of $Na^*(3p^2P)$ by CF_3Cl, for which intercepts in the range ~0.7 to ~0.8 were found, by CH_3CN, for which intercepts of ~0.75 to ~0.9 were found, and by CH_3OH with no argon present, for which intercepts near 0.8 were found. These results would seem to indicate that these three gases would enhance the fluorescence at sufficiently low pressures.

Three possible explanations have apparently been advanced for the kind of enhancements seen here.[25] They are, redistribution of the salt vapor, depolarization of the fluorescence, and collisionally induced dissociation of salt molecules from a shallow well in the upper potential curve. None of these is supported by the failure of several non-quenching gases, including argon, CH_4, C_2H_6 and CF_4, to produce enhancement effects with $Na^*(3p^2P)$. Indeed, in view of the fact that enhancement seems to be dependent on the particular gas, and perhaps on the particular salt, it seems that a better guess concerning its origin is that it results from a real increase in the steady-state concentration of alkali-containing species presumably due to some interaction of the vapor and/or solid salt with the foreign gas. This problem is really a side-issue here, and will be left with this suggestion. In view of the polar nature of most of the enhancing

agents, and of the strong affinity of solid NaI for water, it would seem to be reasonable, although it apparently fails to account for enhancement by H_2.

C. Discussion

1. Quenching Efficiencies

Values of w for all quenching processes studied in these experiments and a few estimated from other studies are given in Table VII. These provide estimates of the quenching efficiencies in terms of the orbiting-dispersion forces model, as discussed in Chapter IV, as they give the ratios of the rate of quenching collisions to the rate of close collisions according to this model. In the orbiting model, $K_6 \propto C_6^{1/3}$, and the Slater-Kirkwood approximation for C_6, in a case in which α_1, the polarizability of the metal atom, is much greater than α_2, the polarizability of the quenching gas, says that K_6(theor) should scale as $\alpha_1^{1/6}(\alpha_2/\mu)^{1/3}$. The values of w listed obviously indicate sizeable deviations from this behavior, and these variations in quenching efficiencies lead to the examination of several factors which might be related to such variations.

There has been considerable discussion to this point concerning the limitations of this model, and it should be clear that the numbers in Table VII must be regarded cautiously in some cases, especially those involving $K^*(5p^2P)$. Such reservations, however, do not alter the fact that there are significant effects in quenching efficiencies which are reflected, though perhaps not quantitatively, by changes in w values. That is, although w may not give accurately the ratio of quenching collisions to "close collisions" in the real case, changes

Table VII. "Quenching efficiencies".*

Atom	$Na^*(3p^2P)$	$K^*(4p^2P)$	$K^*(5p^2P)$
Gas			
C_2H_4	0.68	0.56	0.49
C_6H_6	0.83		
CO_2	0.80	~0.7**	
CH_3CN	0.96		
CF_3Cl	1.0	0.82	1.0
SO_2	1.5	1.3	
I_2	2.2	1.8	0.22
Br_2	2.0		
N_2	~0.2**	~0.2**	0.48
CH_3OH	0.26	0.24	0.74
C_2H_4	0.68	0.56	0.49
C_2D_4			0.50
HCl	~0.8**		0.80
DCl			0.80
H_2	0.18	0.05	0.13
D_2	0.14	0.05	0.11
CF_4	<0.01	<0.01	0.16
CH_4	<0.01	<0.01	0.45
CD_4	<0.01	<0.01	0.30
C_2H_6	<0.01	<0.01	0.58
C_2D_6	<0.01	<0.01	0.41
H_2O	~0.04	~0.03	0.71
D_2O			0.77

Values of polarizabilities used in calculating K_6(theor) from: for M, Ref. 15 of Chap. IV; for CH_3CN, Ref. 26; for CF_3Cl, Ref. 27; for I_2 and Br_2, Ref. 28; for the rest, Ref. 29.

**Values approximated from results in: for $K^*(4p^2P)$-CO_2,N_2, Ref. 10; for $Na^*(3p^2P)$-N_2, Ref. 30; for $Na^*(3p^2P)$-HCl, Ref. 23. All other values from this work.

in w which are outside experimental uncertainties should reflect reasonably well changes in this ratio, and thus may be regarded as significant. With this in mind, the w values do provide a convenient basis for discussion of quenching efficiencies, and, of course, a value of w is, per se, a valid representation of the results in a given case, as it does correspond to a value of k_q under specified conditions.

The simple model used to obtain w values might be expected to apply best for moderately efficient quenching of the first resonance states, as the covalent-ionic curve-crossing distances are in a favorable range, and as strong coupling between the excited and quenched states might be expected to apply, as discussed in Chapter IV. As detailed in the introduction to the present chapter, quenching experiments on $Na^*(3p^2P)$ led to tentative separation of quenchers into four classes. The very inefficient quenching of class A molecules, $w \ll 1$, indicated that strong coupling of the excited and quenched states was not available. This was interpreted predominantly in terms of large negative electron affinities, with the added consideration that these molecules provided no highly exoergic reaction channel with the excited atom. Moderately efficient quenchers of class B, $\sim 0.2 < w < 1.0$, had more favorable electron affinities, as a consequence of possessing low-lying, unfilled molecular orbitals. This made an ionic intermediate available at reasonable separations, thus providing coupling, but the excitation energy had to be dissipated, in a quenching collision, in internal excitation or translational separation, as no highly exoergic reaction channel was available here, either. Class C molecules, again moderately efficient quenchers, with w values generally closer to unity

than for class B, were distinguished from class B primarily by the availability of a highly exoergic reaction path, which was regarded as responsible for their quite efficient quenching. Class D, $w > 1.0$, the "super-efficient" quenchers, included molecules of large electron affinities, for which curve-crossing distances were well outside the expected range of orbiting distances.

Examination of w values for quenching of $Na^*(3p^2P)$ illuminates this breakdown into classes, though distinction between molecules of classes B and C is not clear simply in terms of these numbers. There are some species, notably H_2 and D_2, and perhaps N_2 and CH_3OH, which might be regarded as borderline between classes A and B or C. Subsequent experiments on quenching of $K^*(4p^2P)$ by several gases and of $Na^*(3p^2P)$ by Br_2 have led to no notable departures from the behavior which was expected on the basis of the initial $Na^*(3p^2P)$ work. There does seem to be a decrease in w values for quenching of $K^*(4p^2P)$ as compared to $Na^*(3p^2P)$ for those gases studied with energy dependence, as well as for I_2, but in view of the quality of the data on $K^*(4p^2P)$, this is not necessarily significant. Furthermore, the apparent change in efficiency in going from C_2H_4 (class B) or CF_3Cl (class C) to I_2 or SO_2 (class D), is about the same as in the $Na^*(3p^2P)$ case.

The really interesting results as far as quenching efficiencies are concerned, are found in examining the values for quenching of $K^*(5p^2P)$. Here the only clear separation into classes would probably be noble gases, which do not measurably quench this state, on the one hand, and everything else on the other. The first two gases studied with this state, C_2H_4 and CF_3Cl, held no promise of things to come, as,

within experimental uncertainties, their quenching efficiencies are quite comparable to those for these same gases with the first resonance states. This is also apparently true for HCl, which was studied later. Thus, on the admittedly limited bases of these three molecules, it appears that reasonably efficient quenchers of classes B and C exhibit no particular increase in quenching efficiency with $K^*(5p^2P)$, and show only the nominal increases in quenching cross sections which might be expected in terms of increased dispersion forces, although it is not obvious that such is the true explanation.

Results on N_2, one of the less efficient class B quenchers, indicate an apparently significant, although not really dramatic, increase in quenching efficiency. There are various factors which might be regarded as contributing to this. One is the probably considerably increased quadrupole-quadrupole forces with the more highly excited atom, which are obviously not accounted for by K_6(theor). Another is the availability of four atomic states to which quenching can occur, particularly as two of these states, and 3d and 5s, lie only 3200 and 3700 cm^{-1}, respectively, below the 5p, and provide quenched channels which require transfer of only relatively small amounts of energy. Another factor to consider is the increased density of molecular vibrational levels at energies near the atomic excitation energy.

CH_3OH exhibits a larger apparent increase in quenching efficiency, but even here, the increase is not dramatic, and one might well explain it in terms of the effects considered above. The striking and, in some cases, quite unexpected increases in quenching ability are apparent when one considers the results on a whole group of molecules, from

CF_4 through H_2O and D_2O in Table VII, which are definitely in the inefficient class for quenching first resonance states, but which are promoted to a considerable degree of efficiency on going to the second. The newfound quenching abilities of CH_4 and CF_4, at least, cannot be explained in terms of increased quadrupole interaction. In considering the possible effect of the proximity of the 5s and 3d levels, it was thought that one might see some quenching to these levels by noble gases, yet argon, at 600 Torr, and xenon, at 200 Torr, failed to produce measurable attenuation of the $K^*(5p^2P)$ fluorescence. Indeed, these two gases were the only species studied with $K^*(5p^2P)$ which entirely failed to quench. This at least indicates that quenching does not proceed by purely electronic-translational energy transfer, but that the excitation must find its way into the internal degrees of freedom of the quenching molecule, which process presumably requires fairly intimate contact. It is also interesting in this regard to compare to the case of $Hg^*(6p^3P_1)$,[31] at 4.86 eV, which has the $Hg^*(6p^3P_0)$ metastable state only 0.22 eV (1750 cm^{-1}) below it. It is well established that in many quenching processes this close-lying level does not participate, but rather quenching proceeds directly to the ground state ($6s^1S$). Amongst the gases which do not quench $Hg^*(6p^3P_1)$ efficiently at all are CH_4, C_2H_6 and CF_4. Indeed, this fact contravenes the contention that the quenching efficiencies observed for these gases with $K^*(5p^2P)$ can be explained in terms of increased density of molecular vibrational levels at the higher energies corresponding to the atomic excitation, as the excitation energy of $Hg^*(6p^3P_1)$ is well above that of $K^*(5p^2P)$.

While it would seem reasonable to expect that some of the quenching of $K^*(5p^2P)$ in many, if not most, cases would be to one of the close-lying states, it also seems that the presence of these states, per se, is not a sufficient explanation for fairly efficient quenching by former class A molecules. What other processes which have been made available by the increased excitation energy of the atom might then be considered in investigating these increases in quenching efficiency. First of all, the decreased ionization potential of the atom should lead to the possibility of electron transfer with gases where this was not formerly possible at distances outside the repulsive wall of the potential. That is, the ionic intermediate becomes accessible, whereas it was not with the first resonance states. This situation is illustrated in Fig. V-7, in which rough potential curves, ignoring small attractive forces, indicate approximate crossing distances which might be expected for various values of molecular electron affinities with $K^*(4p^2P)$ and $K^*(5p^2P)$. A value of ~-2.5 to ~-3.5 eV would tend to explain contrasting behavior toward the two atomic states, such as that which is observed with the quenchers under consideration, as the outermost curve-crossing distance in such a case would be on the repulsive part of the potential for $K^*(4p^2P)$, but would be favorably situated for $K^*(5p^2P)$. Appearance potentials in dissociative electron attachment studies on CH_4,[32] H_2O,[32] and CF_4[33] have yielded values for the electron affinities of ~-7.5, ~-5.0 and ~-4.7 eV, respectively. However, Claydon, et al.,[34] have suggested that the lowest negative ion state of H_2O is not seen in such experiments because it is bound relative to dissociation to OH^- and H. They suggest a value greater than -3.28 eV for the vertical

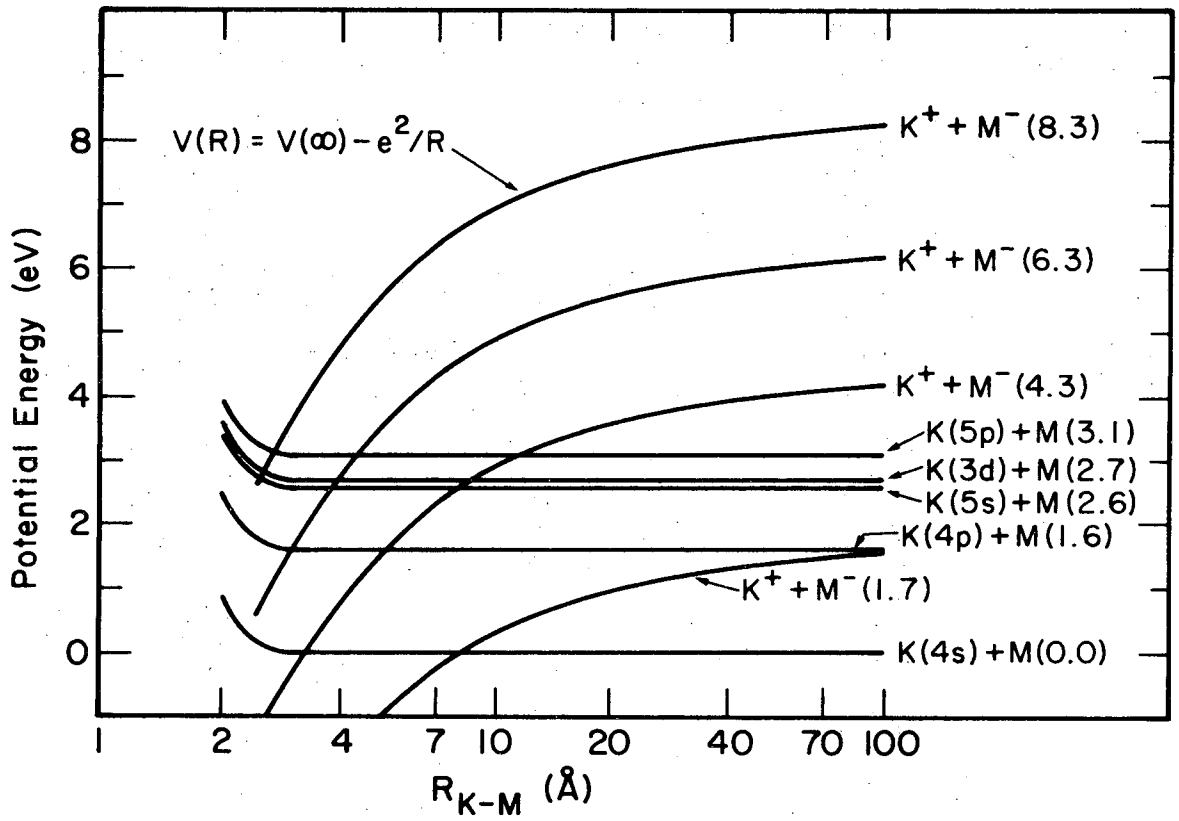

XBL 734-5999

Fig. V-7. Potential curves illustrating crossing distances for ionic and covalent curves for various states of the K atom with gases, M, of various electron affinities. For K + M, numbers in parentheses represent the excitation energy of the atomic state in eV. For $K^+ + M^-$, the numbers in parentheses represent I.P.-E.A., where I.P. is the ionization potential of K(4s), I.P. = 4.3 eV, and E.A. is the electron affinity of M. Thus the four ionic curves shown are appropriate, from bottom to top, to gases of electron affinities +0.6, 0.0, -2.0, and -4.0 eV, respectively.

electron affinity. Similarly, suggestion of a considerably higher electron affinity for CH_4 has been made by Christophorou and Stockdale.[35] Thus, it seems quite possible that one very significant new effect in quenching by former class A molecules is the availability of the ionic intermediate which couples the excited to the quenched state.

Of course, there is still the problem of how the excitation energy is to be dissipated, and the second effect of the increased atomic excitation which might bear strongly on these cases is the much larger exoergicities for possible reactions between the excited atom and the quenching molecule. The effect of highly exoergic reactive channels corresponding to quenching has been referred to previously, and has been granted some importance in the interpretation of quenching efficiencies with first resonance states.[2,4] Reference 2b, in fact, proposes that fairly efficient chemical quenching with low activation energy is likely for reactions which are more than ~20 kcal/mole exoergic. Values of the reaction exoergicity, $\Delta D_o = D_o(M-B) + E^*(M^*) - D_o(A-B)$, where A-B represents a polyatomic molecule, are listed for some possible reactions of interest here in Table VIII, along with the corresponding w values. It can be seen that there is no particular value of ΔD_o which affords efficient quenching in general. However, the very large value for the reaction of $K^*(5p\,^2P)$ with CF_4, and the considerable value for the reaction of this excited atom with H_2O, are comparable in magnitude to the values for $Na^*(3p\,^2P)$ and $K^*(4p\,^2P)$ with CF_3Cl, and to the value for $Na^*(3p\,^2P)$ with CH_3CN. This indicates that, indeed, the reaction path should be considered a probable one for dissipation of excitation in quenching of $K^*(5p\,^2P)$ by H_2O and CF_4, and that this

Table VIII. Reaction exoergicities.*

Atom	Gas	Product	ΔD_o (kcal/mole)	w
$Na^*(3p^2P)$	CH_3CN	NaCN	~46	1.0
	CF_3Cl	NaCl	66	1.0
	HCl	NaCl	43	~0.8
	CH_3OH	NaOH	32	0.26
	CF_4	NaF	36	<0.01
	H_2O	NaOH	10	~0.04
	CH_4	NaH	-6	<0.01
	H_2	NaH	-8	0.18
$K^*(4p^2P)$	CF_3Cl	KCl	59	0.82
	CH_3OH	KOH	35	0.24
	CF_4	KF	31	<0.01
	H_2O	KOH	6	~0.03
	CH_4	KH	-21	<0.01
	H_2	KH	-23	~0.05
$K^*(5p^2P)$	CF_3Cl	KCl	93	1.0
	HCl	KCl	70	0.8
	CH_3OH	KOH	69	0.74
	H_2O	KOH	40	0.71
	CF_4	KF	65	0.16
	CH_4	KH	13	0.45
	H_2	KH	11	0.13

*The reaction exoergicity, $\Delta D_o = D_o(M-B) + E^*(M^*) - D_o(A-B)$, where A-B is the quenching gas. Bond energies from: for NaCN, estimated from arguments given in Ref. 36; for NaF, NaH, KF, KH, from Ref. 37; the rest from Ref. 38.

path may well contribute to quenching efficiency in these cases. However, in a way, this begs the question, as the atom and the molecule must get together before reaction can occur, and this getting together has, for excited alkali atoms, generally been pictured in terms of electron transfer. Once such transfer occurs, quenching may proceed by several paths, and, although some may be somewhat more efficient than others, any distinction among them here is unclear. For instance, CH_4 and C_2H_6, for which the ΔD_o values are not in such a range as to indicate a strong possibility of reaction, apparently possess quenching efficiencies in between those of H_2O and CF_4. Thus, it would seem that the primary recourse in interpreting the quenching efficiencies of the former class A molecules with $K^*(5p^2P)$ would probably be the accessibility of the ionic intermediate.

It is interesting to note that, in all the quenching of $K^*(5p^2P)$, no gas has a value of w greater than unity. So, empirically, at any rate, this method of estimating quenching efficiencies seems to be fairly good. Considering the basis of it, however, this may be purely accidental.

<u>Isotope Effect</u>. So far, the comparison of the hydrogen vs deuterium compounds has not been mentioned, and here an intriguing effect appears. Notably, for CH_4-CD_4 and for C_2H_6-C_2D_6, there is a definite "isotope effect", a ratio of ~1.5 for the quenching efficiencies of the hydrides to those of the deuterides. There is room for such an effect in the results on quenching $Na^*(3p^2P)$ by H_2 and D_2 and possibly on quenching of $K^*(5p^2P)$ by these gases, as well. Note that the observation of this effect for the two hydrocarbon pairs does not necessarily involve

comparison of w values. In these cases, the masses of the partners are sufficiently similar that the measured quenching rate constants or the derived cross sections provide clear evidence of a definite distinction in quenching efficiency, which distinction is then reflected in the w values. The H_2-D_2 case is somewhat trickier. One cannot simply compare measured rate constants, as they correspond to significantly different relative speed distributions, and comparison of K_6(exp) values, which amounts to comparing cross sections for the same value of relative speed, ignores the effect of reduced mass on collision behavior. Thus, it would seem necessary to compare values of w, if one wishes to look for an "isotope effect." In the following, consideration of this effect will be concerned mainly with the hydrocarbon cases, as there is less ambiguity.

Apparently, any possible isotope effect in alkali quenching has not been investigated previously, except for the H_2-D_2 case. In the present work, this effect was observed initially with CH_4-CD_4, and was thought to support the notion of chemically reactive quenching. In fact, experiments were done in which mixtures of these gases were exposed to experimental quenching conditions with K*($5p^2P$) for long periods of time, and subsequent mass spectral analysis was done to see if peaks due to isotope scrambling could be observed. It turned out that such peaks were present, but the same result was found with control samples exposed at 2100Å and 2450Å, where no K*($5p^2P$) could be produced, and, furthermore, the amount of scrambling appeared to be approximately proportional to the length of time for which the mixture was exposed, regardless of the uv wavelength. Thus, these

experiments provided no clear information on the behavior of CH_4 and CD_4 with $K^*(5p^2P)$.

It is now believed that a more plausible explanation for the isotope effect can be found in the Franck-Condon factors involved in making the transition from the molecule to the negative molecular ion when the quenching gas molecule accepts the electron from the excited atom. Since the electron is being put into a strongly antibonding orbital, it is to be expected that the bond distances in the ion will be considerably greater than in the neutral molecule. The larger vibrational amplitudes of the hydrogen-containing species, and the greater non-classical tunneling possibilities, should then make the transition from the neutral molecule to the ion more favorable for hydrogen than for deuterium-containing molecules.

No sooner is this hypothesis adopted, however, than it leads to apparent difficulty in the cases of HCl-DCl and H_2O-D_2O. Why is no isotope effect observed in these cases. (Indeed, this was one reason that a special effort was made to get mass spectrometric analysis of a nominal D_2O sample, despite the difficulties involved.) In seeking an explanation in the HCl-DCl case, one is led to consider the large w values. HCl is apparently quite efficient already in quenching first resonance states, and increased exoergicity for the formation of KCl with $K^*(5p^2P)$ might lead one to expect that this molecule would be a "saturated" quencher. That is, without reference to any model or any particular attractive potential, it could well be that HCl quenches $K^*(5p^2P)$ on essentially every close encounter. As the thermodynamics would be essentially identical for the DCl case, no particular difference in quenching behavior would be expected.

Such an argument might apply in the case of H_2O-D_2O as well, as the ΔD_o values for possible reaction with $K^*(5p\,^2P)$ are quite large, and the w values are comparable to those of HCl and DCl. (The fact that the w value for D_2O is slightly larger than that for H_2O is not regarded as significant.) In this connection, it was thought that an isotope effect with the H_2O-D_2O pair might be observable in the quenching of $Na^*(3p\,^2P)$, as the quenching efficiencies would be very small, and good signal-to-noise was available. As it turned out, however, no quenching at all could be measured with D_2O, and there were complications with slight enhancement of the fluorescence by both gases, so no clear results could be deduced as far as any isotope effect was concerned. In this regard, it is interesting to note that a clear "isotope effect" has been observed[31] in the quenching of $Hg^*(6p\,^3P_1)$ by H_2O and D_2O, and by NH_3 and ND_3; for all these gases, the quenching cross sections are in 0.5-5$Å^2$ range. Curiously, H_2 and D_2 apparently show no isotope effect in quenching this mercury state,[31] but do show one in quenching the $Hg^*(6p\,^3P_0)$ metastable state.[39]

The absence of an isotope effect in the C_2H_4-C_2D_4 situation seemed puzzling at first. Here, however, it was realized that the π^* molecular orbital which would be expected to accept the donated electron is situated on the carbons, so one might regard these molecules, as far as the electron-transfer picture in concerned, as C-C systems, and, in this simple way of thinking, no isotope effect would be expected.

Super-efficient Quenchers. Besides the promotion of several class A quenchers to efficient status on going to $K^*(5p^2P)$, the one formerly super-efficient quencher studied with this state, I_2, suffered a severe demotion in quenching efficiency. As has been mentioned, the analysis of the $K^*(5p^2P) - I_2$ data involved the use of a speed distribution derived for $K^*(4p^2P)$ at 2475Å, and this procedure introduced some additional uncertainty into the results. However, if one analyzes this case as fully thermal, in order to estimate the effect of this uncertainty, one obtains a value for 10^{11} K_6 of 0.98 cm^2-$(cm/sec)^{2/3}$ and for w of 0.25. These values are larger by only 15% than those quoted in Tables V and VII, so the conclusion that I_2 has become an only moderately efficient quencher is not affected by the uncertainty in the analysis.

This striking decrease in quenching efficiency seems to be readily understandable in terms of the curve-crossing picture, as it is found that the $K^*(5p^2P) + I_2$ curve lies above the $K^+ + I_2^-$ curve at all separations. This situation is illustrated in Fig. V-8 for the case of $Na + I_2$, which is exactly analagous. Thus, there is no crossing of the excited covalent curve and the ionic curve, so the quenching efficiency is markedly decreased. One is inclined to wonder how quenching can occur at all, but recourse to vibrational excitation of the I_2^- provides a possible answer. Namely, the excited covalent curve will cross the ionic curves corresponding to highly excited I_2^-. However, such crossing would involve more than 1.5 eV of vibrational excitation in the molecule, and the Franck-Condon factors involved in possible transitions at these crossings would probably be expected to

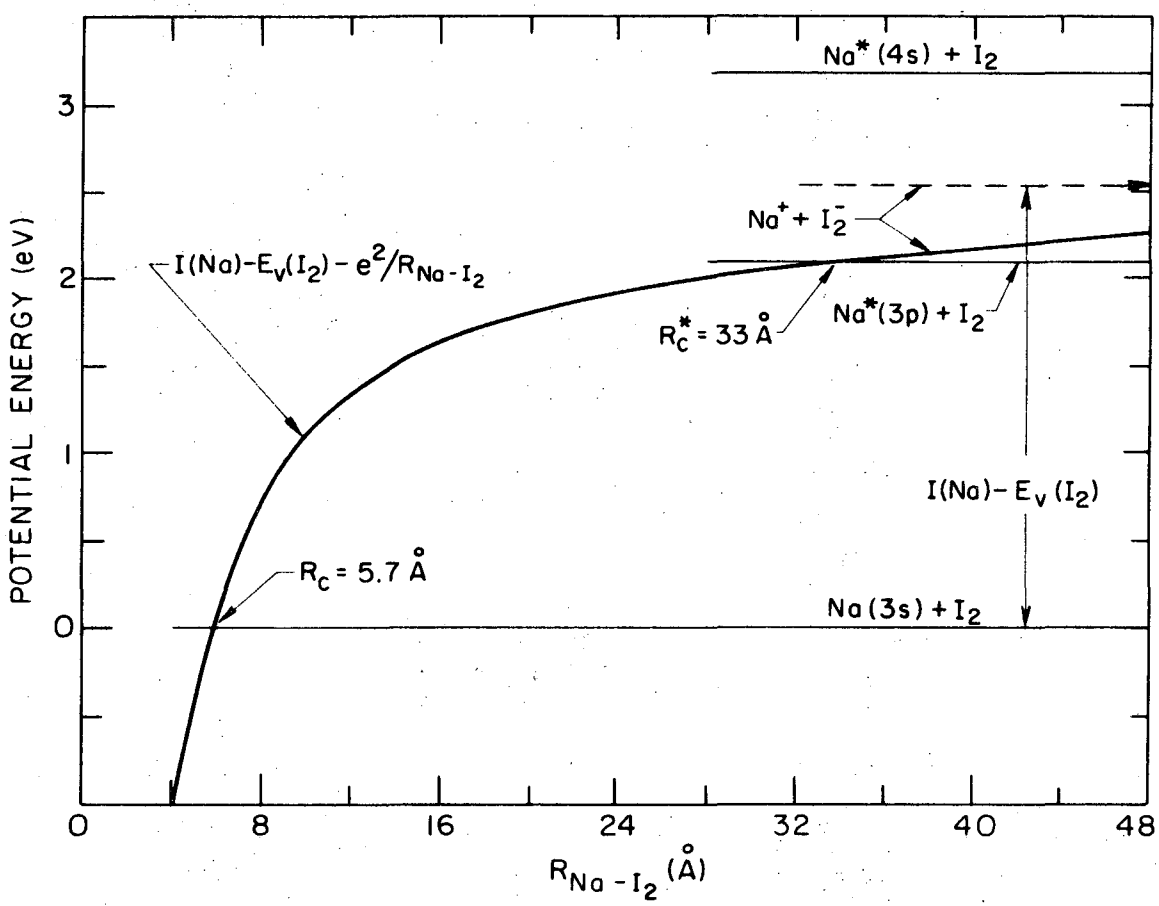

XBL 7110-7442

Fig. V-8. Potential curves for the Na-I_2 system, illustrating that the Na*($4p^2P$)+I_2 curve, which lies above the curve shown for Na*($4s^2S$)+I_2, would not cross the Na^++I_2^- curve. The same situation occurs for K*($5p^2P$)+I_2, as discussed in the text.

to be quite small. Alternatively, one might imagine quenching here as proceeding via curve crossing involving an electronically excited state of I_2^-, which could place the crossing distance at a fairly reasonable value. Here again, the Franck-Condon factors involved would probably be expected to be quite small, due to the rapidly oscillating nature of the continuum ion-state wavefunctions.[40]

This leads to consideration of all the class D quenchers in a bit more detail, in terms of the curve-crossing idea. The outer curve-crossing distances, R_o, calculated approximately from the atomic ionization potentials and the molecular electron affinities are given in Table IX for the cases studied. For SO_2, the crossing distances are not too great, and one might expect a fairly large quenching "efficiency" measured against a cross section of πR_o^2. This provides a very rough estimate of the quenching efficiency in terms of a minimum distance model, with R_o as the minimum distance. If one compares the "average" cross sections for the cases studied to the appropriate values of πR_o^2, one obtains the estimates of quenching efficiencies given in Table IX. Obviously, for the cases listed, larger R_o values result in less efficient quenching, in this picture. The small efficiencies for large R_o's are generally considered to be due to the difficulty of transferring the electron over such large distances. The extent to which this breakdown of the Born-Oppenheimer principle occurs in a given case might be estimated, at least very roughly, from the "efficiencies" given in Table IX. The breakdown would not seem to be very serious for the crossing distances involved in the SO_2 cases, but is clearly quite serious for the I_2 and Br_2 cases.

Table IX. Rough minimum distance efficiencies.

System*	$\sim R_o$ (Å)	"Average" $\langle Q_q \rangle$ ($Å^2$)	"Efficiency" ($\langle Q_q \rangle / \pi R_o^2$)
$Na^*(3p\,^2P)-SO_2$	7.5	120	~0.55
$K^*(4p\,^2P)-SO_2$	9	110	~0.45
$Na^*(3p\,^2P)-Br_2$	32	180	~0.05
$Na^*(3p\,^2P)-I_2$	36	180	~0.05
$K^*(4p\,^2P)-I_2$	120	200	~0.005

*Electron affinities: for SO_2, from Ref. 41, ~1.1 eV; for I_2 and Br_2, Ref. 42 reviews recent measurements which seem to converge on ~2.5 eV for Br_2 and ~2.6 eV for I_2.

Berry, et al.,[43] have discussed this breakdown effect in relation to the branching ratios of neutral atoms to ions in thermal dissociation of alkali halide vapors. Child [44] has obtained an expression for the translational energy dependence of the cross sections for reaction of ground-state alkalis with halogen molecules by calculating the covalent-ionic transition probability as a function of the local radial velocity at R_o. His calculations did not extend to the large R_o values encountered with excited atom-halogen systems, but extrapolation of his results indicates qualitative agreement with the magnitudes and velocity dependences of the quenching cross sections reported here.

One might expect, in quenching by I_2 and Br_2, that the initial covalent-to-ionic transition is made to an ionic curve corresponding to a vibrationally excited negative ion, placing the curve-crossing distance at a more favorable value for the electron jump. Examining the rough potential curves of Ref. 40 indicates that an optimum vibrational overlap for the $I_2 \rightarrow I_2^-$ transition would probably be realized for ~0.5-0.7 eV vibrational excitation of I_2^-, which would place the crossing distance at ~12-18Å for the cases involved here. Inside this "optimum Franck-Condon distance", the curve crossing picture might be regarded as a trade-off between the Born-Oppenheimer principle and the Franck-Condon principle. That is, at smaller separations, the vibrational overlap becomes progressively worse, but the ease of transferring the electron over the distance involved becomes greater, other things being equal. In considering this picture with regard to the present situation, it is interesting to note that Br_2 and I_2 with $Na^*(3p^2P)$ have nearly indentical R_o values, and that the measured

$\langle Q_q \rangle$ vs $\langle g \rangle$ values lie essentailly on the same curve. The I_2 quenching $K^*(4p^2P)$ cross section is a bit below this curve, but perhaps not significantly so, considering the quality of the data.

2. Comparison to Other Alkali Quenching Work

There has been relatively little study of quenching of excited alkalis by the sorts of molecules which were the primary concern of this study, with the exception of I_2 and Br_2 quenching $Na^*(3p^2P)$. Comparison to the direct lifetime measurement results of Brus[3] on these two quenchers has already been made. The I_2 comparison is shown in Fig. V-4. Brus's value of ~180Å^2 for the quenching cross section of Br_2 at a nominal relative speed of 1.4 km/sec has been noted as agreeing well with the results displayed in Fig. V-5. Also, measurements on quenching of $Na^*(3p^2P)$ by N_2, which are not referred to elsewhere, gave rate constants which agreed within 15% with the recent results of Weston and Barker, which were also obtained by direct lifetime measurement. One of the first quenchers studied here was CO_2 with $Na^*(3p^2P)$, and the results were compared to those of Hanson[23] as an initial check of the experiment. It was found that the agreement was good.

Aside from comparison to these other photodissociation studies, it is also worthwhile to compare results with inherently thermal studies. These latter fall into two general classes, atomic vapor and flame, as discussed in Chapter I. As the results generated by these two methods cover a very wide range of temperatures, it is convenient to convert the reported cross sections into K_6(exp) values for purposes of comparison, using Eqs. (32) and (37) of Chapter IV. The results of these manipulations are given in Table X, along with the reported

Table X. Comparison to thermal studies.

Atom-Gas	Method	Ref.	T (°K)	$\langle Q_q \rangle$ ($Å^2$)	10^{11} K_6(exp)	10^{11}(K_6(exp) This Work
$Na^*(3p^2P)-H_2$	Vapor	1*	400	23	0.85	
	Vapor	45(ℓ)**	400	16	0.60	
	Vapor	46(ℓ)	~600	12	0.50	0.48
	Flame	47	1600	9	0.53	
	Flame	8	1900	8	0.51	
$Na^*(3p^2P)-D_2$	Vapor	45(ℓ)	400	10	0.30	0.32
	Vapor	46(ℓ)	~600	10	0.34	
$Na^*(3p^2P)-CO_2$	Flame	47	1600	49	1.4	1.6
	Flame	8	1900	50	1.5	
$Na^*(3p^2P)-C_2H_4$	Vapor	1*	400	138	2.8	1.7
$Na^*(3p^2P)-C_6H_6$	Vapor	1*	400	230	4.1	2.1
	Vapor	46	~600	95	2.0	
$K^*(4p^2P)-H_2$	Vapor	9	350	5	0.17	0.15
	Vapor	6	400	~5	0.18	
	Vapor	5(ℓ)	400	9	0.33	
	Flame	7	1600	3.1	0.19	
	Flame	8	1900	3.4	0.21	
$K^*(4p^2P)-D_2$	Vapor	6	400	~1.5	0.05	0.12
	Vapor	8	400	10	0.24	
	Vapor	9	350	3.5	0.10	
$K^*(5p^2P)-H_2$	Flame	8	1900	60	3.8	0.58
$K^*(5p^2P)-H_2O$	Flame	8	2100	10	0.33	2.1
$K^*(5p^2P)-N_2$	Flame	8	1900	48	1.5	1.4

*As discussed in the text, results of Ref. 1 are probably affected by radiation imprisonment.

**(ℓ) denotes measurement by a lifetime method, in Ref. 46 by phase-shift, and in Refs. 5 and 45 by monitoring the decay of the excited population following a pulse. All other atomic vapor studies were by the steady-state method.

cross sections and temperatures in each case, where they are compared to the K_6(exp) values derived from the experimental results of this study. The overall agreement between this work and the thermal studies, as well as among all the studies, is quite good. There are, however, a few points which require discussion.

The values from Norrish and Smith[1] are about a factor of two higher than those of any other studies with which they can be compared. Reference 1 was perhaps the first atomic vapor study to get quenching cross sections anywhere close to values obtained in later studies. Two early studies[48,49] obtained astronomically high values for quenching cross sections for N_2 (190 and 90Å^2) and H_2 (54Å^2) with Na*($3p^2P$), presumably because they operated at excessively high temperatures, ~500°K. These studies are subject to considerable difficulty with radiation imprisonment, and this might explain the anomalously large cross sections. It is worth noting that Norrish and Smith did investigate an impressive variety of hydrocarbons, and divided them into efficient (unsaturated) and inefficient (saturated) quenchers. It is also interesting in reading their paper to note that, as of 1940, the importance of electron transfer in alkali quenching had apparently not been recognized.

With respect to the problem of temperature, or, more directly, vapor pressure, in atomic vapor studies, it should be noted that the value of ~600°K quoted with the results of Ref. 46 is the temperature of the quenching region. Their measured value of the lifetime for the excited population, by a phase shift method, of 1.66 nsec indicates that the vapor pressure was determined by a much lower temperature,

which is apparently not given in their paper. The use of a lifetime measurement technique may make their results a bit more reliable than those of atomic vapor studies which used steady-state measurements. The latter include all except Refs. 5, 45 and 46.

The results displayed in Table X for quenching of $K^*(4p^2P)$ by D_2 seem to be in a rather sad state of disorder. The results on this process and on $K^*(4p^2P) - H_2$ from Refs. 5 and 6 were produced by Krause and his co-workers. The values from Ref. 6 were obtained by measurements on separated doublet lines by a steady state technique, while those from Ref. 5 are the results of lifetime measurements on both components together. Results of other workers generally support the former measurement for H_2, but for D_2, the results of Refs. 5 and 6 represent the extremes, with the other two available measurements intermediate.

Finally, in regard to Table X, consider the results on quenching of $K^*(5p^2P)$. The values from Ref. 8 for H_2 and H_2O essentially reverse the values of the present work, while the value for N_2 agrees well. The flame measurements on quenching by these gases were done in flames containing combinations of 2 or 3 gases, so extraction of cross sections required knowledge of flame composition. Examination of the results indicates, however, that the value for N_2 should be unequivocal, as it depends only on knowing how much N_2 is introduced into the flame. The values for H_2O and H_2, however, depend on calculation of equilibrium concentrations following combustion of H_2 and O_2. Noting that the sum of the H_2 and H_2O cross sections is very similar to that obtained here, it seems possible that the results of Ref. 8 might be compromised by inaccurate knowledge of flame composition.

3. Comparison with Other Systems

Other "Electron-Transfer" Systems. In considering the covalent-ionic curve-crossing picture of alkali quenching, it is instructive to examine other processes which are also generally thought of in terms of this picture. Perhaps the prototypical electron-transfer process is the reaction of a ground state alkali atom with a molecule of a large electron affinity, such as I_2. Processes of this sort have been referred to in Chapter IV in connection with the notion of strong coupling between the initial and final (in this case, reacted) states.

Davidovits and his co-workers[50] have recently measured what should be quite reliable cross sections for reactions of the alkali metals with I_2. They produce ground-state alkali atoms, by photodissociation of the alkali iodide, in the presence of I_2, monitor the alkali concentration by measuring the absorption of resonance radiation through the reaction cell, and extract reaction cross sections from the decay rate of the alkali population.

Using a similar technique, they have also measured cross sections[51] for quenching of metastable $Tl^*(6p\,^2P_{3/2})$ atoms by I_2 and for reaction of ground state Tl atoms with I_2. As the ionization potential of Tl is only 6.106 eV, it is often thought of as "alkali-like", and these processes are also considered as proceeding via electron-transfer. The experimental results in Refs. 50 and 51 have been compared to cross sections calculated from a modified orbiting theory due to Anderson,[52] which approximately takes into account the interaction between the ionic and covalent electronic terms in the potential curve for the approach of the reactants. Computer solution is required to obtain a value for

the calculated cross-section. Good agreement was obtained between these calculated cross sections and the experimental results. Gislason[53] has recently calculated reaction cross sections for these systems using the multiple curve-crossing method described in Chapter IV (Ref. 26 of Chapter IV) in connection with the $Na^*(3p^2P) - N_2$ quenching calculations. He reports that good agreement with experimental results of Ref. 50 is obtained by this method also.

The experimental cross sections from Refs. 50 and 51 are shown in Table XI, along with the cross section obtained by Brus[3] for quenching of $Tl^*(7s^2S)$ by I_2. In addition, cross sections for quenching of $Na^*(3p^2P)$ and $K^*(4p^2P)$ by I_2, extrapolated from the results of this work to the conditions of the measurements on the corresponding ground state alkali reactions, are given for comparison. Likewise, these quenching cross sections are extrapolated to the nominal speed of Brus' $Tl^*(7s^2S) - I_2$ measurement for comparison to that cross section.

Taking ratios of measured cross sections from Ref. 50 to values of πR_o^2, one obtains a value near unity for the $Na-I_2$ reaction, and decreasing values as one goes to the K-, Rb- and $Cs-I_2$ cases, with a value of ~0.5 in the last case. As with the "super-efficient" quenchers, these numbers might be considered as roughly reflecting the extent of the Born-Oppenheimer breakdown in a given case, with larger values indicating less serious breakdown. For the reaction of Tl with I_2, $\pi R_o^2 \approx 55$, and for quenching of metastable Tl, $\pi R_o^2 \approx 100$, both values being well below the measured cross sections. The larger measured cross-sections may be simply due to the effect of attractive forces, as, in these cases, the R_o values are considerably smaller than in the

Table XI. Comparison to other "electron-transfer" systems.

Process	$\sim R_o$ (Å)	Measured $\langle Q \rangle$ (Å^2)	Conditions	Ref.
$Na+I_2 \rightarrow NaI+I$	6	97	860°K Thermal	50
$Na^*(3p\,^2P)+I_2 \rightarrow Na+I_2$, $NaI+I$	36	300	860°K Thermal	This* Work
$K+I_2 \rightarrow KI+I$	8	127	860°K Thermal	50
$K^*(4p\,^2P)+I_2 \rightarrow K+I_2$, $KI+I$	120	260	860°K Thermal	This* Work
$Rb+I_2 \rightarrow RbI+I$	9	167	860°K Thermal	50
$Cs+I_2 \rightarrow CsI+I$	11	195	860°K Thermal	50
$T\ell(6p\,^2P_{1/2})+I_2 \rightarrow T\ell I+I$	4.5	105	600°K Thermal	51
$T\ell^*(6p\,^2P_{3/2})+I_2 \rightarrow T\ell(6p\,^2P_{1/2})+I_2$	6	159	860°K Thermal	51
$T\ell^*(7s\,^2S)+I_2 \rightarrow$ any of several combinations	65	480	g = 0.35 km/sec	3
$Na^*(3p\,^2P)+I_2 \rightarrow Na+I_2$, $NaI+I$	36	560	g = 0.35 km/sec	This* Work
$K^*(4p\,^2P)+I_2 \rightarrow K+I_2$, $KI+I$	120	430	g = 0.35 km/sec	This* Work

*These values were extrapolated from the results of this work to the given conditions.

alkali cases, and little or no breakdown of the Born-Oppenheimer principle might be expected.

Referring to the quenching of $Tl^*(7s^2S)$, it is seen that, first, R_o is extremely large, and, second, the cross sections for quenching of this state and of $K^*(4p^2P)$ and $Na^*(3p^2P)$ by I_2 are nearly equal at the same relative speed. The cross section for quenching of $Na^*(3p^2P)$ by Br_2 would be essentially equal to these, as well, since it appears to be nearly identical to the $Na^*(3p^2P)$ - I_2 quenching cross section. In all these cases, the Born-Oppenheimer breakdown at R_o is quite serious, and, as opined earlier, one might expect that the initial covalent-ionic transition would occur at some smaller distance, at a crossing point involving an ionic curve corresponding to a vibrationally excited halogen molecule negative ion.

The main feature of these electron-transfer systems, particularly as they are combined here with highly exoergic reactive channels, is the very large cross sections. These indicate again the strong coupling between initial and final states. The agreement between the experimental cross sections and those calculated from the modified orbiting theory indicates this, as the theory rests on the assumption that penetration of the centrifugal barrier is the critical factor in producing a reactive collision, in just the same way as does the ordinary orbiting theory. Reference 50, however, cautions that the particulary good agreement found probably would not be expected from such a simple theory, and may be, to some degree, accidental.

Quenching of Excited Mercury. Quenching of mercury $Hg^*(6p^3P_1)$ has been studied perhaps more than that of any other excited atom. The properties and behavior of this species provide interesting comparisons to the excited alkalis. Several references have already been made to quenching of this state, and it will be discussed a bit more here, based on data from several sources collected in Calvert and Pitts.[31]

Perhaps the most significant contrast in the properties of $Hg^*(6p^3P_1)$ as compared to the excited alkali metals, is that its excitation energy of 4.86 eV is sufficient to break many chemical bonds. This has the consequence that photosensitized reactions play very important roles in quenching this state. In fact, the analysis of the products of such reactions is a considerable field in the study of $Hg^*(6p^3P_1)$.

Another difference in the mercury case, at least from first resonance states of alkalis, is the presence of the close-lying $6p^3P_0$ state, only 0.22 eV below the $^3P_1$ state. Interestingly enough, however, quenching to this metastable $^3P_0$ state is not regarded as important in most cases, including quenching by hydrocarbons. N_2 is one well-established exception, but its quenching cross section is only $\sim 0.2 Å^2$.

The importance of reactive quenching of $Hg^*(6p^3P_1)$ is illustrated by the fact that H_2 and D_2 both quench with cross sections of gas-kinetic magnitude, $\sim 9 Å^2$ and $\sim 12 Å^2$, respectively, via photosensitized decomposition of the molecule, whereas N_2, which cannot be decomposed by 4.86 eV, does not quench nearly so strongly.

Extensive studies have been made of quenching of $Hg^*(6p^3P_1)$ by saturated and unsaturated hydrocarbons. At first glance, these results might seem comparable to those for first resonance states of alkalis,

as small saturated hydrocarbons have very small cross sections, and unsaturated hydrocarbons display cross sections of ~25-~50Å^2. However, larger saturated molecules are generally quite strong quenchers of Hg*(6p^{3}P$_1$), with cross sections comparable to those for the unsaturated molecules. N-heptane and n-hexane for example, possess quenching cross sections of ~20Å^2 and ~30Å^2, respectively. Norrish and Smith,[1] studying quenching of Na*(3p^{2}P), found no significant increase in quenching ability of saturated hydrocarbons as molecular size and complexity increased. The overall process by which saturated molecules quench Hg*(6p^{3}P$_1$) is generally recognized to involve decomposition of the molecule, and the increased reactivity of certain molecular sub-groups is regarded as responsible for the quenching ability of the large molecules. The mechanisms and particular trends in reactivity are a subject of considerable complexity and research. However, the basic fact of reactive quenching seems to be clear, in contrast to excited alkalis, where such a process is energetically forbidden for first resonance states, and probably not very likely even for second resonance states.

In quenching of Hg*(6p^{3}P$_1$) by unsaturated hydrocarbons, the situation is considerably different, due to the possibility of triplet energy transfer, as the lowest triplet states of the molecules lie below the atomic excitation energy. Thus, the electronic structure of the molecule is regarded as contributing directly to its quenching ability, much as with excited alkalis, but in the mercury case, the quenching proceeds again via decomposition of the quenching molecule.

Another important difference in the properties of $Hg^*(6p\,^3P_1)$ is that its ionization potential is 5.5 eV, greater even than those of ground state alkalis. This has the consequence that an ionic intermediate coupling the initial and final states would become energetically available only at very small separations with most gases. This may explain why the largest cross sections observed for quenching of $Hg^*(6p\,^3P_1)$ are only of gas kinetic magnitude, while much larger cross sections for quenching of excited alkalis are commonplace.

D. Conclusion

On the basis of the quenching measurements reported here, combined with other data, it is felt that a reasonably good guess could be made as to the quenching ability of a good many molecules with alkali atom resonance states. With first resonance states, the molecular parameters which seem to be important, at least empirically, are the electron affinity and the presence or absence of a highly exoergic reaction path. Results on $K^*(5p\,^2P)$ indicate that everything except noble gases is a moderately efficient quencher, and this would probably extend to most other second resonance states, and possibly to more highly excited states as well, although the kinds of interactions to be expected become less clear.

One intriguing future experimental possibility is the study of $Na^*(4p\,^2P)$, "anomalous" amongst the second resonance states of alkalis in possessing a negative polarizability. Due to the impossibility of obtaining accurate knowledge of photodissociatively produced speed distributions with second and higher resonance states, and the problems involved in thermalizing, as well as the difficulties with uv intensity,

0 0 0 0 3 9 0 7 3 3 7

it seems that the photodissociation method is not the best for studying these more highly excited states. Probably, one should go to atomic vapors, and possibly utilize a laser as the excitation source. This would also permit excitation of extremely highly excited states, with the possibility of looking for ionizing collisions.

Another, probably more complicated, experiment, which would be good to see is the measurement of the vibrational energy distribution in N_2 or CO following quenching, as comparison to calculations could be made. There was indication that such work was in progress a few years ago,[54] but if quantitative results have been obtained, they have escaped notice here.

REFERENCES

1. R. G. W. Norrish and W. Mac F. Smith, Proc. Roy. Soc. London A176, 295 (1940).
2. (a) D. J. Dowling and E. Warhust, Trans. Far. Soc. 55, 532 (1959).
   (b) D. J. Dowling, G. R. H. Jones and E. Warhurst, ibid., p. 537.
3. L. E. Brus, J. Chem. Phys. 52, 1716 (1970) and references therein.
4. B. L. Earl, R. R. Herm, S-M. Lin and C. A. Mims, J. Chem. Phys. 56, 867 (1972).
5. G. Copley and L. Krause, Can. J. Phys. 47, 533 (1969).
6. D. A. McGillis and L. Krause, Can. J. Phys. 46, 25 (1968).
7. W. M. Smith, S. A. Stewart and G. W. Taylor, Can. J. Chem. 32, 961 (1954).
8. D. R. Jenkins, Proc. Roy. Soc. A303, 453 (1968).
9. H. P. Hoomayers and P. L. Lijnse, J. Quant. Spectrosc. and Radiat. Trans. 9, 995 (1969).
10. J. Gatzke, Z. Phyzik. Chem. (Leipzig) 223, 321 (1963).
11. W. L. Wiese, M. W. Smith and B. M. Miles, Atomic Transition Probabilities (Nat. Stand. Ref. Data Ser., Nat. Bur. Stand. (U.S.), 22, 1964), Vol. II.
12. Sidney W. Benson, Thermochemical Kinetics (John Wiley and Sons, New York, 1968), Table A.11.
13. American Petroleum Institute Research Project 44. Selected Mass Spectral Data (Thermodynamics Research Center, Departement of Chemistry, Texas A and M Univeristy, College Station, Texas).
14. A. Corme and R. Massot, Compilation of Mass Spectral Data (Heyden and Son, Ltd., London, 1966).

15. Dr. C. W. Koch, University of California, Berkeley (private communication).

16. F. W. Lampe, J. L. Franklin and F. H. Field, J. Am. Chem. Soc. 79, 6129 (1957).

17. G. H. Herzberg, Electronic Spectra of Polyatomic Molecules (D. van Nostrand Company, Inc., Princeton, 1967), p. 534.

18. Ronald R. Herm and Dudley R. Herschbach, Inhomogeneous Electric Deflecting Field for Analysis of Rotational Excitation in Reactive Scattering of Molecular Beams, UCRL-16039, 1965.

19. John L. Margrave, The Characterization of High Temperature Vapors (John Wiley and Sons, New York, 1967), p. 503.

20. D. R. Stull, Ind. and Eng. Chem. 39, 517 (1947).

21. J. A. R. Samson, Techniques of Vacuum Ultraviolet Spectroscopy (John Wiley and Sons, New York, 1966), p. 300.

22. Diffraction Grating Handbook (Baush and Lomb, Inc., Rochester, New York, 1972).

23. H. G. Hanson, J. Chem. Phys. 23, 1391 (1955).

24. V. A. Dudkin, V. I. Malyshev and V. N. Soroken, Opt. Spectrosc. 20, 313 (1966).

25. H. G. Hanson, J. Chem. Phys. 47, 4773 (1967).

26. E. P. Lipincott, G. Nagarajan and J. M. Stutman, J. Phys. Chem. 70, 78 (1966).

27. W. N. Hess, R. L. Mather and R. A. Nobles, J. Chem. Eng. Data 7, 317 (1962).

28. J. H. Birely, R. R. Herm, K. R. Wilson and D. R. Herschbach, J. Chem. Phys. 47, 993 (1967).

29. Landolt-Bornstein Zahlenwerte und Functionen, A. M. Hellwege and K. H. Hellwege, eds. (Springer, Berlin, 1951), Vol. 1, pt. 3, p. 510.

30. J. R. Barker and R. E. Weston, Jr., Chem. Phys. Letters 19, 235 (1973).

31. Jack G. Calvert and James N. Pitts, Jr., Photochemistry (John Wiley and Sons, New York, 1966), Chapter 2 gives an extenstive review of mercury quenching.

32. L. G. Christophorou, Atomic and Molecular Radiation Physics (John Wiley and Sons, New York, 1971).

33. K. A. G. MacNeil and J. C. J. Thynne, Int. J. Mass Spectrom. Ion Phys. 3, 455 (1970).

34. C. R. Claydon, G. A. Segal and H. S. Taylor, J. Chem. Phys. 54, 3799 (1971).

35. L. G. Christophorou and J. A. D. Stockdale, J. Chem. Phys. 48, 1956 (1968).

36. R. R. Herm and D. R. Herschbach, J. Chem. Phys. 52, 5783 (1970).

37. A. G. Gaydon, Dissociation Energies and Spectra of Diatomic Molecules (Chapman and Hall, London, 1968).

38. B. de B. Barwent, Bond Dissociation Energies in Simple Molecules (Nat. Stand. Ref. Data Ser., Nat. Bur. Stand. (U.S.), 31, 1970).

39. A. C. Vikis and H. C. Moser, J. Chem. Phys. 53, 1491 (1970).

40. D. R. Herschbach, Advances in Chemical Physics X. Molecular Beams, John Ross, ed. (Interscience, New York, 1966), Chapter 9.

41. K. Kraus, W. Muller-Dzying and H. Neuert, Z. Zaturforsch. 16a, 1385 (1961).

42. A. P. M. Baede, Physica 59, 541 (1972).

0 0 0 0 3 9 0 7 5 3 9

43. J. J. Ewing, R. Milstein and R. S. Berry, J. Chem. Phys. 51, 4173 (1971).

44. M. S. Child, Mol. Phys. 16, 313 (1969).

45. B. P. Kibble, G. Copley and L. Krause, Phys. Rev. 159, 11 (1967).

46. C. Baestlein, G. Baumgartner and B. Brosa, Z. Physik. 218, 319 (1969).

47. D. R. Jenkins, Proc. Roy. Soc. (London) 293, 493 (1966).

48. R. Mannkopff, Z. Physik. 36, 22 (1926).

49. L. von Hamos, Z. Physik. 74, 379 (1932).

50. S. A. Edelstein and P. Davidovits, J. Chem. Phys. 55, 5164 (1971).

51. A. Gedeon, S. A. Edelstein and P. Davidovits, ibid., p. 5171.

52. Roger Anderson, Ph. D. Thesis, Harvard University, Cambridge, Mass. 1968.

53. E. A. Gislason, University of Chicago-Chicago Circle (private communication).

54. J. C. Hassler and J. C. Polanyi, Disc. Far. Soc. 44, 157 (1967).

ACKNOWLEDGEMENTS

It is a pleasure to acknowledge the very large part played by Professor Ronald R. Herm in the success of this project. He initiated it, and his assistance, scientific advice, and moral support were essential to its completion. For what has been learned, by me and by the reader, his insight is primarily responsible.

Several people played significant roles in assisting along the way: Tom Weber, with the construction of the H_2 arc; Maynard Chen, with collecting some of the NaI data; Chuck Mims and Shen-Maw Lin with assembly of the apparatus and early experiments. Lin, in addition, deserves special credit for his contributions to the data analysis.

In 1969, before I started this project, I seriously considered quitting graduate school. Professor William D. Gwinn urged me to continue, and influenced in no small way my decision to do so. For his confidence in me and his contribution to my career, I am grateful.

The staffs of the chemistry department and LBL have contributed much to the progress of this work. Especially the efforts of the very talented people in the departmental machine shop and the glass shops of both the department and LBL have been of great help. In addition, the efforts of Nancy Monroe and Gloria Pelatowski in preparing the figures, and especially of Jean Wolslegel in typing the manuscript, have made the preparation of this thesis go very smoothly, and deserve special thanks.

Among the things which contributed significantly to keeping me on a more or less even keel, especially through the less fruitful

experimental periods, were the works of J. S. Bach, W. A. Mozart, L. van Beethoven, and all that they made possible.

This work has been done under the auspices of the U. S. Atomic Energy Commission.

LEGAL NOTICE

This report was prepared as an account of work sponsored by the United States Government. Neither the United States nor the United States Atomic Energy Commission, nor any of their employees, nor any of their contractors, subcontractors, or their employees, makes any warranty, express or implied, or assumes any legal liability or responsibility for the accuracy, completeness or usefulness of any information, apparatus, product or process disclosed, or represents that its use would not infringe privately owned rights.

TECHNICAL INFORMATION DIVISION
LAWRENCE BERKELEY LABORATORY
UNIVERSITY OF CALIFORNIA
BERKELEY, CALIFORNIA 94720